
**Facultad**
**de**
**Ciencias**

# DISSECTING THE CMB ANGULAR POWER SPECTRA

Diseccionando los espectros angulares de potencia del FCM

Trabajo de Fin de Grado
para acceder al

**GRADO EN FÍSICA**

**Autor:** Miguel Ruiz Granda
**Director:** Patricio Vielva Martínez

**Junio 2021**

# Contents

**Acknowledgements** **III**

**Abstract** **V**

**Foreword** **VII**

**1 Introduction** **1**

1.1 The CMB temperature power spectrum . . . . . 1

1.2 The CMB polarization power spectra . . . . . 3

1.3 Observing the CMB: temperature and polarization . . . . . 7

1.4 CMB anisotropies theory: temperature and polarization . . . . . 10

**2 Methodology** **14**

2.1 Cosmic Linear Anisotropy Solving System (CLASS) . . . . . 14

2.2 Simulation of the CMB power spectra . . . . . 19

2.2.1 Generating the theoretical power spectra . . . . . 19

2.2.2 Healpy . . . . . 19

2.2.3 Planck frequency maps and their properties . . . . . 21

2.2.4 Simulating temperature and polarization maps . . . . . 21

2.3 Bayesian inference in cosmology . . . . . 25

2.3.1 The Prior . . . . . 25

2.3.2 The Likelihood . . . . . 26

2.3.3 Sampling for parameter estimation . . . . . 27

2.3.4 Markov Chain Monte Carlo (MCMC) sampling . . . . . 28

**3 Results** **30**

3.1 Fitting to ΛCDM cosmological parameters . . . . . 30

3.2 Fitting ΛCDM plus one phenomenological amplitude . . . . . 33
3.3 Fitting ΛCDM plus several phenomenological amplitudes . . . . . 40

**4 Conclusions and future work** **46**

**Bibliography** **48**

**A Cosmological parameters** **51**

**B Fitting $A_s$ plus the six phenomenological amplitudes** **57**

**C Code used in this project** **59**

# Acknowledgements

Este trabajo supone la finalización de una etapa que empecé hace ya cinco años y, en cierto modo, la consecución de un sueño que tengo desde que tenía doce años. Los que me conocen bien saben que fue el gusto por la Astronomía lo que me llevó a querer ser físico, por lo que tener la oportunidad de realizar el Trabajo Fin de Grado en el campo de la Astrofísica tiene una gran importancia para mí.

En primer lugar, querría dar las gracias a Patricio por el tiempo que dedicó hace ya más de un año para que escogiera un proyecto que me gustase y la constante dedicación y disposición a ayudarme durante toda la duración de este trabajo. Agradecer también a Julien Lesgourgues, ya que fue un correo suyo el que motivó la realización de este proyecto, y a Aída Palacio, por la ayuda en la utilización del Supercomputador Altamira.

Mi agradecimiento también a mis amigos, por el apoyo recibido durante toda la carrera. En particular, agradecer a Mario toda la ayuda que me brindó en el complicado mundo de la instalación y ejecución de programas en Linux. Sin lugar a duda este proyecto habría sido infinitamente más difícil sin su ayuda.

Por último, me gustaría dedicar este trabajo a mis padres, por todo el apoyo y ayuda recibida a lo largo de toda mi carrera académica. Gracias de corazón.

# Abstract

The aim of this project is to perform an extra parametrization of the standard cosmological model, ΛCDM, to weight the different physical processes that define the pattern of the Cosmic Microwave Background, CMB, angular power spectra. We define six different phenomenological amplitudes to account for the Sachs-Wolfe, early and late Integrated Sachs-Wolfe, polarization, Doppler and lensing effects. To this end, we have modified `CLASS` Boltzmann code and adapted the Markov Chain Monte Carlo (MCMC) sampler from `Cobaya` to introduce these new parameters. Simulations of the CMB angular power spectra obtained by Planck mission were used to test the capability of this experiment to constrain different combinations of cosmological and phenomenological amplitudes. Deviations of the mean values of the phenomenological amplitudes from the ΛCDM model predictions would imply inconsistencies in the cosmological standard model and would be helpful to resolve the existing cosmological tensions.

The results presented in this work show Planck experiment might be able to constrain ΛCDM plus one physical contribution, except the late Integrated Sachs-Wolfe effect. However, all the cosmological and phenomenological parameters cannot be constrained simultaneously due to a existing degeneracy between the scalar amplitude, $A_s$, and the phenomenological amplitudes. Other combinations have been studied throughout this work and in all the simulations performed the joint use of CMB temperature and polarization data has proven to be beneficial in constraining the phenomenological amplitudes.

**Keywords**: CMB, cosmology, physical processes in the CMB, Markov Chain Monte Carlo.

# Resumen

El objetivo de este proyecto es realizar una parametrización adicional del modelo cosmológico estándar, ΛCDM, para pesar los distintos procesos físicos que determinan la forma de los espectros angulares de potencia del Fondo Cósmico de Microondas, FCM. Hemos definido seis amplitudes fenomenológicas distintas para considerar el efecto Sachs-Wolfe, los efectos integrados Sachs-Wolfe temprano y tardío, el efecto de polarización, el efecto Doppler y el efecto de lensado. Para este fin, hemos modificado el código Boltzmann `CLASS` y adaptado el muestreador Markov Chain Monte Carlo (MCMC) de `Cobaya` para introducir estos nuevos parámetros. Simulaciones de los espectros angulares del FCM obtenidos por la misión de Planck fueron usados para comprobar la capacidad de este experimento para constreñir distintas combinaciones de parámetros cosmológicos y fenomenológicos. Desviaciones de los valores medios de las amplitudes fenomenológicas respecto a las predicciones realizadas por el modelo ΛCDM implicarían inconsistencias en el modelo estándar cosmológico y serían de ayuda para resolver las distintas tensiones cosmológicas existentes.

Los resultados presentados en este trabajo muestran que la misión Planck sería capaz de constreñir los parámetros del modelo ΛCDM y una amplitud fenomenológica adicional, a excepción del efecto integrado Sachs-Wolfe tardío. Sin embargo, todos los parámetros cosmológicos y fenomenológicos no pueden ser constreñidos simultáneamente debido a la degeneración existente entre la amplitud escalar, $A_s$, y los parámetros fenomenológicos. Otras combinaciones han sido estudiadas en este trabajo y, en todas las ejecuciones del muestreador MCMC, el uso conjunto de datos de temperatura y polarización del FCM ha probado ser beneficioso en la constricción de los parámetros fenomenológicos.

**Palabras clave**: FCM, cosmología, procesos físicos en el FCM, Markov Chain Monte Carlo.

# Foreword

This thesis is the result of a project which started a year ago under the supervision of Dr. Patricio Vielva and has been supported by a Collaboration Grant with University Departments from the Spanish Ministry of Education, Culture and Sports in the Modern Physics Department at the University of Cantabria. Due to the important computational component of this work, the Altamira Supercomputer at the Institute of Physics of Cantabria (IFCA-CSIC), member of the Spanish Supercomputing Network, was used for performing simulations.

Our work aims to perform an extra parametrization of the standard cosmological model, ΛCDM, to weight the different physical processes that define the pattern of the Cosmic Microwave Background, CMB, angular power spectra. Six different physical processes, weighted by their corresponding phenomenological amplitudes, have been considered in this work: the Sachs-Wolfe, early and late Integrated Sachs-Wolfe, polarization, Doppler and lensing effects. Using simulations of the CMB angular power spectra recovered by Planck mission, we tested how well different combinations of cosmological and phenomenological parameters can be constrained. Deviations of the mean values of the phenomenological amplitudes from the ΛCDM model predictions would imply inconsistencies in the cosmological standard model and would be helpful to resolve the existing cosmological tensions.

This work is structured as follows. In Chapter 1, we introduce the Cosmic Microwave Background explaining its origin, their temperature and polarization constituents, different experimental aspects and the different physical processes that determine the shape of the CMB angular power spectra. Chapter 2 focuses on explaining the different software used (`CLASS` [1], `healpy` [2], `Cobaya`[3] and `GetDist`[4]) to perform the simulations of the CMB angular power spectra and the bayesian analysis techniques used to recover the values of the ΛCDM and phenomenological parameters. The most important part of our work are presented in Chapter 3, where the results of the different MCMC runs for different combinations of cosmological and phenomenological parameters are shown and analysed. In Chapter 4, the conclusions of this project and future work are described. Finally, three appendices are included and, in particular, Appendix C contains a significant part of the code modified and created for this project.

[1] `http://www.class-code.net/`
[2] `https://healpy.readthedocs.io/en/latest/`
[3] `https://cobaya.readthedocs.io/en/latest/`
[4] `https://getdist.readthedocs.io/en/latest/`

# Chapter 1

# Introduction

The Universe in its origin was very hot, dense and opaque as the electrons were free and scattered very well photons due to Thomson scattering. In this early phase, radiation and matter were in thermal equilibrium. As the Universe was expanding, it cooled down progressively and when it reached a temperature of around 3.000 K the Universe became transparent. Radiation decouples with matter and photons escaped.

This radiation emitted when the Universe was 375.000 years old, 13.8 billion years ago, is observed nowadays in the microwave range as an almost perfect black-body spectrum with a characteristic temperature of $T_0 = 2.72548 \pm 0.00057$ K [1] and, for that reason, is named the Cosmic Microwave Background (CMB). Although the CMB is extremely homogeneous, small temperature anisotropies has been observed at the $10^{-5}$ K level, which contains valuable information about the primordial density perturbations and the characteristics of our Universe. The existence of temperature fluctuations imply that CMB radiation must be polarized as a consequence of the directional dependence of the Thomson scattering, which was confirmed this century. The CMB is a cornerstone of the hot Big Bang model and provides precise measurements of the properties of the Universe. In particular, it can be used to constrain the cosmological parameters that appear in the standard cosmological model, named $\Lambda$CDM, which describes a flat Universe containing three major components: Baryonic or ordinary Matter, Cold Dark Matter (weakly interacting non-relativistic matter detected only by its gravitational effects) and Dark Energy (consistent with a cosmological constant $\Lambda$, causing the current accelerated expansion of the Universe).

The CMB radiation was discovered by Penzias and Wilson in 1965, however it is not until COBE when the temperature fluctuations were detected in 1992. Afterwards, other experiments such as WMAP (2001) and more recently Planck, whose final data release is from 2018, has improved the measurement precision of temperature and polarization fluctuations generated on the last scattering surface [2].

## 1.1 The CMB temperature power spectrum

The CMB temperature anisotropy field is defined as the relative temperature fluctuations $\Delta T$ from its average blackbody temperature $T = T_0$, $\frac{\Delta T}{T}(\mathbf{x}, t, \hat{\mathbf{q}})$, and is a function of

position $\mathbf{x}$, time $t$ and photon direction $\hat{\mathbf{q}}$. All current CMB experiments are located on Earth (or near it) so both position and time could be considered as constants and these arguments might be suppressed. For that reason, $\frac{\Delta T}{T}(\hat{\mathbf{q}})$ is a function on the unit sphere, $\hat{\mathbf{q}} = (\theta, \phi) \in \mathbb{S}^2$, as it only depends on the photon direction and the temperature fluctuations can be expanded on the basis of spherical harmonics, $Y_{\ell m}$, as shown in equation (1.1).

$$\frac{\Delta T}{T}(\hat{\mathbf{q}}) = \sum_{\ell=2}^{+\infty} \sum_{m=-\ell}^{\ell} a_{\ell m}^T Y_{\ell m}(\hat{\mathbf{q}}), \tag{1.1}$$

where $a_{\ell m}^T$ are the spherical harmonic coefficients of the temperature anisotropy field

$$a_{\ell m}^T = \int_{\mathbb{S}^2} d\Omega_{\hat{\mathbf{q}}} \frac{\Delta T}{T}(\hat{\mathbf{q}}) Y_{\ell m}^*(\hat{\mathbf{q}}), \tag{1.2}$$

and $d\Omega_{\hat{\mathbf{q}}} = \sin\theta d\theta d\phi$ is a differential solid angle. The equation (1.2) has been obtain using the orthonormal property of spherical harmonics

$$\int_{\mathbb{S}^2} d\Omega_{\hat{\mathbf{q}}} Y_{\ell' m'}^*(\hat{\mathbf{q}}) Y_{\ell m}(\hat{\mathbf{q}}) = \delta_{\ell\ell'}\delta_{mm'} \tag{1.3}$$

in equation (1.1).

The temperature fluctuations are assumed to be a random statistically homogeneous and isotropic field. This means that the expectation values over an ensemble of Universes is independent of position and the distribution of $\frac{\Delta T}{T}(\hat{\mathbf{q}})$ is the same for all directions $\hat{\mathbf{q}}$. It is connected with the fact that the process generating the initial perturbations has a quantum origin as predicted by inflation. Consequently, the $a_{\ell m}^T$ coefficients has mean zero and non zero variance and are normally distributed. The variance of the $a_{\ell m}^T$'s is called $C_\ell^{TT}$, more commonly known in the scientific literature as the CMB temperature power spectrum.

$$\langle a_{\ell m}^T \rangle = 0 \qquad \langle a_{\ell m}^T a_{\ell' m'}^{T*} \rangle = \delta_{\ell\ell'}\delta_{mm'} C_\ell^{TT} \tag{1.4}$$

Because of statistical isotropy the random variables $a_{\ell m}^T$ for different values of $\ell$'s and $m$'s are not correlated, hence their covariance is zero. The reason for this is that the $\ell$ coefficient is related with the angular scale of the temperature fluctuations, $\alpha \approx \frac{\pi}{\ell}$, and different values of $m$ are related with different orientations. From equation (1.4) an estimator of the temperature power spectrum, $\hat{C}_\ell^{TT}$, can be derived:

$$\hat{C}_\ell^{TT} = \frac{1}{2\ell+1} \sum_{m=-\ell}^{\ell} |a_{\ell m}^T|^2. \tag{1.5}$$

The reader can easily realize that for a given $\ell$, each $a_{\ell m}^T$ has the same variance. In a certain Universe realisation, for each value of $\ell$ there are $2\ell+1$ possible values of $m$ which are sampled from the distribution. When the $\ell$ value is high the number of $a_{\ell m}^T$ coefficients used to calculate the variance is also high and it will give a good approximation of the underlying angular power spectrum of the distribution. However, when the $\ell$ value is low, for example in the case of the quadrupole ($\ell = 2$), only five coefficients contributes to calculate $C_2^{TT}$, which will not give much information as statistical fluctuations dominate.

Thus, there is an intrinsic uncertainty to determine the $C_\ell^{TT}$'s which is called cosmic variance.

Assuming that the initial quantum fluctuations are Gaussian, an estimation of the cosmic variance shows that the uncertainty scales as the square root of the number of possible samples:

$$(\Delta C_\ell^{TT})^2 = \frac{2(C_\ell^{TT})^2}{(2\ell+1)f_{sky}}, \tag{1.6}$$

where $f_{sky}$ is the fraction of sky observed by the experiment.

This means that larger scales (smaller values of $\ell$) are more affected by cosmic variance than smaller scales (larger values of $\ell$) and all experiments that exists nowadays have to deal with it inevitably [3].

In real space, the CMB power spectrum is related with the expectation value of the correlation function of the temperature fluctuation between two points in the sky, named the 2-point correlation function,

$$C(\hat{\mathbf{q}}, \hat{\mathbf{q}}') = \left\langle \frac{\Delta T}{T}(\hat{\mathbf{q}}) \frac{\Delta T}{T}(\hat{\mathbf{q}}') \right\rangle = \frac{1}{4\pi} \sum_{\ell=0}^{+\infty} (2\ell+1) C_\ell^{TT} P_\ell(\hat{\mathbf{q}} \cdot \hat{\mathbf{q}}'), \tag{1.7}$$

where $P_\ell$'s are the Legendre polynomials.

In the 2-point correlation function, the expectation value that appears is understood as an averaging over directions $\hat{\mathbf{q}}$ and $\hat{\mathbf{q}}'$ with a fixed opening angle $\cos\beta = \hat{\mathbf{q}} \cdot \hat{\mathbf{q}}'$. Under the assumption of statistical isotropy, theoretical ensemble average and the previous one are equal.

Under the hypothesis of Gaussian temperature fluctuations, which is the situation in simple inflationary models, all higher point correlation functions are related to $C(\hat{\mathbf{q}}, \hat{\mathbf{q}}')$. Consequently, in this situation the $C_\ell^{TT}$'s would contain all the statistical information to characterize the temperature fluctuations field [4] [5] [6].

## 1.2 The CMB polarization power spectra

Another key CMB observable is polarization. This observed polarization is caused by Thomson scattering during recombination, since at early times Thomson scattering is too efficient for the generation of polarization, while after recombination scatterings are very rare [7].

Consider scattering of an unpolarized electromagnetic wave travelling in the $x$-direction which has equal intensities in the $y$ and $z$ directions. Assuming it scatters off an electron at the origin and gets deflected in the $z$ direction, only the intensity component perpendicular to the $z$ direction, i.e., the $y$ component, will be transmitted. The net result is outgoing polarization in the $y$ direction as it is shown in Figure 1.1(a).

Now suppose two unpolarized electromagnetic waves coming to an electron (located at the origin) from the $x$ and $y$ direction. Assuming that they are scattered by the electron both in the $z$ direction, the intensity of the outgoing ray along the $x$ axis comes from the radiation incident from the $y$ direction, while the outgoing $y$ intensity comes from the

radiation incident from the $x$ axis. If the intensity of both electromagnetic waves were the same, the outgoing wave would be unpolarized as it is shown in Figure 1.1(b). However, if the intensity of the electromagnetic waves are different, a situation which arises when the radiation comes from a hot spot (higher intensity) and from a cold spot (lower intensity), then we would get polarized light, as it can be seen in Figure 1.1(c). In summary, it is mandatory to have a quadrupole anisotropy ($\ell = 2$) to get polarized light because neither a monopole ($\ell = 0$) nor a dipole ($\ell = 1$) would give a polarized output [3].

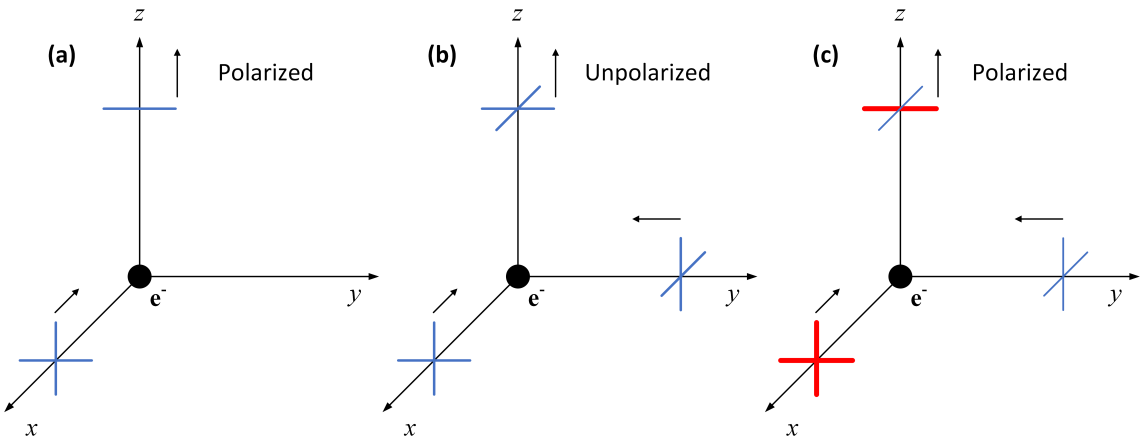


Figure 1.1: ***(a)*** *Unpolarized radiation moving toward the origin along the $x$-axis is scattered by an electron into the $z$ direction. Only the $y$ component of the radiation remains after scattering. As a result, the outgoing radiation is polarized in the $y$ direction.* ***(b)*** *Incoming isotropic radiation produces no polarization. Here, since the incoming amplitudes from the $x$ and $y$ directions are equal, the outgoing intensities along both of these directions are equal, leading to unpolarized radiation.* ***(c)*** *Incoming quadrupole radiation produces outgoing polarized light. The outgoing radiation has greater intensity along the $y-$axis than in the $x$ direction. This is a direct result of the hotter radiation incident from the $x$ direction. Images and description adapted from [3].*

Polarized light is conventionally described in terms of the Stokes parameters. Consider a monochromatic plane electromagnetic wave propagating in the $z-$direction with frequency $\omega$. The components of the wave's electric field vector at a given point in space can be written as

$$E_x = a_x \cos(\omega t - \xi_x), \quad E_y = a_y \cos(\omega t - \xi_y), \tag{1.8}$$

where $a_x$ and $a_y$ are the amplitudes and $\xi_x$ and $\xi_y$ are the phases. If some correlation exists between the two components in equation (1.8), then the wave is polarized.

The Stokes parameters are the intensity, $I$, the linear polarization parameters, $Q$ and $U$, and circular polarization parameter, $V$, as shown in the following equations:

$$I = a_x^2 + a_y^2, \tag{1.9}$$

$$Q = a_x^2 - a_y^2, \tag{1.10}$$

$$U = 2a_x a_y \cos(\xi_x - \xi_y), \tag{1.11}$$

$$V = 2a_x a_y \sin(\xi_x - \xi_y). \tag{1.12}$$

The parameter $I$ gives the intensity of the radiation, which is always positive, and is related to the temperature anisotropy field explained in Section 1.1. The other three parameters define the polarization state of the wave and can have either sign. The parameter $Q$ quantifies the polarization in the $x-y$ directions while $U$ quantifies it along axes rotated by 45°. As the Thomson scattering induces no circular polarization, the circular polarization parameter $V$ vanishes in CMB observations. Consequently, $I$, $Q$ and $U$ Stokes parameters are the only ones necessary to characterize linearly polarized light [8].

While the parameters $I$ and $V$ are physical observables independent of the coordinate system, the parameters $Q$ and $U$ depend on the orientation of the $x$ and $y$ axes [9]. If a given wave is described by the parameters $Q$ and $U$ for a certain orientation of the coordinate system, then after a rotation of the $x-y$ plane through an angle $\phi$, the same wave is now described by the parameters

$$Q' = Q\cos(2\phi) + U\sin(2\phi), \quad U' = -Q\sin(2\phi) + U\cos(2\phi), \tag{1.13}$$

or more simply

$$Q' \pm iU' = e^{\mp 2i\phi}(Q \pm iU). \tag{1.14}$$

Hence $Q \pm iU$ transforms like spin-2 variables with a magnetic quantum number $\pm 2$ under rotations around the direction $\hat{\mathbf{q}}$. A scalar field on the sphere, like the CMB temperature on the sky, can be expanded in spherical harmonics, $Y_{\ell m}$. These functions are not appropriate to expand spin weighted functions with $s = 2$ like $Q \pm iU$. There exist analog sets of functions that can be used to expand spin-2 functions, the so called spin-2 spherical harmonics ${}_{\pm 2}Y_{\ell m}$ which verifies the same orthogonal property of spherical harmonics explained in the previous section.

We may therefore expand $Q \pm iU$ in the appropriate spin-weighted basis:

$$(Q \pm iU)(\hat{\mathbf{q}}) = \sum_{\ell=2}^{+\infty} \sum_{m=-\ell}^{\ell} a_{\ell m}^{(\pm 2)}\ {}_{\pm 2}Y_{\ell m}(\hat{\mathbf{q}}). \tag{1.15}$$

To perform this expansion, $Q$ and $U$ in equation (1.15) are measured relative to $(\hat{\mathbf{q}}_1, \hat{\mathbf{q}}_2) = (\hat{\mathbf{q}}_\theta, \hat{\mathbf{q}}_\phi)$, the unit vectors of the spherical coordinate system.

To obtain spin zero quantities like temperature it can be used the raising, $\eth$, and lowering, $\eth^*$, operators:

$$\eth^2({}_{-2}Y_{\ell m}) = (\eth^*)^2({}_{+2}Y_{\ell m}) = \sqrt{\frac{(\ell+2)!}{(\ell-2)!}}Y_{\ell m}, \tag{1.16}$$

These have the advantages of being rotationally invariant and no ambiguities connect with the rotation of coordinate system arise. Acting twice with $\eth$ and $\eth^*$ on $Q \pm iU$ in equation 1.15 leads to

$$(\eth^*)^2(Q+iU)(\hat{\mathbf{q}}) = \sum_{\ell=2}^{+\infty} \sum_{m=-\ell}^{\ell} a_{\ell m}^{(+2)} \sqrt{\frac{(\ell+2)!}{(\ell-2)!}} Y_{\ell m}(\hat{\mathbf{q}}), \tag{1.17}$$

$$\eth^2(Q-iU)(\hat{\mathbf{q}}) = \sum_{\ell=2}^{+\infty} \sum_{m=-\ell}^{\ell} a_{\ell m}^{(-2)} \sqrt{\frac{(\ell+2)!}{(\ell-2)!}} Y_{\ell m}(\hat{\mathbf{q}}). \tag{1.18}$$

The expressions for the spin-2 spherical harmonics coefficients are

$$a_{\ell m}^{(+2)} = \int_{\mathbb{S}^2} d\Omega_{\hat{\mathbf{q}}} (Q + iU)(\hat{\mathbf{q}})_{+2}Y^*_{\ell m}(\hat{\mathbf{q}}) = \sqrt{\frac{(\ell-2)!}{(\ell+2)!}} \int_{\mathbb{S}^2} d\Omega_{\hat{\mathbf{q}}} (\eth^*)^2 (Q + iU)(\hat{\mathbf{q}}) Y^*_{\ell m}(\hat{\mathbf{q}}), \tag{1.19}$$

$$a_{\ell m}^{(-2)} = \int_{\mathbb{S}^2} d\Omega_{\hat{\mathbf{q}}} (Q - iU)(\hat{\mathbf{q}})_{-2}Y^*_{\ell m}(\hat{\mathbf{q}}) = \sqrt{\frac{(\ell-2)!}{(\ell+2)!}} \int_{\mathbb{S}^2} d\Omega_{\hat{\mathbf{q}}} \eth^2 (Q - iU)(\hat{\mathbf{q}}) Y^*_{\ell m}(\hat{\mathbf{q}}). \tag{1.20}$$

Instead of $a_{\ell m}^{(+2)}$ and $a_{\ell m}^{(-2)}$, it is convenient to introduce their linear combinations:

$$a^E_{\ell m} = -\frac{1}{2}\left(a_{\ell m}^{(+2)} + a_{\ell m}^{(-2)}\right), \quad a^B_{\ell m} = \frac{i}{2}\left(a_{\ell m}^{(+2)} - a_{\ell m}^{(-2)}\right). \tag{1.21}$$

With this, we can define the scalar quantities, $E$ and $B$, which like temperature fluctuations are rotationally invariant:

$$E(\hat{\mathbf{q}}) \equiv -\frac{1}{2}\left[(\eth^*)^2(Q + iU) + \eth^2(Q - iU)\right] = \sum_{\ell=2}^{+\infty} \sum_{m=-\ell}^{\ell} \sqrt{\frac{(\ell+2)!}{(\ell-2)!}} a^E_{\ell m} Y_{\ell m}(\hat{\mathbf{q}}), \tag{1.22}$$

$$B(\hat{\mathbf{q}}) \equiv \frac{i}{2}\left[(\eth^*)^2(Q + iU) - \eth^2(Q - iU)\right] = \sum_{\ell=2}^{+\infty} \sum_{m=-\ell}^{\ell} \sqrt{\frac{(\ell+2)!}{(\ell-2)!}} a^B_{\ell m} Y_{\ell m}(\hat{\mathbf{q}}). \tag{1.23}$$

This scalar quantities are named in analogy with electric and magnetic field and a graphical example of $E-$mode and $B-$mode patterns are drawn in Figure 1.2.

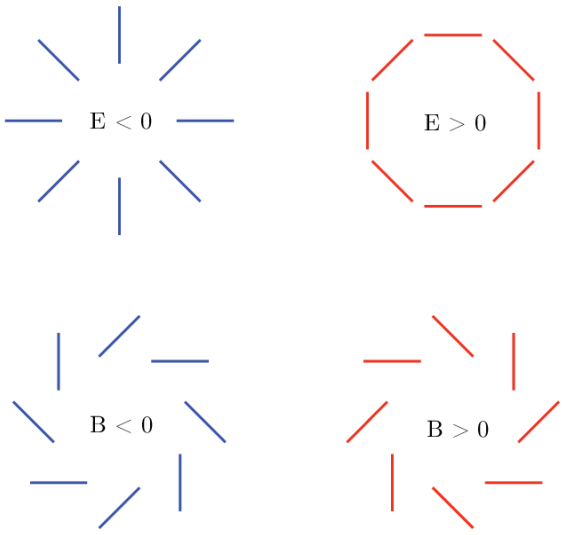


Figure 1.2: *Examples of $E-$mode and $B-$mode patterns of polarization. Source: [10].*

To characterize the statistics of the CMB perturbations only four spectra are needed, those for $T$, $E$, $B$ and the cross correlation beetween $T$ and $E$. The cross correlation

between $B$ and $E$ or $B$ and $T$ vanished because $B$ has the opposite parity of $T$ and $E$. As the temperature power spectrum was explained in the previous section, now we will focus on the other spectra:

$$\langle a^X_{\ell m} a^{X*}_{\ell' m'} \rangle = \delta_{\ell\ell'}\delta_{mm'} C^{XX}_\ell,\ X = \{E,\ B\}; \quad \langle a^T_{\ell m} a^{E*}_{\ell' m'} \rangle = \delta_{\ell\ell'}\delta_{mm'} C^{TE}_\ell, \tag{1.24}$$

where $C^{EE}_\ell$ and $C^{BB}_\ell$ are respectively the $E$ and $B$ polarization power spectra and $C^{TE}_\ell$ is the cross correlation power spectrum.

The polarization magnitudes observed from CMB experiments are actually the $Q$ and $U$ Stokes parameters, so it is very useful to rewrite equation (1.15) as:

$$Q(\hat{\mathbf{q}}) = -\sum_{\ell=2}^{+\infty} \sum_{m=-\ell}^{\ell} a^E_{\ell m} X_{1,\ell m}(\hat{\mathbf{q}}) + i a^B_{\ell m} X_{2,\ell m}(\hat{\mathbf{q}}) \tag{1.25}$$

$$U(\hat{\mathbf{q}}) = -\sum_{\ell=2}^{+\infty} \sum_{m=-\ell}^{\ell} a^B_{\ell m} X_{1,\ell m}(\hat{\mathbf{q}}) - i a^E_{\ell m} X_{2,\ell m}(\hat{\mathbf{q}}) \tag{1.26}$$

where we have introduced $X_{1,\ell m}(\hat{\mathbf{q}}) = \{{}_{+2}Y_{\ell m}(\hat{\mathbf{q}}) + {}_{-2}Y_{\ell m}(\hat{\mathbf{q}})\}/2$ and $X_{1,\ell m}(\hat{\mathbf{q}}) = \{{}_{+2}Y_{\ell m}(\hat{\mathbf{q}}) - {}_{-2}Y_{\ell m}(\hat{\mathbf{q}})\}/2$ [11].

From full-sky CMB maps and using equation (1.24), we can construct the following rotationally-invariant estimators for the polarization and cross correlation power spectra:

$$\hat{C}^{XX}_\ell = \frac{1}{2\ell+1} \sum_{m=-\ell}^{\ell} |a^X_{\ell m}|^2,\ X = \{E, B\}; \quad \hat{C}^{TE}_\ell = \frac{1}{2\ell+1} \sum_{m=-\ell}^{\ell} a^{T*}_{\ell m} a^E_{\ell m}. \tag{1.27}$$

Analogously to the temperature spectrum explained in Section 1.1, the polarization and cross correlation spectra suffer from cosmic variance as shown in equation (1.28) under gaussian hypothesis [4] [12].

$$\begin{aligned} (\Delta C^{XX}_\ell)^2 &= \frac{2(C^{XX}_\ell)^2}{(2\ell+1) f_{sky}},\ X = \{E, B\}, \\ (\Delta C^{TE}_\ell)^2 &= \frac{1}{(2\ell+1) f_{sky}} \left[ (C^{TE}_\ell)^2 + C^{TT}_\ell C^{EE}_\ell \right]. \end{aligned} \tag{1.28}$$

## 1.3 Observing the CMB: temperature and polarization

In section 1.1 the cosmic variance was presented, an intrinsic uncertainty connected with the fact that only one realization of the Universe is available. When an experiment observes the CMB temperature and polarization field, other sources of errors must also be taken into consideration like foregrounds, instrumental noise, atmospheric effects, etc.

In this project, a simplified experimental situation is assumed. We begin with a temperature and polarization maps without foreground contaminants and the only instrumental effects affecting our data are the finite resolution of an instrumental beam and the instrumental random noise. We will explain in detail only the temperature fluctuation field and describe what happen to the polarization and cross correlation spectra. First, we will only

consider the effect of the instrumental beam. The CMB temperature anisotropy signal $\widetilde{\frac{\Delta T}{T}}(\hat{\mathbf{q}})$ can be expresed as the convolution of the true sky $\frac{\Delta T}{T}(\hat{\mathbf{q}})$ with the instrumental beam function $B(\hat{\mathbf{q}}, \hat{\mathbf{q}}')$ as shown in equation (1.29):

$$\widetilde{\frac{\Delta T}{T}}(\hat{\mathbf{q}}) = \int_{\mathbb{S}^2} d\Omega_{\hat{\mathbf{q}}'} \frac{\Delta T}{T}(\hat{\mathbf{q}}') B(\hat{\mathbf{q}}, \hat{\mathbf{q}}'). \tag{1.29}$$

At this point, we can relate the 2-point correlation function of the CMB anisotropy signal between two directions $\hat{\mathbf{q}}$ and $\hat{\mathbf{q}}'$ to to the power spectrum by

$$\widetilde{C}(\hat{\mathbf{q}}, \hat{\mathbf{q}}') = \left\langle \widetilde{\frac{\Delta T}{T}}(\hat{\mathbf{q}}) \widetilde{\frac{\Delta T}{T}}(\hat{\mathbf{q}}') \right\rangle = \frac{1}{4\pi} \sum_{\ell=0}^{+\infty} (2\ell+1) C_\ell W_\ell(\hat{\mathbf{q}}, \hat{\mathbf{q}}'), \tag{1.30}$$

where $W_\ell(\hat{\mathbf{q}}, \hat{\mathbf{q}}')$ is the window function whose equation is

$$W_\ell(\hat{\mathbf{q}}, \hat{\mathbf{q}}') = \int_{\mathbb{S}^2} d\Omega_{\hat{\mathbf{q}}_1} \int_{\mathbb{S}^2} d\Omega_{\hat{\mathbf{q}}_2} B(\hat{\mathbf{q}}, \hat{\mathbf{q}}_1) B(\hat{\mathbf{q}}', \hat{\mathbf{q}}_2) P_\ell(\hat{\mathbf{q}}_1 \cdot \hat{\mathbf{q}}_2). \tag{1.31}$$

Considering a spherically symmetric Gaussian beam, the window function is simplified to

$$W_\ell(\hat{\mathbf{q}}, \hat{\mathbf{q}}') = B^2_{\ell,TT} P_\ell(\hat{\mathbf{q}} \cdot \hat{\mathbf{q}}'), \tag{1.32}$$

where $B_{\ell,TT} = \exp(-\frac{1}{2}\ell(\ell+1)\sigma_B^2)$ is the beam function in $\ell$ space [4] [13].

Substituting equation (1.32) in equation (1.30) and comparing with equation (1.7) it is evident that

$$C_\ell^{\text{signal}} = B^2_{\ell,TT} C_\ell^{\text{sky}}. \tag{1.33}$$

When dealing with polarization and cross correlation spectra, the beam function changes to $B_{\ell,EE} = B_{\ell,BB} = B_{\ell,TT} \exp(2\sigma_B^2)$ and $B_{\ell,TE} = B_{\ell,TT} \exp(\sigma_B^2)$ respectively. The difference is subtle, affecting only low $\ell$ values [14].

Furthermore, all the theoretical explanations developed in this section uses continuous temperature anisotropy and polarizations maps. However, due to the finite resolution of the experiments actually we have discrete maps. This fact has several consequences, for instance, you are experimentally limited to observe up to a maximum $\ell$ value or the existence of a pixel window function for temperature, $p_{\ell,T}$, and polarization, $p_{\ell,P}$, which takes into account the pixelation effect produced when a function is discretised and transform equation (1.33) into

$$C_\ell^{\text{signal},X} = B^2_{\ell,X} p^2_{\ell,Y} C_\ell^{\text{sky},X}, \tag{1.34}$$

where $X = TT$ and $Y = T$, or $Y = P$ and $X = \{EE, BB, TE\}$.

Having a temperature anisotropy pixel map implies having to deal with pixels and its positions. Assuming that we have a map with $N_{pix}$ pixels, the coefficients $a_{\ell m}^{\text{map}}$ can be approximated to

$$a_{\ell m}^{\text{map}} = \int_{\mathbb{S}^2} d\Omega_{\hat{\mathbf{q}}} \frac{\Delta T}{T}^{\text{map}}(\hat{\mathbf{q}}) Y^*_{\ell m}(\hat{\mathbf{q}}) \approx \sum_{j=1}^{N_{pix}} \frac{4\pi}{N_{pix}} \frac{\Delta T_j}{T}^{\text{map}} Y^*_{\ell m}(\hat{\mathbf{q}}_j) \tag{1.35}$$

where $\hat{\mathbf{q}}_j$ are the coordinates of the pixel $j$. An analogous expression can be obtained for the equations (1.19) and (1.20) corresponding to polarization.

Now, the observed temperature anisotropy in each pixel $j$ can be decompose into two contributions: signal and noise. In this way,

$$\frac{\Delta T_j}{T}^{\text{map}} = \frac{\Delta T_j}{T}^{\text{signal}} + \frac{\Delta T_j}{T}^{\text{noise}}. \tag{1.36}$$

If we assume that each pixel has the same rms noise, $\sigma_{pix,T}$, and that the noise is uncorrelated with that in any other pixel and with the cosmological signal, i.e.

$$\left\langle \frac{\Delta T_i}{T}^{\text{noise}} \frac{\Delta T_j}{T}^{\text{noise}} \right\rangle = T_0^2 \sigma_{pix,T}^2 \delta_{ij} \quad \text{and} \quad \left\langle \frac{\Delta T_i}{T}^{\text{signal}} \frac{\Delta T_j}{T}^{\text{noise}} \right\rangle = 0,$$

then after some calculus, that the reader could find in detail in [15], the temperature power spectrum of the map can be related to the power spectrum of the signal and the noise. A generalised result for both temperature and polarization is shown in the following equation:

$$C_\ell^{\text{map}} = C_\ell^{\text{signal}} + C_\ell^{\text{noise}} = B_{\ell,X}^2 p_{\ell,Y}^2 C_\ell^{\text{sky}} + \frac{4\pi\sigma_{pix,Y}^2}{N_{pix}}. \tag{1.37}$$

If temperature and polarization are obtained from the same experiment by adding and subtracting the intensities between two orthogonal polarizations, $Q$ and $U$, then the rms noise in temperature, $\sigma_{pix,T}$, and polarization, $\sigma_{pix,P}$, are related by $\sigma_{pix,T}^2 = \sigma_{pix,P}^2/2$. We assume this experimental configuration, which is approximately correct for Planck mission.

At this point, it is interesting to deconvolve the effects of the beam and the pixel to obtain an estimate of $C_\ell^{\text{map}}$ as close as possible to $C_\ell^{\text{sky}}$:

$$C_\ell^{\text{map'}} = \frac{C_\ell^{\text{map}}}{B_{\ell,X}^2 p_{\ell,Y}^2} = C_\ell^{\text{sky}} + \frac{4\pi\sigma_{pix,Y}^2}{B_{\ell,X}^2 p_{\ell,Y}^2 N_{pix}}. \tag{1.38}$$

After doing this, the constant noise power spectrum that we have in equation (1.37) exploits at high $\ell$ after deconvolution due to the dominant contribution of $B_{\ell,X}$ and $p_{\ell,Y}$.

To compare maps (produced by different experiment) with different instrumental noise per pixel, $\sigma_{pix,Y}$, and different pixel angular size, $\Omega_{pix}$, is very useful to introduce the magnitude called weight per solid angle

$$w_Y = (\sigma_{pix,Y}^2 \Omega_{pix})^{-1} = \left( \frac{4\pi\sigma_{pix,Y}^2}{N_{pix}} \right)^{-1}, \; Y = \{T, P\}. \tag{1.39}$$

Even if we are able to deconvolve the beam and the pixel window function with extremely high precision, it will introduce an additional term in the uncertainty of $C_\ell$'s:

$$(\Delta C_\ell^{\text{map'},XX})^2 = \frac{2}{(2\ell+1) f_{sky}} \left( C_\ell^{XX} + \frac{1}{w_Y B_{\ell,XX}^2 p_{\ell,Y}^2} \right)^2, \tag{1.40}$$

$$(\Delta C_\ell^{\text{map'},TE})^2 = \frac{\left[(C_\ell^{EE})^2 + \left(C_\ell^{TT} + \frac{1}{w_T B_{\ell,TT}^2 p_{\ell,T}^2}\right)\left(C_\ell^{EE} + \frac{1}{w_P B_{\ell,EE}^2 p_{\ell,P}^2}\right)\right]}{(2\ell+1) f_{sky}}, \tag{1.41}$$

where $X = Y = T$ or $Y = P$ and $X = \{E, B\}$, and $f_{sky}$ is the fraction of sky observed by the experiment.

This means that there exist uncertainty at low $\ell$ due to having a single Universe realization and also at large $\ell$ due to noise [16] [17].

For graphical purposes, in this project we are going to plot $D_\ell$, instead of $C_\ell$ which are easily related by:

$$D_\ell \equiv \frac{\ell(\ell+1)}{2\pi} C_\ell. \tag{1.42}$$

## 1.4 CMB anisotropies theory: temperature and polarization

In the previous sections we have studied the power spectrum, $C_\ell$, a key magnitude in CMB science, and how is related to observational data taken from experiments. In this section, we will focus on how is calculated the CMB power spectra for temperature and polarization.

The CMB anisotropies observed in the CMB experiments are $O(10^{-5})$, which lead to the development of the linear cosmological perturbation theory. In this project, the main objective is to study scalar perturbations, which represent the response of the metric to an irrotational distribution of matter and generalize Newton's theory of gravitation.

In this section, the Newtonian gauge will be used for pedagogical purposes. A gauge is a way to slice the space-time in equal-time hypersurfaces. In an idealised FLRW (Friedmann-Lemaitre-Robertson-Walker) Universe, there is only one time slicing compatible with the assumption of homogeneity and isotropy. Conversely, in a perturbed Universe, there is an infinity. To correct this issue one possibility is to fix the gauge, i.e. imposing a restriction such that time slicing is fixed. For scalars using the Newtonian gauge (units such $c = 1$ and conformal time, $\eta$) the line element, $ds$, is defined by:

$$ds^2 = a^2(\eta)[-(1 + 2\Psi(\mathbf{x}, \eta))d\eta^2 + (1 - 2\Phi(\mathbf{x}, \eta))d\mathbf{x}^2], \tag{1.43}$$

where $a(\eta)$ is the scale factor and the linear perturbations $\Psi$ and $\Phi$ are the Newtonian potential and spatial perturbation to the metric, respectively. The conformal time is a measure of time based on the comoving distance travelled by a photon and is related to proper time by $dt = a(\eta)d\eta$ [18].

Within the framework of the minimal $\Lambda$CDM model, zero spatial curvature ($K = 0$) is assumed. In this situation, to calculate the scalar power spectra in $\ell$ space, we need to solve the following integral

$$C_\ell^{XY} = 4\pi \int \frac{dk}{k} \Delta_\ell^X(k, \eta_0)\Delta_\ell^Y(k, \eta_0)\mathcal{P}_\mathcal{R}(k), \tag{1.44}$$

where $X, Y \in \{T, E, B\}$, $\Delta_\ell^Y(k, \eta_0)$ is a photon transfer function, $\mathcal{P}_\mathcal{R}(k)$ is the curvature power spectrum, $k$ is the wavenumber and $\eta_0$ is the conformal time today.

The single-field inflation theory predicts a nearly scale-invariant curvature power spectrum, $\mathcal{P}_{\mathcal{R}}(k)$. To account deviations from a scale-invariant power spectrum, it is customary to introduce a power-law primordial spectrum

$$\mathcal{P}_{\mathcal{R}}(k) = A_s k^{n_s - 1}, \tag{1.45}$$

where $A_s$ is the scalar spectrum amplitude and $n_s$ is called the scalar tilt.

Other important components of equation (1.44) are the photon transfer functions. These functions can be obtained by a time integral of a set of source functions multiplied by certain radial functions. To calculate the source functions we will use the total angular momentum method. This technique introduced in [19] simplifies the radiation transport problem under gravity and scattering processes, dealt by Boltzmann equation, for temperature and polarization anisotropies in the CMB. The total angular momentum method leads to a unified set of simple integrals accounting for temperature $T$ and $E$ and $B$ polarization modes which allow to split the source functions in a set of physical contributions. This is the key aspect of this project: multiplying phenomenological amplitudes to each physical contribution permit to weight them. The resulting photon transfer functions for scalar modes are:

$$\begin{aligned}
\Delta_\ell^T(k,\eta_0) &= A_{SW}\int_{\eta_{ini}}^{\eta_0} d\eta g(\eta)[\Theta_0(k,\eta)+\Psi(k,\eta)]j_\ell(k(\eta_0-\eta))+ \\
&+ \int_{\eta_{ini}}^{\eta_0} d\eta f(\eta)e^{-\tau}(\Phi'(k,\eta)+\Psi'(k,\eta))j_\ell(k(\eta_0-\eta))+ \\
&+ A_{Dop}\int_{\eta_{ini}}^{\eta_0} d\eta \frac{g(\eta)\theta_b}{k} j'_\ell(k(\eta_0-\eta))+ \\
&+ A_{Pol}\int_{\eta_{ini}}^{\eta_0} d\eta \frac{g(\eta)}{2} P^{(0)}[3j''_\ell(k(\eta_0-\eta))+j_\ell(k(\eta_0-\eta))] \\
\Delta_\ell^E(k,\eta_0) &= A_{Pol}\int_{\eta_{ini}}^{\eta_0} d\eta \sqrt{\frac{9(\ell+2)!}{4(\ell-2)!}} g(\eta)P^{(0)}\frac{j_\ell(k(\eta_0-\eta))}{(k(\eta_0-\eta))^2} \\
\Delta_\ell^B(k,\eta_0) &= 0
\end{aligned} \tag{1.46}$$

where $P^{(0)}$ is the scalar polarization source function, $j_\ell(k(\eta_0-\eta))$ are the spherical Bessel functions, $\tau$ is the optical depth at a given conformal time, $g(\eta) = -\tau' e^{-\tau}$ is the visibility function, $\Theta_0$ is the temperature monopole, $\theta_b = \nabla\cdot\vec{v}_b$ is the divergence of the bulk velocity of baryons, equal to that of electrons due to tight Coulomb interactions and associated with the existence of a CMB dipole. Finally, the function

$$f(\eta) = \begin{cases} A_{eISW} \text{ for } z \geq 30. \\ A_{lISW} \text{ for } z < 30. \end{cases} \tag{1.47}$$

The reason for choosing redshift $z = 30$ as a turning point between the early and late Integrated Sachs-Wolfe contributions is merely a phenomenological one. As is explained in [20], when plotting the integrand $e^{-\tau}(\Phi' + \Psi')$ as a function of redshift, one can see that its minimum lies near $z = 30$ [21].

The optical depth that appears in equation (1.46), $\tau = \tau(\eta)$, represents the opacity of the Universe at a given time, $\eta$. It is related to the Thomson scattering rate, $\Gamma(\eta)$, by

$$\tau(\eta) = \int_{\eta}^{\eta_0} d\eta \Gamma(\eta). \tag{1.48}$$

It tends to infinity when $\eta \to 0$, falls below one at recombination and stabilize at a value of the order of 0.1 between recombination and reionization, when the first stars began to form. After reionization it decreases smoothly and reaches zero today by definition. From the CMB power spectra, an effective value of $\tau$ can be estimated. The parameter is named optical depth to reonization, $\tau_{reio}$, and measures the opacity of the Universe between $z = 0$ and $z = z_{reio}$.

The visibility function, $g(\eta) = -\tau' e^{-\tau}$, gives the probability that a CMB photon seen today experienced its last scattering at time $\eta$. It starts from negligible values at high redshift (suppressed by the $e^{-\tau}$ factor). It has a narrow spike around the time of recombination, and then it falls again to negligible values due to the smallness of $\tau'$ between recombination and reionization. It develops a second smaller and wider spike around reionization. This function shows that most CMB photons did not interact between the last scattering surface and today, while a minority rescattered at reionization. The width of the recombination spike gives an indication on the thickness of the last scattering surface. Connecting this knowledge with equation (1.46) means that the first, third and fourth terms of the temperature photon transfer function are sourced primarily at the surface of last scattering while the second term is sourced at all points along the way as the visibility function does not appear.

At this point, we have explained all the components that appears in the temperature transfer function of equation (1.46), but we have not yet explained what they are accounting for. The first term, weighted by a phenomenological amplitude $A_{SW}$, comprise the Sachs-Wolfe (SW) effect and includes the intrinsic temperature term $\Theta_0$ modified by the gravitational redshifting or blueshifting of the CMB photons as they leave the last scattering surface due to the effect of potential $\Psi$. The second term accounts for the Integrated Sachs-Wolfe (ISW) effect, parametrized by $A_{eISW}$ for early times and by $A_{lISW}$ for late times, and contains all non-conservative effect occurring in a Universe with non-static metric fluctuations, for instance, if a potential well is getting shallower in time, photons receive a net blueshift in crossing the well and the CMB appears hotter. The third term accounts for the Doppler shifting of CMB photons, modulated by a phenomenological parameter $A_{Dop}$, and produces a gravitational redshifting/blueshifting from scattering off moving matter [7]. Finally, the fourth term is the CMB polarization contribution to the CMB power spectra, modulated by the parameter $A_{Pol}$, and is related to the directional dependence of Thomson Scattering and the existence of a quadrupolar component [22]. The combination of this four contributions gives the CMB temperature power spectrum as it might be seen in Figure 1.3. If $\Lambda$CDM predictions are correct, one would expect to obtain $A_{Pol} = A_{Dop} = A_{eISW} = A_{lISW} = A_{SW} = 1$ and obtaining values that differ from this prediction would indicate inconsistencies with the theory.

If we analyse Figure 1.3, we could establish the regions of the spectrum where each physical contribution dominate. In the low $\ell$ region ($\ell \leq 10$), the main contributions come from the Sachs-Wolfe (SW) effect and from the late Integrated Sachs-Wolfe (lISW) effect. In fact, this zone of the spectrum is called the Sachs-Wolfe plateau. In the intermediate $\ell$ region, comprising $10 < \ell \leq 500$ and including the first peak, the most important contributions come from the Sachs-Wolfe (SW) effect, the Doppler effect and the early Integrated Sachs Wolfe (eISW) effect. Finally, the last region covers the small scales ($\ell \geq 500$) where the main contributions are the Sachs-Wolfe (SW) effect and the Doppler effect. However, the polarization effect, although minor, contributes to the temperature

power spectrum at small scales.

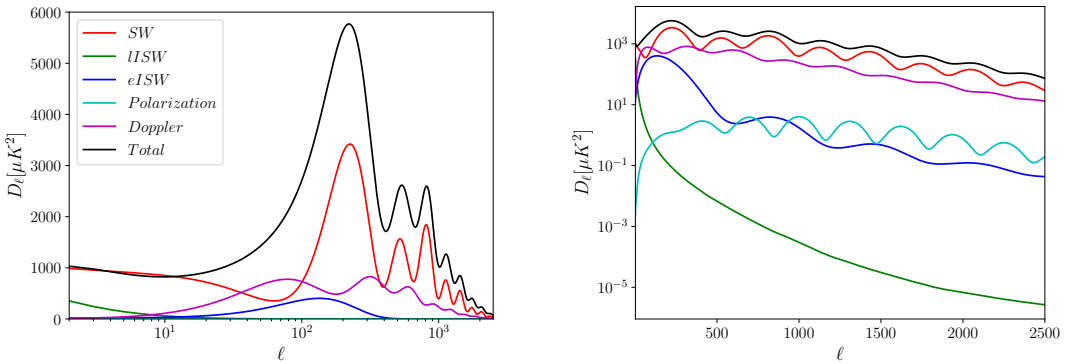


Figure 1.3: *Plots in linear and logarithmic scales of the physical contributions to the CMB temperature power spectrum using the best fit parameters obtained by Planck mission.*

The polarization spectra do not include the physical contributions explained previously because they have a gravitational origin, except for $A_{Pol}$ that rescales the $EE$ and $TE$ power spectra. However, these physical contributions have important effects in the cross correlation power spectrum between temperature and $E$ mode.

For a complete parametrization of physical contributions, one last effect need to be considered: the lensing effect. On their path from the last scattering surface to the CMB experiments, the CMB photons are deflected by the perturbed gravitational field which has an imprint in the temperature and polarization power spectra [4]. In particular, scalar perturbations does not produce $B$ polarization mode, however, when lensing is included a non-zero $B$ mode power spectrum is expected due to the effect of lensing transforming $E$ mode into $B$ mode. This lensing contribution is determined by the lensing power spectrum, $C_\ell^\Psi$, and can be rescaled by a phenomenological parameter $A_L$ as:

$$C_\ell^\Psi \rightarrow A_L C_\ell^\Psi. \tag{1.49}$$

As it has been mentioned before, we are using the minimal ΛCDM model which has six free parameters:

$$\{A_s, n_s, \omega_b, \omega_c, H_0, \tau_{reio}\}, \tag{1.50}$$

where $\tau_{reio}$, $A_s$ and $n_s$ has been explained earlier. The Hubble parameter today, $H_0$, accounts for the expansion rate of the Universe. This magnitude can be expressed in terms of a dimensionless reduced Hubble parameter $h$:

$$H_0 = 100h \text{ (km/s)/Mpc}. \tag{1.51}$$

The last magnitudes to be considered are the physical cold dark matter density, $\omega_c = h^2\Omega_c = h^2(\rho_c/\rho_{crit})$, and the physical baryon density, $\omega_b = h^2\Omega_b = h^2(\rho_b/\rho_{crit})$, which measure the quantity of dark matter and baryonic matter present in our Universe, respectively [23].

# Chapter 2

# Methodology

## 2.1 Cosmic Linear Anisotropy Solving System (CLASS)

The Cosmic Linear Anisotropy Solving System (`CLASS`) [1] [24] is a Boltzmann code that we have modified and used to compute the CMB lensed temperature and polarization scalar power spectra. It is written in C, but it is possible to execute through Python thanks to the existence of a Python wrapper, which allows to import `CLASS` as a package. `CLASS` is a common usage software for cosmologists and it has a fundamental advantage for this project: it is easy to modify. Structured in 11 modules (each one including a .c and .h files as is proper of C programming language), we will list and explain briefly each one in the order they are executed in `CLASS` [25], focusing especially in the ones we have modified (see Appendix C):

1. **Input**. It reads the input parameters, sets all the parameters to their default values and replace some of them with the values read. This part was modified to allow reading the type double input variables associated with the phenomenological amplitudes.

2. **Background**. This module solves the background equations (in particular, the Friedmann equation).

3. **Thermodynamics**. This module solves for the thermodynamical evolution with `RECFAST`.

4. **Perturbations**. It solves the evolution of all perturbations, calculating the source functions. This module contains some variables that allows to consider or not each physical contribution. For this project, these variables were used for a bit different purpose but it was not necessary to modify them. The only part of this module that was modified was to account correctly for the early and late ISW effect.

5. **Bessel**. This module computes the spherical Bessel functions.

6. **Transfer**. This module computes the transfer functions $\Delta_\ell(k)$, by convolving source functions and Bessel functions.

[1] `http://www.class-code.net/`

7. **Primordial**. This module computes the primordial power spectra.

8. **Spectra**. This module computes observable power spectra out of source functions, transfer functions and primordial spectra.

9. **Non linear**. This module gives an estimate of the non-linear version of the previous spectra, according to some scheme chosen by the user. In this project, a linear primordial power spectrum is assumed so this module is not used.

10. **Lensing**. This module computes the lensed temperature and polarization CMB spectra, using the unlensed spectra and the CMB lensing potential spectrum. We have introduced the phenomenological amplitude $A_L$ to weight the lensing effect, as it was not originally included in `CLASS`.

11. **Output**. It writes the output in some files. In the case of executing CLASS from Python no files are generated, instead, you receive the output in a dictionary structure.

In the following Figures we show the effects in the temperature and polarization power spectra of varying each of the phenomenological amplitudes introduced. Except for the lensing and polarization effects, the $E$-mode and $B$-mode polarization power spectra are not shown because no effects were observed. First, in Figure 2.1 the Sachs-Wolfe effect is considered. As it can be observed, changing $A_{SW}$ affects the hole temperature and cross polarization power spectra. In particular, increasing the $A_{SW}$ parameter increases both peaks and troughs in the temperature power spectrum, while for the cross correlation between temperature and $E$ polarization mode the peaks are increased and the troughs are decreased.

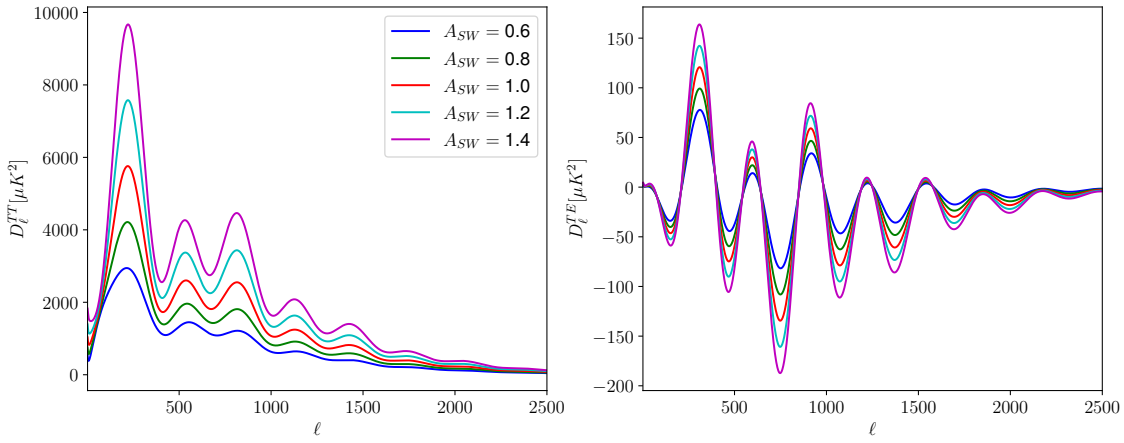


Figure 2.1: *Plots of the impact of varying the $A_{SW}$ parameter in the temperature and cross polarization power spectra. The red line correspond to the power spectra predicted by $\Lambda CDM$ model for the best fit parameters from Planck mission. Both plots have the same legend.*

In Figure 2.2 the effects of varying the $A_{eISW}$ parameter are shown. As it can be inferred from Figure 1.3, the early integrated Sachs-Wolfe effect has its greatest impact in

the first peak both in temperature and cross-spectrum, increasing the height of the first peak when $A_{eISW}$ is increased.

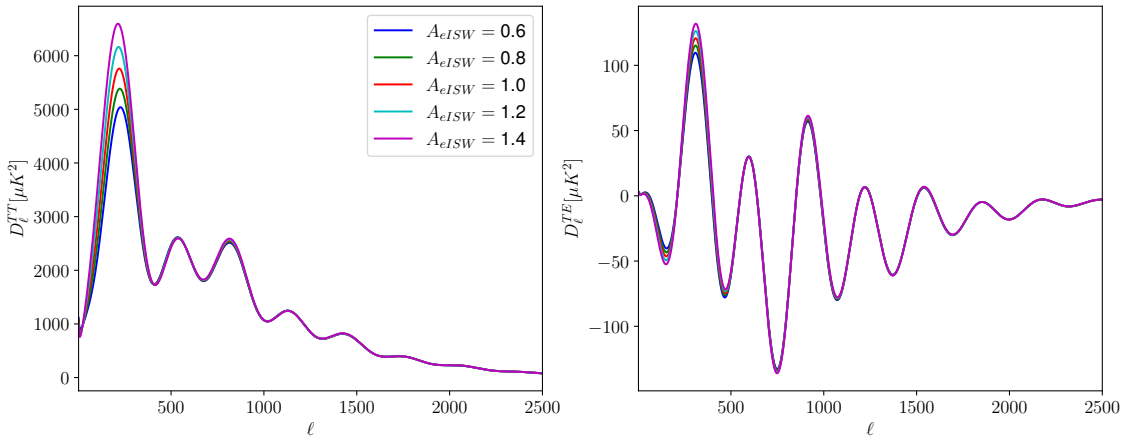


Figure 2.2: *Plots of the impact of varying the $A_{eISW}$ parameter in the temperature and cross polarization power spectra. The red line correspond to the power spectra predicted by $\Lambda CDM$ model for the best fit parameters from Planck mission. Both plots have the same legend.*

In Figure 2.3 the effects of varying the $A_{lISW}$ parameter are shown. As it can be inferred from Figure 1.3, the late integrated Sachs-Wolfe effect has its greatest impact in the large scales ($\ell \leq 30$) both in temperature and cross correlation between temperature and $E$ polarization mode, increasing the height of the temperature power spectrum and decreasing the height of the cross correlation power spectrum at low $\ell$'s when $A_{lISW}$ is increased.

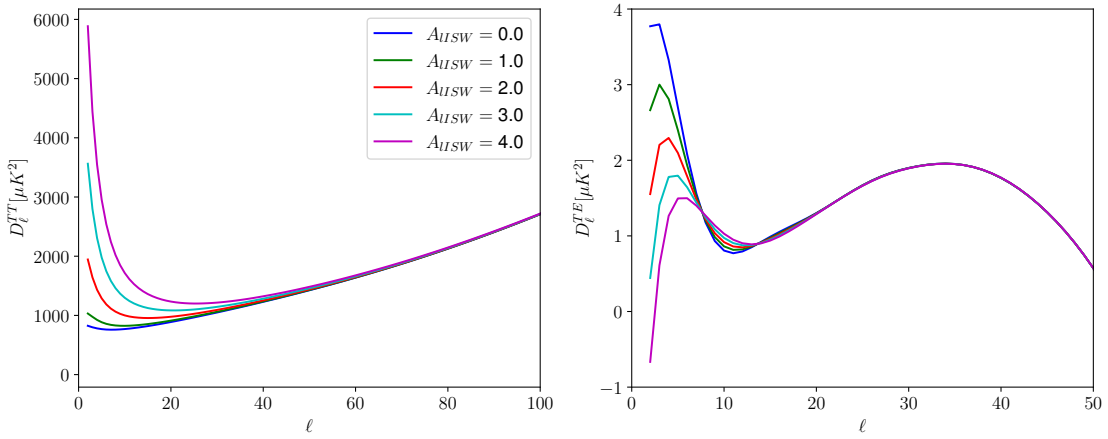


Figure 2.3: *Plots of the impact of varying the $A_{lISW}$ parameter in the temperature and cross polarization power spectra. The green line correspond to the power spectra predicted by $\Lambda CDM$ model for the best fit parameters from Planck mission. Both plots have the same legend.*

In Figure 2.4 the effects of varying the $A_{Pol}$ parameter are shown. The polarization effect produces a phase shift, both in temperature and cross correlation between temperature and $E$ polarization mode, affecting mainly the second and following peaks. Also, this effect lifts the temperature and polarization power spectra when $A_{Pol}$ is increased, specially for the $EE$ and $TE$ power spectrum because $A_{Pol}$ acts as a multiplicative constant to the spectrum in those two situations.

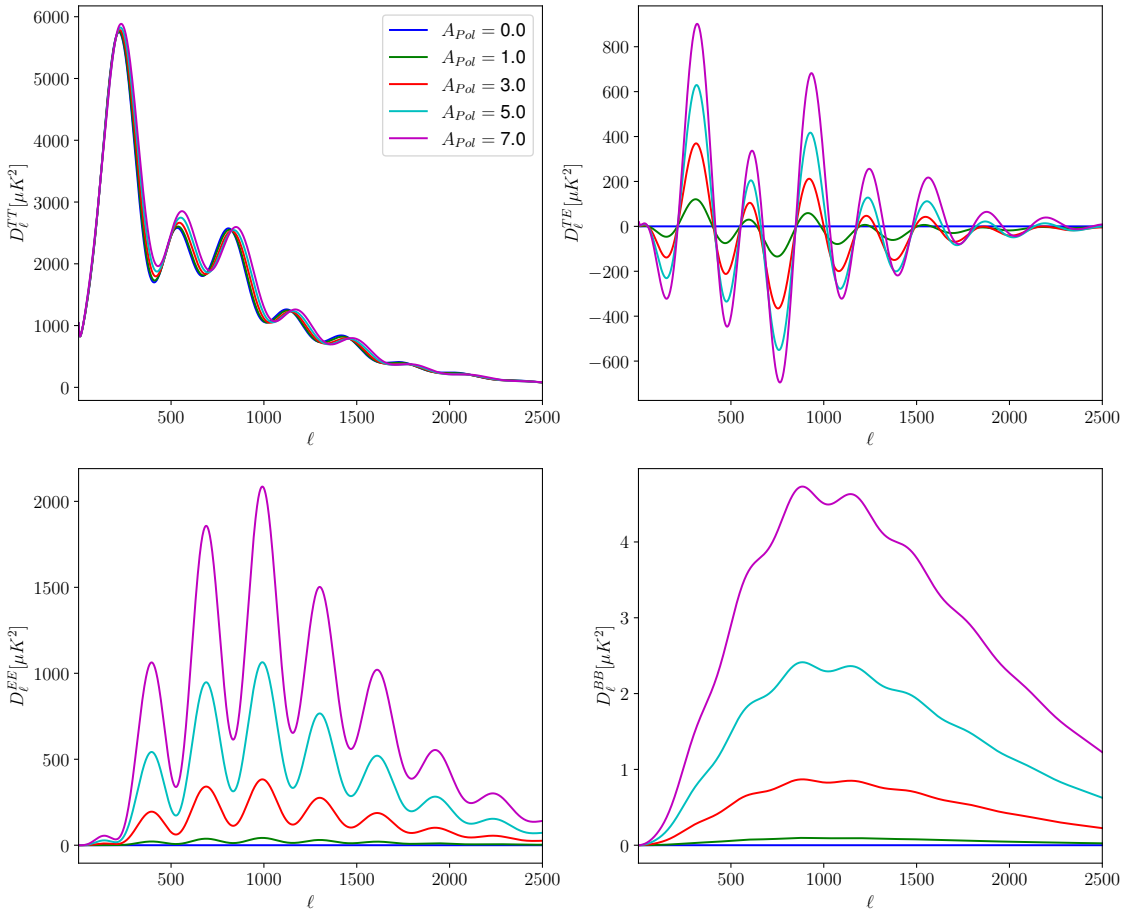


Figure 2.4: *Plots of the impact of varying the $A_{Pol}$ parameter in the temperature and polarization power spectra. The green line correspond to the power spectra predicted by $\Lambda CDM$ model for the best fit parameters from Planck mission. All plots have the same legend.*

In Figure 2.5, the effects of varying the $A_{Dop}$ parameter are shown. As it can be inferred from Figure 1.3, the Doppler effect is important in the intermediate and small scales ($\ell \geq 10$). It increases both peaks and troughs in the temperature power spectrum, while for the cross correlation between temperature and $E$ polarization mode the peaks are increased and the troughs are decreased.

In Figure 2.6, the effects of varying the $A_L$ parameter are shown. The lensing effect smooths the power spectra, especially in small scales and for the $TT$, $EE$ and $TE$ power spectra. However, for the $BB$ power spectrum increasing $A_L$ increases the power spectrum, as it is caused by the transforming power of the lensing effect from $E$ to $B$ polarization modes.

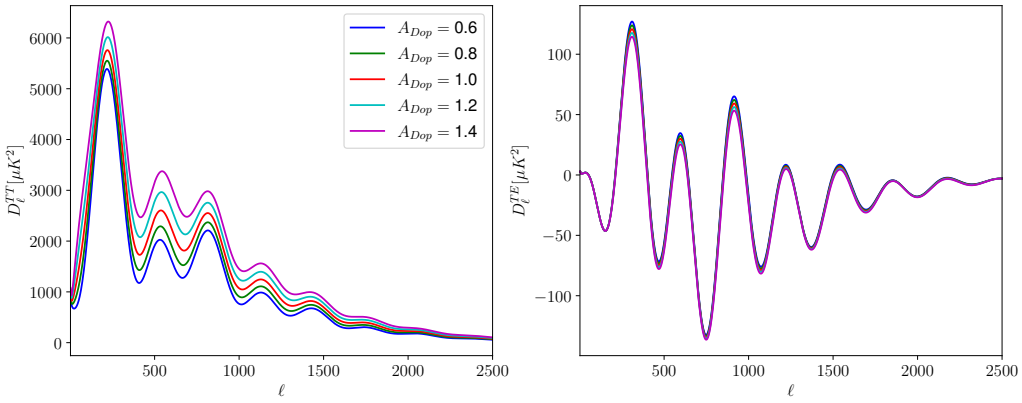


Figure 2.5: *Plots of the impact of varying the $A_{Dop}$ parameter in the temperature and cross polarization power spectra. The red line correspond to the power spectra predicted by $\Lambda CDM$ model for the best fit parameters from Planck mission. Both plots have the same legend.*

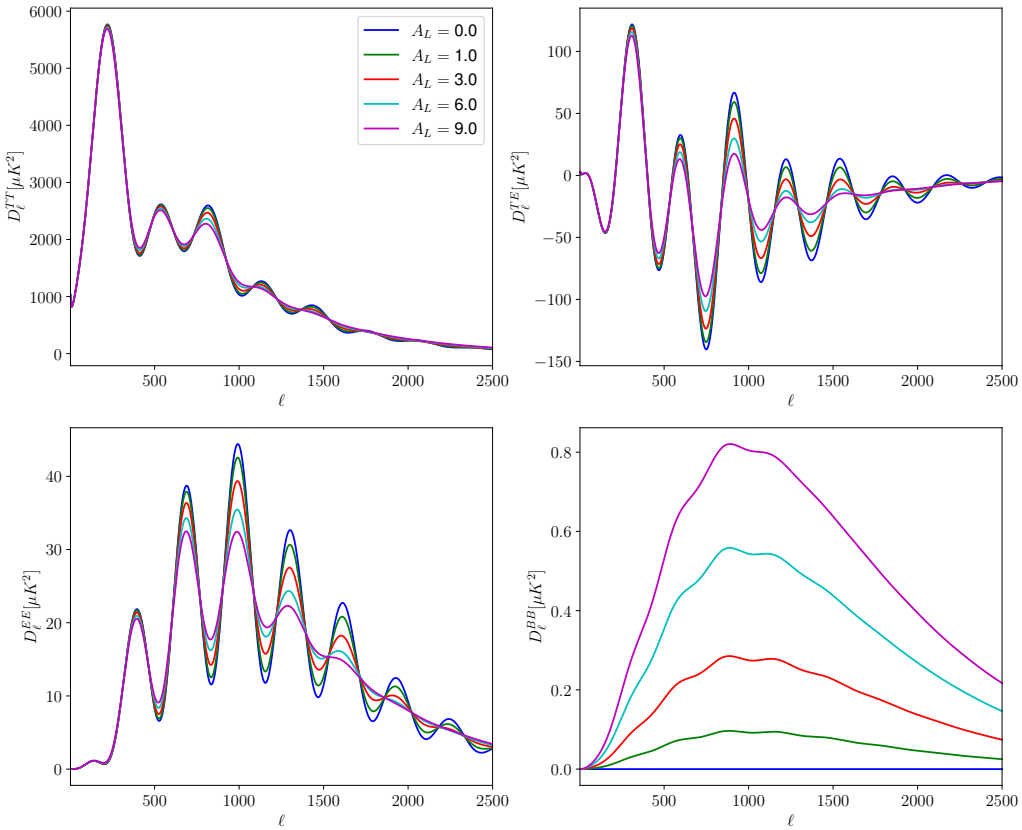


Figure 2.6: *Plots of the impact of varying the $A_L$ parameter in the temperature and polarization power spectra. The green line correspond to the power spectra predicted by $\Lambda CDM$ model for the best fit parameters from Planck mission. All plots have the same legend.*

The effect of varying the cosmological parameters is plotted in the Appendix A, as it is not the important part of the project.

## 2.2 Simulation of the CMB power spectra

In this section, it is explained how to simulate the power spectra, both temperature and polarization, recovered by Planck mission for a given set of cosmological parameters and phenomenological amplitudes. First, the theoretical CMB power spectra are simulated and used to generate simulated map realisations of the temperature and polarization Gaussian random fields observed by Planck. Performing an harmonic transform, the power spectra could be recovered for a posterior analysis.

### 2.2.1 Generating the theoretical power spectra

The CMB lensed power spectra, both temperature ($C_\ell^{TT}$) and polarization ($C_\ell^{EE}$, $C_\ell^{BB}$ and $C_\ell^{TE}$), are simulated using `CLASS` from $\ell = 2$ (without the monopole and dipole) to $\ell_{max} = 2500$. We take into account only scalar modes and all phenomenological amplitudes are set to 1 as is shown in Table 2.1 with the rest of cosmological parameters used.

| $\omega_b$ | $\omega_c$ | $H_0$ / (km/s)/Mpc | $\tau_{reio}$ | $\ln(10^{10}A_s)$ | $n_s$ |
|---|---|---|---|---|---|
| 0.0224 | 0.12 | 67.4 | 0.055 | 3.05 | 0.965 |
| $A_{SW}$ | $A_{eISW}$ | $A_{lISW}$ | $A_{Pol}$ | $A_{Dop}$ | $A_L$ |
| 1.0 | 1.0 | 1.0 | 1.0 | 1.0 | 1.0 |

Table 2.1: Cosmological parameters and phenomenological amplitudes used in the simulation with `CLASS`.

The parameters that appears in Table 2.1 are not the only ones required to execute a simulation with `CLASS`. However, we do not mentioned the others because they are not an active part of the project and are set to the default value assigned by `CLASS`.

### 2.2.2 Healpy

`healpy`[2] [26] is a Python package based on the Hierarchical Equal Area isoLatitude Pixelation (HEALPix[3]) software. It has implemented different methods to perform numerical analysis of functions on the sphere. For that purpose, the sphere is tessellated, which means that the sphere is partitioned into finite area elements verifying:

1. The elements of partition has equal areas. This implies that signals are sampled without regional dependence.

2. The data base has a hierarchical structure. Consequently, elements which are near in the tree structure are also near in the sphere, which improves the performance.

[2]Documentation available at `https://healpy.readthedocs.io/en/latest/`
[3]`https://healpix.sourceforge.io/`

3. The discrete area elements on a sphere has an iso-Latitude distribution. This property is critical for computing speed of all operations involving evaluation of spherical harmonics.

The base-resolution comprises a partition of the sphere in twelve pixels. The resolution of the grid is expressed by the parameter $N_{side}$ which defines the number of divisions along the side of a base-resolution pixel that is needed to reach a desired high-resolution partition. The total number of pixels $N_{pix}$ is related with the parameter $N_{side}$ by $N_{pix} = 12N_{side}^2$. Four examples are shown in Figure 2.7.

For Planck data is typical to use a $N_{side}$ value of 2048, corresponding to $N_{pix} \approx 5 \cdot 10^7$ pixels. As a result, the angular resolution of a single pixel is $\theta_{pix} = 1.72'$ [27].

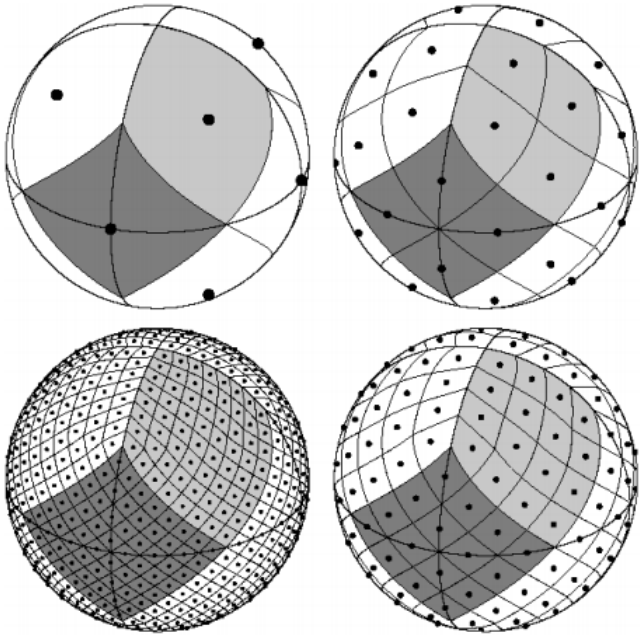

Figure 2.7: *Moving clockwise from the upper left sphere, the sphere is partitioned with a grid resolution parameter* $N_{side} = 1, 2, 4, 8$ *corresponding to a total number of pixels* $N_{pix} = 12, 48, 192, 768$. *Source: [27].*

Given a theoretical power spectra, `healpy` has a function called *synfast* that can be used to create temperature and polarization maps as realisations of random Gaussian fields on the sphere with a temporal complexity of $O(N_{pix}^{1/2}\ell_{max}^2)$, where $\ell_{max}$ is the limiting spherical harmonics order. The programme uses the known $C_\ell$'s, which are the expected variance of the $a_{\ell m}$ at that $\ell$, to generate the real and imaginary part of the $2\ell + 1$ $a_{\ell m}$ values for each $\ell$ and spectrum:

$$\begin{aligned} a_{\ell m}^T &= \zeta_1 (C_\ell^{TT})^{1/2}, \\ a_{\ell m}^E &= \zeta_1 \frac{C_\ell^{TE}}{(C_\ell^{TT})^{1/2}} + \zeta_2 \left( C_\ell^{EE} - \frac{(C_\ell^{TE})^2}{C_\ell^{TT}} \right)^{1/2}, \\ a_{\ell m}^B &= \zeta_3 (C_\ell^{BB})^{1/2}, \end{aligned} \tag{2.1}$$

where for each value of $\ell$ and $m > 0$ three complex numbers $(\zeta_1, \zeta_2, \zeta_3)$ are drawn from a Gaussian distribution with unit variance, i.e., both $\sqrt{2}Re(\zeta_i)$ and $\sqrt{2}Im(\zeta_i)$ are drawn

from a normal distribution $N(0,1)$. For $m = 0$ the same equations hold but the $\zeta_i$ should be real and drawn from a normal distribution $N(0,1)$. Finally, for $m < 0$ the coefficients are given by the reality condition

$$a^{X*}_{\ell m} = (-1)^m a^X_{\ell -m}, \tag{2.2}$$

where $X = \{T, E, B\}$ [15].

At this point, using equations (1.1), (1.25) and (1.26) with $\ell$ from 2 to $\ell_{max} = 2500$, which correspond approximately the maximum $\ell$ measured by Planck, the temperature ($T$) and polarization ($Q$ and $U$) maps are obtained.

Given the temperature and polarization maps, `healpy` has a function named *anafast* which performs harmonic analysis over the maps and returns the recovered power spectra $C_\ell$'s via an harmonic transform with a temporal complexity of $O(N_{pix}^{1/2}\ell^2_{max})$. It uses basically equation (1.35) for the temperature map, and a similar one from the discretisation of equations (1.19) and (1.20) for polarization maps.

We use also other useful functions that `healpy` provides, for instance, *gauss_beam*, which computes the spherical transform of a Gaussian beam given the value of fwhm, and *pixwin*, which returns the pixel window function for a given $N_{side}$.

### 2.2.3 Planck frequency maps and their properties

Planck satellite uses an array of 74 detectors to analyse the sky in nine bands, covering frequencies between 25 and 1000 GHz, imaging the sky with angular resolution between 33' and 5'. Table 2.2 includes the main characteristics of the nine bands.

| Central band / GHz | 30 | 44 | 70 | 100 | 143 | 217 | 353 | 545 | 857 |
|---|---|---|---|---|---|---|---|---|---|
| Effective beam FWHM[4] / arcmin | 32.29 | 27.94 | 13.08 | 9.66 | 7.22 | 4.90 | 4.92 | 4.67 | 4.22 |
| Temperature noise level / $\mu$K deg | 2.5 | 2.7 | 3.5 | 1.29 | 0.55 | 0.78 | 2.56 | | |
| Temperature noise level / kJy sr$^{-1}$ deg | | | | | | | | 0.78 | 0.72 |

Table 2.2: Main characteristics of the nine Planck frequency bands [28].

Our simulations take as reference the 143 GHz band for the effective beam profile and the temperature noise level because it balances the foreground intensity, which dominates at high frequencies, and the effective beam resolution, which increases as the frequency decreases. This leads to a noise per pixel $\sigma_{pix} = 7.049 \cdot 10^{-6}$ and effective experimental beam standard deviation $\sigma_B = 8.919 \cdot 10^{-4}$.

### 2.2.4 Simulating temperature and polarization maps

In Figure 2.8 the theoretical power spectra ($D_\ell^{TT,\text{sky}}$, $D_\ell^{EE,\text{sky}}$, $D_\ell^{TE,\text{sky}}$ and $D_\ell^{BB,\text{sky}}$) calculated with `CLASS` as explained in section 2.2.1 and their convolution with an instrumental beam and a pixel window function are shown. The effects of the beam and the pixelation produce a damping effect in the power spectra at small scales (large $\ell$'s) and affect the resolution of the experiment and it is very important to correct it.

[4]FWHM and standard deviation, $\sigma$, are easily related by $\sigma = FWHM/\sqrt{8\ln 2}$.

Using $D_\ell^{\text{signal}}$ for the different spectra and the function *synfast* from `healpy`, a temperature ($T$) and polarization ($Q$ and $U$) maps could be generated. Afterwords, adding white noise for each map, i.e., the noise for each pixel of each map is sampled from two independent normal distributions: $N(0, \sigma^2_{pix,T})$ ($T$) and $N(0, 2\sigma^2_{pix,T})$ ($Q$ and $U$). Non-correlated noise between temperature and polarization is assumed. The simulated Planck maps are shown in Figures 2.9 and 2.10.

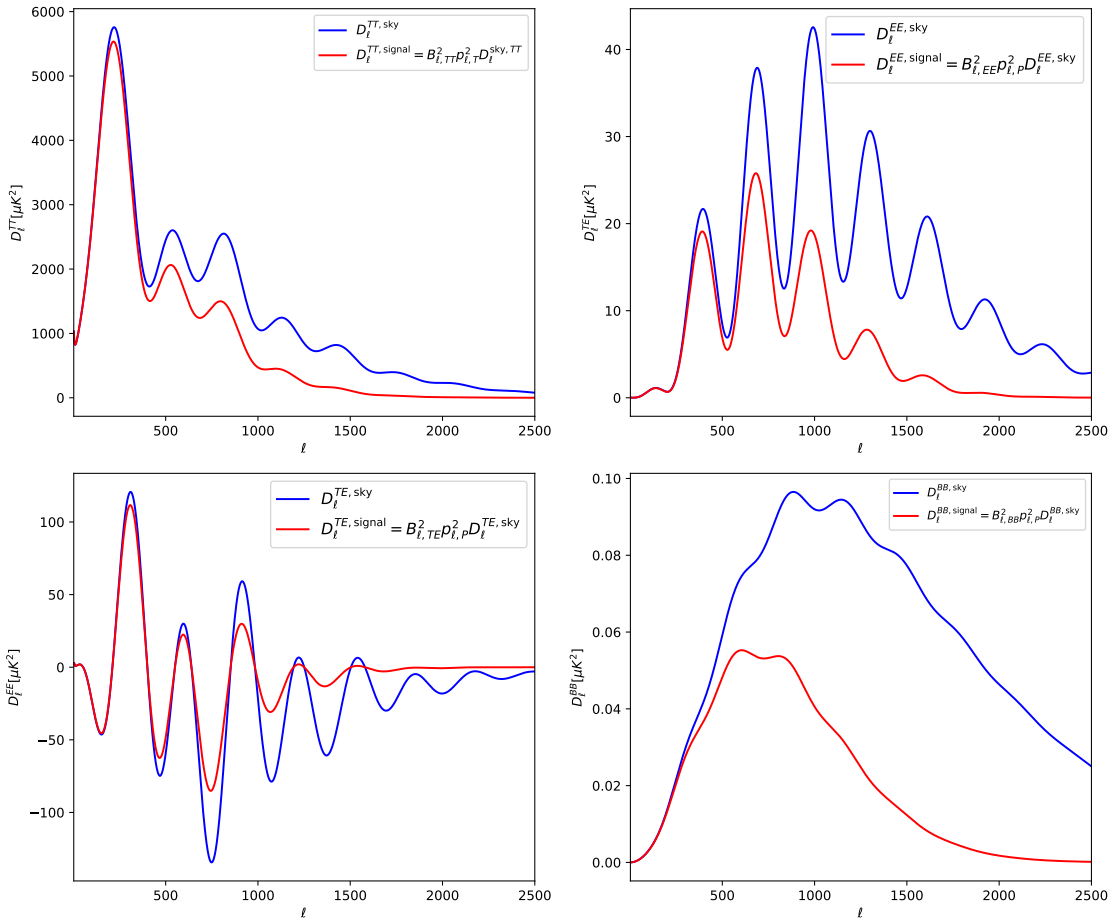


Figure 2.8: *Simulation of the TT, TE, EE and BB power spectrum from* `CLASS` *and convolved with the beam and pixel window function obtained with* `healpy`.

Performing a harmonic transform of the maps using function *anafast* from `healpy` allows us to recover the power spectra. After this, a deconvolution of the beam and the pixel window function is performed. As explained in section 1.3, the noise causes the values of $D_\ell$'s to increase dramatically for high $\ell$'s. For visualization purposes, in Figures 2.11, 2.12 and 2.13 the recovered and deconvolved power spectra are plotted with the noise removed. A quick analysis of these Figures shows how the cosmic variance affects low and high $\ell$'s. In fact, Figures 2.12 and 2.13 which correspond to the $E$ mode polarization spectrum and temperature-polarization cross-correlation are limited to a $\ell_{max}$ value of 2000 due to the dominant contribution of noise over the data. The $B$ mode power spectrum is not plotted as Planck mission is unable to resolve it.

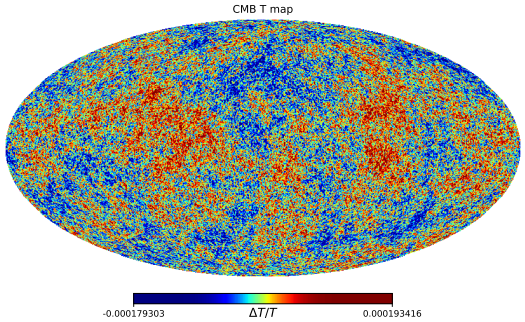


Figure 2.9: *Simulated temperature map obtained using the 143 GHz band properties of Planck mission.*

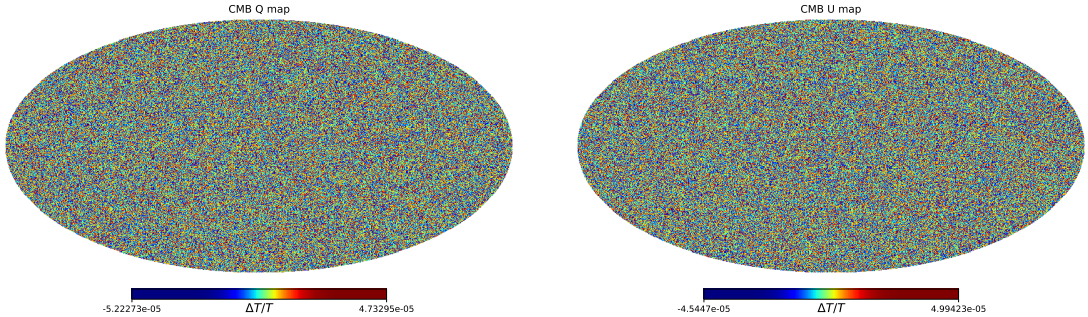


Figure 2.10: *Simulated Q and U mode polarization maps obtained using the 143 GHz band properties of Planck mission.*

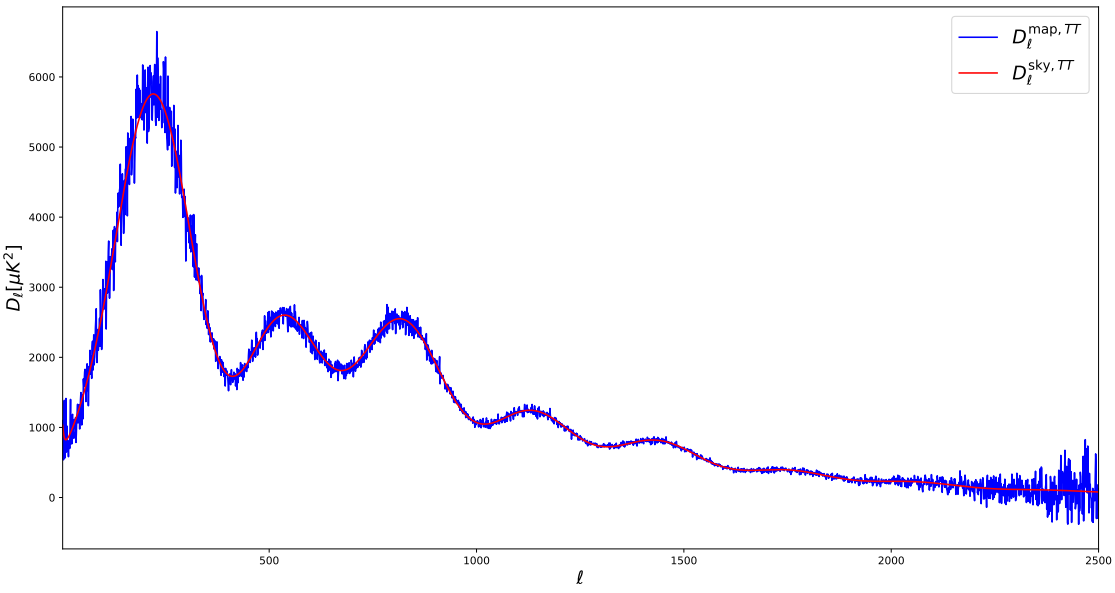


Figure 2.11: *Simulated temperature CMB spectrum (TT) obtained by the Planck mission (in blue) compared with the theoretical temperature spectrum calculated with* `CLASS` *(in red).*

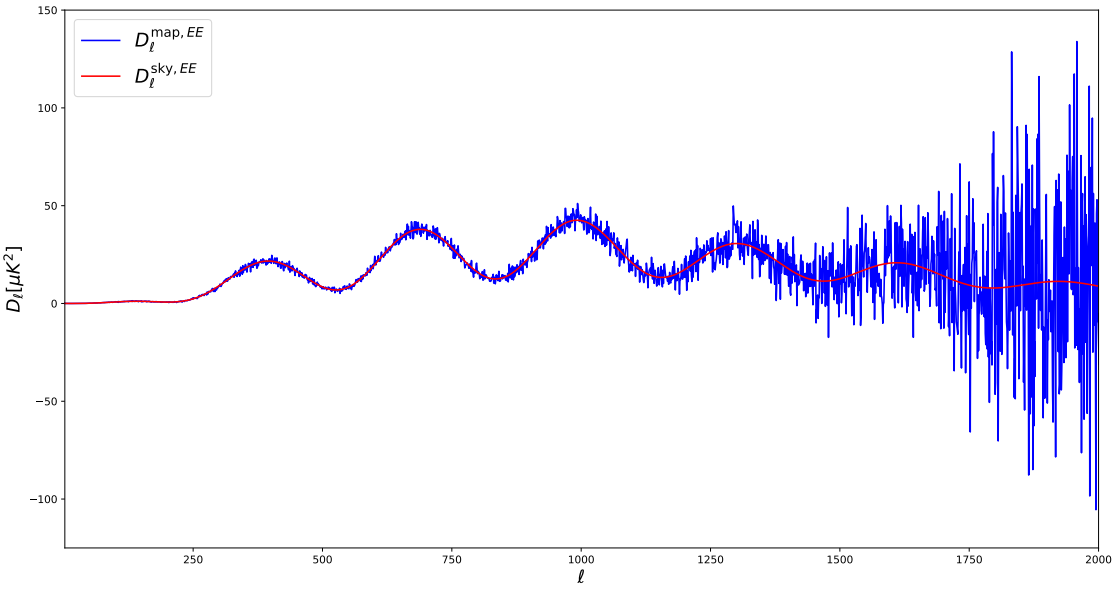


Figure 2.12: *Simulated E mode polarization CMB spectrum (EE) obtained by the Planck mission (in blue) compared with the theoretical E mode polarization spectrum calculated with* `CLASS` *(in red).*

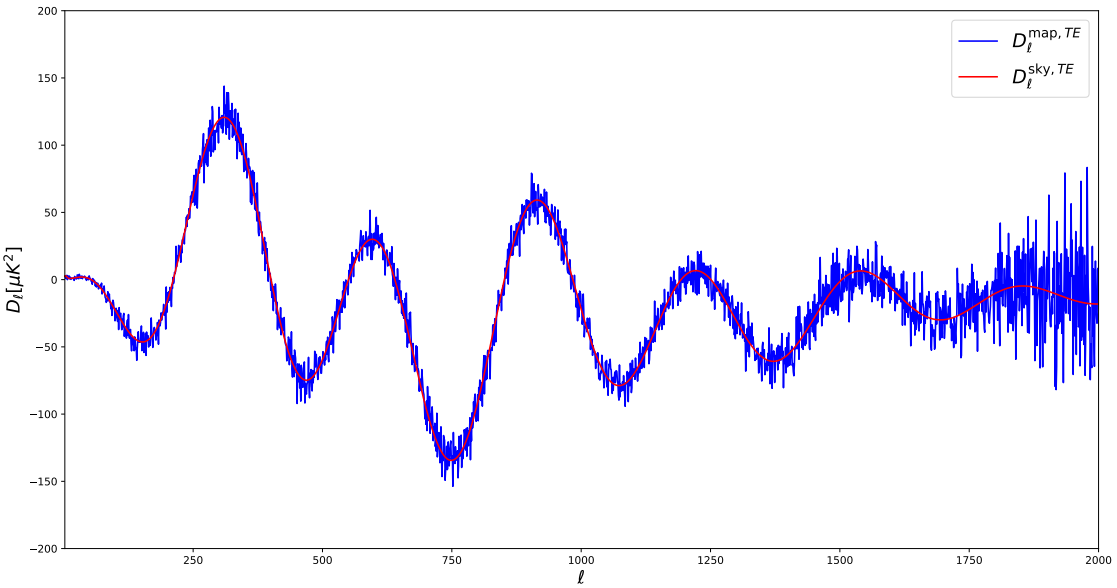


Figure 2.13: *Simulated temperature-polarization cross-correlation CMB spectrum (TE) obtained by the Planck mission (in blue) compared with the theoretical temperature-polarization cross-correlation spectrum calculated with* `CLASS` *(in red).*

## 2.3 Bayesian inference in cosmology

Given a model $\mathcal{M}$ parametrized by a collection of parameters $\theta$ and data $D$, the objective of using bayesian inference is to obtain credible regions in which, given a model, the parameters can be constrained [29]. By the product rule, the joint probability of model and data factorizes:

$$\begin{array}{ccccc} P(\theta)\ P(D \mid \theta) & = & P(\theta, D) & = & P(D)\ P(\theta \mid D) \\ \textbf{Prior} \times \textbf{Likelihood} & = & \textbf{Joint} & = & \textbf{Evidence} \times \textbf{Posterior} \\ \pi(\theta)\ \mathcal{L}(\theta) & = & \cdots & = & E\ \mathcal{P}(\theta) \\ \text{Inputs} & & & & \text{Outputs} \end{array} \tag{2.3}$$

where:

- The Prior, $\pi(\theta)$, contains a priori information on the parameters. This probability has been controversial because no matter how sophisticated is the methodology used, in the end it consists in an informal assignment of what is thought to be reasonable based on the knowledge available.
- The Likelihood, $\mathcal{L}(\theta)$, represents the probability distribution of the data for each allowed input $\theta$. It models the instrument response to known inputs $\theta$, which can usually be estimated by calibration. In the worst case scenario, they can be left as nuisance parameters which can be incorporated in $\theta$ as extra parameters to be determined.
- The Posterior, $\mathcal{P}(\theta)$, represents our inferred distribution of probability given a model and the data.
- The Evidence, $E$, represents how well the original assignments manage to predict the data.

Our objective is to estimate the Posterior distribution using the known Prior and Likelihood. It could be done using the expression of the posterior which can be derived from equation (2.3):

$$\mathcal{P}(\theta) = \frac{\pi(\theta)\ \mathcal{L}(\theta)}{E} \quad \text{where } E = \int \pi(\theta)\ \mathcal{L}(\theta) d\theta. \tag{2.4}$$

### 2.3.1 The Prior

The priors used in this project are Uniform and Gaussian distributions. In Table 2.3 the parameters of the priors used in this work are shown. When a different prior for a certain parameter is used, it will be specified. The only difference between the priors used in the temperature, $TT$, and temperature and polarization, $TT + EE + TE$, is the prior in $\tau_{reio}$. There is a well known degeneracy in the CMB temperature data between the scalar amplitude, $A_s$, and the optical depth to reionization, $\tau_{reio}$. This degeneracy is broken when $\ell \leq 20$ $EE$ data is introduced, so a Gaussian prior of $\tau_{reio} = 0.055 \pm 0.008$ is used for temperature data to account for the constrain from low $\ell$ region of the $EE$ power spectrum introduced by Planck experiment [22].

| $\ln(A_s)$ | $n_s$ | $\omega_b$ | $\omega_{cdm}$ | $H_0$ | $\tau_{reio}$ $(TT)$ | $\tau_{reio}$ $(TT+EE+TE)$ |
|---|---|---|---|---|---|---|
| $U(1.61, 3.91)$ | $U(0.8, 1.2)$ | $U(0.005, 0.1)$ | $U(0.001, 0.99)$ | $U(20, 100)$ | $\mathcal{N}(0.055, 6.4 \cdot 10^{-5})$ | $U(0.01, 0.8)$ |
| $A_{SW}$ | $A_{eISW}$ | $A_{lISW}$ | $A_{Dop}$ | $A_{Pol}$ | $A_L$ | $\sigma_{pix,T}$ |
| $U(0.75, 1.25)$ | $U(0.75, 1.25)$ | $U(0, 3)$ | $U(0.75, 1.25)$ | $U(0, 3)$ | $U(0.75, 1.25)$ | $\mathcal{N}(7.05 \cdot 10^{-6}, 10^{-16})$ |

Table 2.3: Priors used for $TT$ and $TT + EE + TE$ data. The uniform distribution is represented by $U(a, b)$ where $a$ and $b$ are the minimum and maximum values of the interval. The Gaussian distribution is represented by $\mathcal{N}(\mu, \sigma^2)$ where $\mu$ is the mean and $\sigma^2$ is the variance. The only difference between the two datasets is in the prior of the optical depth to reionization, $\tau_{reio}$.

### 2.3.2 The Likelihood

Assuming that the theoretical CMB signal is normally distributed and the signals are statistically isotropic, the CMB power spectra contains all the information about the model, and all of the constrains of the parameters of the theory can be obtained from the $C_\ell$ probability distribution. Consequently, the likelihood as a function of some cosmological parameters, $\theta$, is just the likelihood as a function of the power spectra determined from those parameters: $\mathcal{L}(\theta) = P(D \mid \theta) = P(D \mid C_\ell(\theta))$.

While the CMB temperature and polarization are normally distributed, the $C_\ell$ are not: the uncertainties in the determination of the power spectra are not Gaussian-distributed. At high $\ell$, the Central Limit will ensure that the likelihood is well approximated by a Gaussian but at low $\ell$ this is not the case. As a result, the likelihood must be non-Gaussian.

Consider an experiment covering a fraction of the sky, $f_{sky}$, with a uniform pixel noise and finite beam. First, we will assume that only the temperature data is available, which leads to an expression of the log-likelihood shown in equation (2.5):

$$\ln \mathcal{L} = -\frac{1}{2} \sum_{\ell=2}^{2500} (2\ell + 1) f_{sky} \left[ \ln \left( \frac{C_\ell^{TT} + \mathcal{N}_\ell^{TT}}{\hat{C}_\ell^{TT}} \right) + \left( \frac{\hat{C}_\ell^{TT}}{C_\ell^{TT} + \mathcal{N}_\ell^{TT}} \right) - 1 \right], \tag{2.5}$$

where $\hat{C}_\ell^{TT}$ is the temperature power spectrum recovered by the experiment, $C_\ell^{TT}$ is the theoretical power spectrum given by the model and $\mathcal{N}_\ell^{TT} = \frac{1}{w_T B_{\ell,TT}^2 p_{\ell,T}^2}$ is the power spectrum of the noise, calculated in Section 1.4. For Planck experiment, $f_{sky}$ is set to a value of 0.7, which correspond to the portion of sky where the CMB signal could be recovered properly.

This likelihood is maximized at $C_\ell^{TT} = \hat{C}_\ell^{TT} - \mathcal{N}_\ell^{TT}$. If the likelihood is evaluated at its peak, the standard error on a $C_\ell^{TT}$ is then given by:

$$\Delta C_\ell^{TT} = (C_\ell^{TT} + \mathcal{N}_\ell^{TT}) \sqrt{\frac{2}{(2\ell + 1) f_{sky}}}, \tag{2.6}$$

which coincides with the expression of the cosmic variance of equation (1.40). However, uncertainties derived in this manner are larger if $\hat{C}_\ell^{TT}$ has fluctuated upward from the underlying "real" value and smaller for a downward fluctuation [30].

To include polarization, we have taken into consideration that in Planck experiment, while temperature data is available up to $\ell = 2500$, we only have polarization data until $\ell = 2000$. The following equation corresponds to the likelihood which combines the

temperature and polarization data:

$$\begin{aligned}\ln\mathcal{L} = &-\frac{1}{2}\sum_{\ell=2}^{2000}(2\ell+1)f_{sky}\left[\ln\left(\frac{(C_\ell^{TT}+\mathcal{N}_\ell^{TT})(C_\ell^{EE}+\mathcal{N}_\ell^{EE})-(C_\ell^{TE})^2}{\hat{C}_\ell^{TT}\hat{C}_\ell^{EE}-(\hat{C}_\ell^{TE})^2}\right)+\right.\\ &\left.+\left(\frac{\hat{C}_\ell^{TT}(C_\ell^{EE}+\mathcal{N}_\ell^{EE})+(C_\ell^{TT}+\mathcal{N}_\ell^{TT})\hat{C}_\ell^{EE}-2\hat{C}_\ell^{TE}C_\ell^{TE}}{(C_\ell^{TT}+\mathcal{N}_\ell^{TT})(C_\ell^{EE}+\mathcal{N}_\ell^{EE})-(C_\ell^{TE})^2}\right)-2\right]+\\ &-\frac{1}{2}\sum_{\ell=2001}^{2500}(2\ell+1)f_{sky}\left[\ln\left(\frac{C_\ell^{TT}+\mathcal{N}_\ell^{TT}}{\hat{C}_\ell^{TT}}\right)+\left(\frac{\hat{C}_\ell^{TT}}{C_\ell^{TT}+\mathcal{N}_\ell^{TT}}\right)-1\right],\end{aligned} \tag{2.7}$$

where $\hat{C}_\ell^{TT}$, $\hat{C}_\ell^{EE}$ and $\hat{C}_\ell^{TE}$ are the power spectra recovered from the experiment; $C_\ell^{TT}$, $C_\ell^{EE}$ and $C_\ell^{TE}$ are the theoretical power spectra given by the model and $\mathcal{N}_\ell^{TT}$ and $\mathcal{N}_\ell^{EE}$ are the noise power spectra for temperature and E-mode polarization respectively [17]. Again, $f_{sky}$ is set to a value of 0.7 assuming an equal covering in temperature and polarization maps.

### 2.3.3 Sampling for parameter estimation

The goal of the project is to obtain estimates of the parameters and their error bars given the data and the model. From the posterior probability distribution we can answer statistical questions about functions of the parameters, $P(f(\theta) \mid \mathcal{P}(\theta))$. For example, the expected value of a function of parameters $f(\theta)$ is given by

$$\langle f(\theta)\rangle = \int d\theta f(\theta)\mathcal{P}(\theta). \tag{2.8}$$

If we want to find the expectation value of a cosmological parameter (for instance, $f(\theta) = H_0$), the posterior probability distribution must be evaluated in the full multidimensional parameter space to perform the integral of equation (2.8) for the expectation value of $H_0$. In principle, this integral can be calculated numerically, however, if there are $n$ parameters then the posterior is an $n$-dimensional scalar-valued function. The simplest computational method would sum over an evenly spaced grid, which has to cover a large volume of parameter space to analyse all the regions in which $f(\theta)\mathcal{P}(\theta)$ is significantly non-zero. If the width of the parameter space in a dimension, i.e., for a certain parameter, is $w_i$ and the required resolution is $\Delta_i$, the number of grid points is $\prod_{i=1}^{n}(w_i/\Delta_i) \approx (w_1/\Delta_1)^n$ (approximation only valid if all dimensions have a similar structure). As a result, there is an exponential scaling in the number of grid points with the number of dimensions, which makes direct integration numerically prohibitive in large dimensions.

A good alternative is to try to compress the posterior $\mathcal{P}(\theta)$ into a small manageable collection of numbers by sampling. The probability of taking a sample from a given position in parameter space $\theta$ is proportional to the probability $\mathcal{P}(\theta)$ at that position in parameter space. A set of $m$ samples $\{\theta_i\}$ specifies $m$ positions in parameter space and therefore consists of $n \times m$ numbers. The number density of samples should then be proportional to the probability distribution itself.

From the set of samples $\{\theta_i\}$, through the calculation of $P(f(\theta) \mid \{\theta_i\})$, we can infer properties of the full distribution, $P(f(\theta) \mid \mathcal{P}(\theta))$. An estimation of the expectation value

of $f(\theta)$ can be obtained using the following estimator:

$$\hat{E}_f = \frac{1}{m}\sum_{i=1}^{m} f(\theta_i), \tag{2.9}$$

which verifies that the expected value of $\hat{E}_f$ is $\langle \hat{E}_f \rangle = \langle f(\theta) \rangle$.

The Central Limit Theorem states that for a large number of samples and if $f(\theta_i)$ has finite variance, $P(\hat{E}_f)$ tends to the normal distribution $\mathcal{N}(\langle f(\theta)\rangle, \sigma_f^2/m)$, where $\sigma_f^2$ is the true variance of $f(\theta)$.

### 2.3.4 Markov Chain Monte Carlo (MCMC) sampling

The Markov Chain Monte Carlo sampling is a local sampling method which sets up a random walk through parameter space so that only regions with fairly high probability are explored. This method is based on a rule for choosing a sequence of points in parameter space such that after a long time the probability of the current position being $\theta_i$ is proportional to the posterior $\mathcal{P}(\theta_i)$, this is why it is common to remove the first samples, which is called burn in and in this project is set to a value of 30 %. If the rule for moving from $\theta_i$ to $\theta_{i+1}$ depends only on $\theta_i$, then the sequence of points is called a Markov chain.

The generation of the elements of the chain is described by a transition probability, $T(\theta_i, \theta_{i+1})$, that determines the probability of the chain moving from $\theta_i$ to $\theta_{i+1}$ in parameter space. A sufficient condition to obtain a Markov Chain is that the transition probability satisfies the detailed balanced condition:

$$\mathcal{P}(\theta_{i+1})T(\theta_{i+1}, \theta_i) = \mathcal{P}(\theta_i)T(\theta_i, \theta_{i+1}). \tag{2.10}$$

The Metropolis-Hastings algorithm is one of the simplest and most popular MCMC algorithms to construct a Markov chain satisfying the detailed balance condition. It uses a proposal density distribution $q(\theta_i, \theta_{i+1})$ to propose a new point $\theta_{i+1}$ given the chain is currently at $\theta_i$. The proposed new point is then accepted with probability

$$\alpha(\theta_i, \theta_{i+1}) = \min\left\{1, \frac{\mathcal{P}(\theta_{i+1})q(\theta_{i+1}, \theta_i)}{\mathcal{P}(\theta_i)q(\theta_i, \theta_{i+1})}\right\}, \tag{2.11}$$

so the total transition probability is $T(\theta_i, \theta_{i+1}) = \alpha(\theta_i, \theta_{i+1})q(\theta_i, \theta_{i+1})$ which verifies the detailed balance condition.

Notice from equation (2.11) that only the unnormalized posterior is required, as there is a quotient of posteriors in the equation. Another important aspect is the choice of the proposal distribution $q$ for the efficient exploration of the posterior. If the scale of $q$ is too small compared to the scale of the target distribution, the algorithm will spend too much locally and the exploration will be poor. If the scale of $q$ is too large, the chain will get stuck as it will not jump very frequently [29] [31]. Having a covariance matrix, that can be obtained from a pre-run is advisable.

In this project, we have used `Cobaya` [5] [32] (Code for Bayesian Analysis) which is a general-purpose Bayesian analysis code that allows to explore the posterior using a range of

[5] `https://cobaya.readthedocs.io/en/latest/`

Monte Carlo samplers. The MCMC sampler used in `Cobaya` is from `CosmoMC` [33] [34] [35], which calls `CLASS` code for the likelihood calculation. This code uses a generalized version of the $R-1$ Gelman-Rubin statistic to check for convergence. In general, the $R-1$ parameter is set to a value of 0.05, but in certain situations when the convergence is difficult to achieve it will be set to 0.1. `Cobaya` has been adapted to allow sampling the phenomenological parameters introduced in this project.

To analyse the samples, a Python package called `GetDist`[6] [36] has been used. This program allows to calculate quantities of interest from the samples, as parameter means, credible intervals and marginalized densities. With `GetDist` 2D contour plots containing the 68 % and 95% of the samples can be obtained, which help us to study degeneracies among parameters.

[6] `https://getdist.readthedocs.io/en/latest/`

# Chapter 3

# Results

In this chapter we will analyse how well we recover the cosmological and phenomenological parameters from simulations. We will analyse the correlation and degenerations between the different parameters and establish different combinations of parameters that Planck experiment might be able to constrain successfully using only the temperature power spectrum and using the combination of temperature and polarization power spectra.

## 3.1 Fitting to ΛCDM cosmological parameters

The first logical step is trying to fit the ΛCDM parameters to our simulations using only temperature data and a combination of temperature and polarization data.

The two types of simulations that we are going to use are:

- Theoretical temperature and polarization power spectra generated by `CLASS` (without using `healpy`) added to a theoretical noise power spectra calculated with the noise and finite beam characteristics of Planck experiment. From now on, we will call this dataset Theoretical.
- Simulated temperature and polarization power spectra using `CLASS` and `healpy` as explained in section 2.2.4 using the noise and finite beam characteristics of Planck experiment. From now on, we will call this dataset Simulated.

In Figure 3.1 the cosmological parameters are recovered using the dataset Theoretical. In Figure 3.2 the cosmological parameters are recovered using the dataset Simulated. The $TT$ spectrum only and the $TT + EE + TE$ spectra were considered for the four different runs of MCMC software that led to those Figures. In Table 3.1, the mean and 68% credible intervals are shown for the different parameters considered.

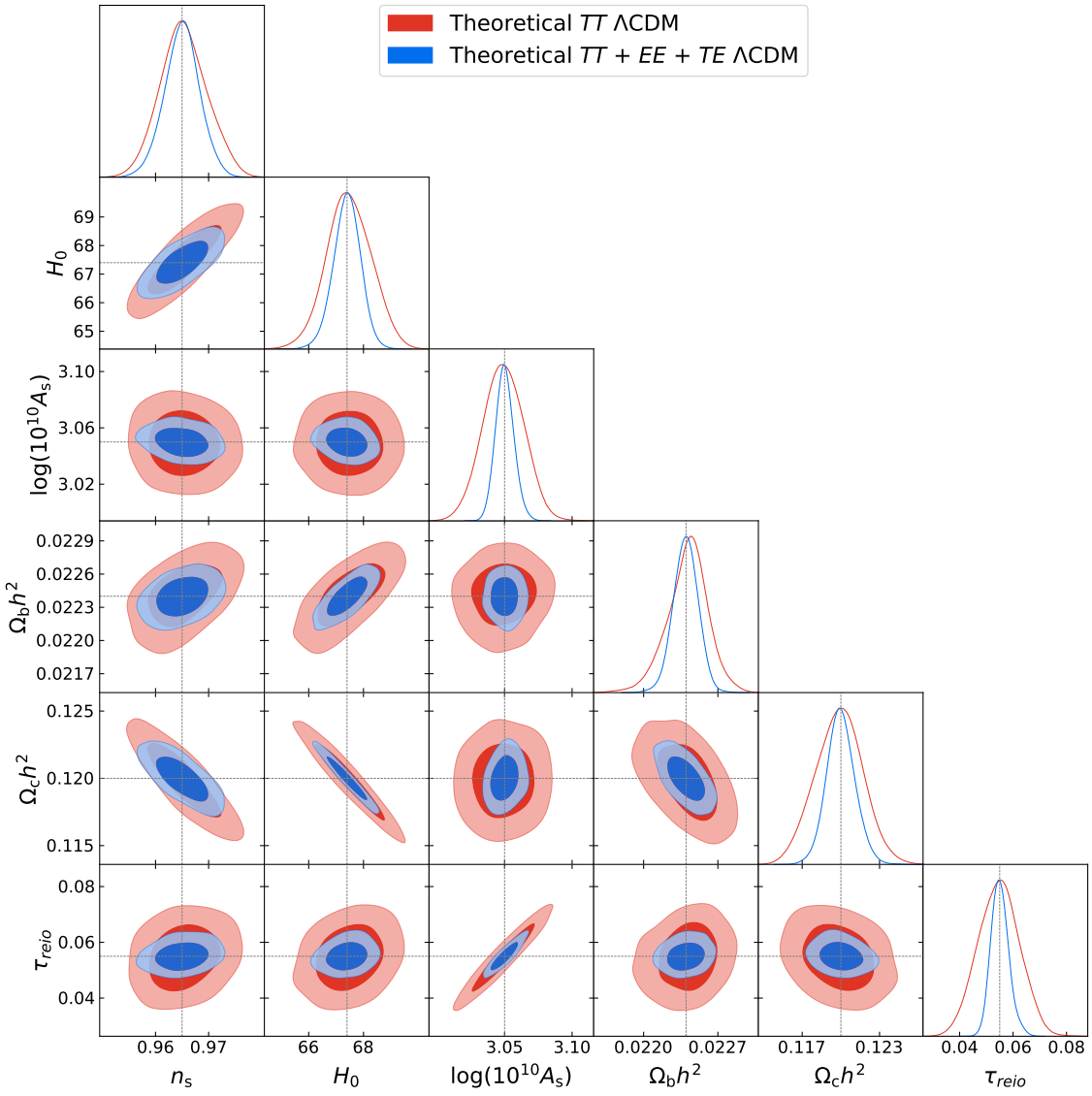


Figure 3.1: *Plots of the marginalized posterior for the parameters of the minimal ΛCDM model using the temperature data, TT, and the temperature and polarization data, $TT + EE + TE$, from the Theoretical dataset. The contours display the 68% and 95% limits and the black dotted lines represent the original parameter values used in the simulations. The $R - 1$ parameter for these two runs was set to 0.05. The priors and likelihoods used in this plot are described in detail in sections 2.3.1 and 2.3.2, respectively.*

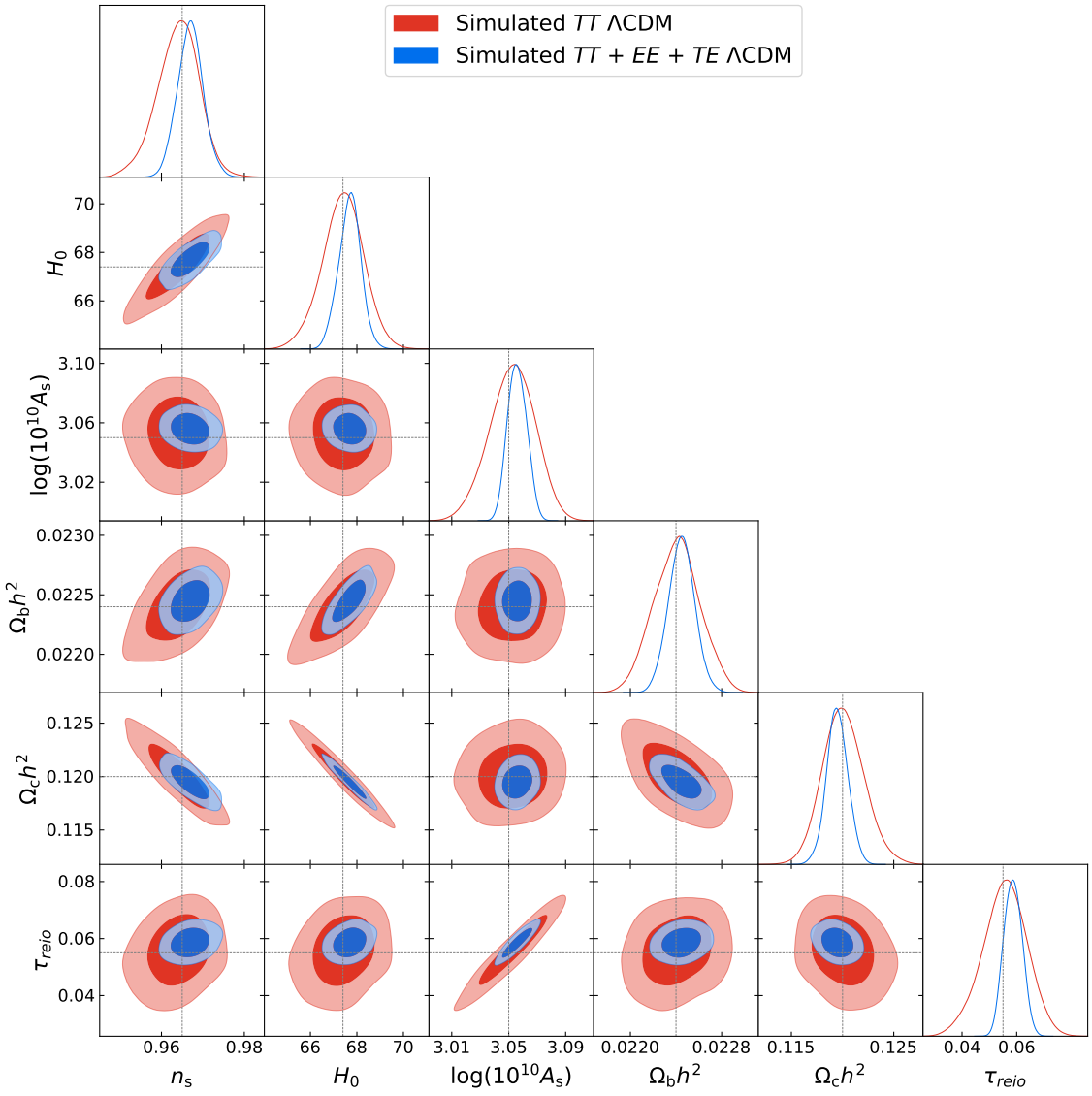


Figure 3.2: *Plots of the marginalized posterior for the parameters of the minimal ΛCDM model using the temperature data, TT, and the temperature and polarization data, TT+EE+TE, from the Simulated dataset. The contours display the 68% and 95% limits and the black dotted lines represent the original parameter values used in the simulations. The $R-1$ parameter for these two runs was set to 0.05. The priors and likelihoods used in this plot are described in detail in sections 2.3.1 and 2.3.2, respectively.*

| | Theoretical | | Simulated | |
|---|---|---|---|---|
| Param. | $TT$ | $TT+EE+TE$ | $TT$ | $TT+EE+TE$ |
| $n_s$ | $0.9653 \pm 0.0044$ | $0.9650 \pm 0.0033$ | $0.9640^{+0.0053}_{-0.0045}$ | $0.9670 \pm 0.0031$ |
| $H_0$ | $67.48 \pm 0.81$ | $67.40 \pm 0.50$ | $67.40 \pm 0.89$ | $67.69^{+0.49}_{-0.45}$ |
| $100\omega_b$ | $2.241^{+0.020}_{-0.017}$ | $2.240 \pm 0.012$ | $2.241 \pm 0.020$ | $2.245 \pm 0.011$ |
| $\omega_c$ | $0.1199 \pm 0.0018$ | $0.1200 \pm 0.0011$ | $0.1201^{+0.0019}_{-0.0021}$ | $0.1195 \pm 0.0010$ |
| $\tau_{reio}$ | $0.0546 \pm 0.0077$ | $0.0551^{+0.0029}_{-0.0036}$ | $0.0557^{+0.0084}_{-0.0076}$ | $0.0586 \pm 0.0033$ |
| $\ln(10^{10}A_s)$ | $3.049 \pm 0.015$ | $3.0502 \pm 0.0068$ | $3.053^{+0.017}_{-0.015}$ | $3.0560 \pm 0.0066$ |

Table 3.1: Mean values and 68% credible intervals for the minimal ΛCDM parameters for the MCMC chains fit to Theoretical and Simulated datasets. The values of the parameters used to generate the different simulations are in Table 2.1.

Comparing Figures 3.1 and 3.2 the results obtained from both simulations are quite similar. The greatest difference is observed in the mean values recovered from the MCMC samples with the $TT+EE+TE$ Simulated dataset, which differ a bit from the parameters used for the simulations shown in Table 2.1. This is the expected behaviour when using the Simulated dataset, as cosmic variance is directly included in the dataset and produces these "noisy" power spectra that are plotted in Figures 2.11, 2.12 and 2.13. Also, other important aspect is the 68 % credible intervals obtained from each parameter is similar when comparing the samples from the Theoretical and Simulated datasets. As the results are quite similar in both cases and the MCMC simulations are expensive, we decide to perform MCMC analysis only on the Theoretical dataset for the following runs because we know that the mean values will not be shifted and understanding the results obtained will be easier.

If we focus on the Figures 3.1 and 3.2, we will be able to establish relations between the ΛCDM parameters. The first relation is observed between $A_s$ and $\tau_{reio}$. These two parameters are correlated because $A_s$ lifts and $\tau_{reio}$ lowers the CMB power spectra when both parameters are increased, as it can be observed in Figures A.1 and A.6. These two parameters are mostly uncorrelated with the rest of cosmological parameters. The physical cold dark matter density, $\omega_c$, is anti-correlated with the scalar tilt, $n_s$, the Hubble parameter, $H_0$, and the physical baryonic density, $\omega_b$. Finally, $n_s$ is correlated with $\omega_b$ and $H_0$, and $\omega_b$ is correlated with $H_0$. Analysing these relations are important to know if there has been a change, when including the phenomenological amplitudes.

Comparing the 68% credible intervals for $TT$ and $TT+EE+TE$ datasets showed in Table 3.1 with the credible intervals obtained by Planck mission [37] we see a very good coincidence for the $TT$ dataset. However, for the $TT+EE+TE$ dataset, the uncertainty in the parameters $\ln(10^{10}A_s)$ and $\tau_{reio}$ is reduced a half compared to $TT$ data only. This reduction is not observed when dealing with real data, due to the fact that the likelihood used in Planck is more complicated than the likelihood used in this project in several aspects, for instance, it has to deal with existence of systematics that affects differently each spectrum. As the scalar amplitude and optical depth to reionization are global effects in the sense that affects each $C_\ell$ equally, they are very sensitive to systematics.

## 3.2 Fitting ΛCDM plus one phenomenological amplitude

In this section, we want to analyse how well we are able to constrain the ΛCDM cosmological parameters plus one phenomenological amplitude using the Theoretical $TT$ and the

Theoretical $TT + EE + TE$ datasets.

In [22] it was studied how including one phenomenological amplitude in addition to the ΛCDM parameters could improve the ΛCDM fit to the $TT$ Planck power spectrum. The results obtained by [22] showed that, when the phenomenological parameters $A_{SW}$, $A_{eISW}$, $A_{Dop}$, $A_{Pol}$ and $A_L$ are taken into consideration, the best fit is obtained when $A_L$ is used, which is a phenomenological amplitude used by Planck Collaboration to relieve the tension between low $\ell$ and high $\ell$ data. Focusing on the part that affects our project, this article showed that the five phenomenological amplitudes enumerated previously can be constrained while still being able to place strong constrains to ΛCDM parameters.

In this work, we wanted not only to check the results presented in [22], but to go further by testing an additional phenomenological amplitude named $A_{lISW}$ and to analyse if tighter constrains can be achieved when including polarization data.

In Tables 3.2 and 3.3 the mean and 68% credible intervals are shown for the different phenomenological parameters considered for the Theoretical $TT$ dataset and for the Theoretical $TT + EE + TE$ dataset, respectively. In Figures 3.3 and 3.4 the results obtained using the Theoretical $TT$ dataset are shown, while in Figures 3.5 and 3.6 the Theoretical $TT + EE + TE$ dataset is used.

| Param. | $+ A_{SW}$ | $+ A_{eISW}$ | $+ A_{lISW}$ | $+ A_L$ | $+ A_{Dop}$ | $+ A_{Pol}$ |
|---|---|---|---|---|---|---|
| $n_s$ | $0.9650^{+0.0050}_{-0.0056}$ | $0.9643 \pm 0.0069$ | $0.9650 \pm 0.0048$ | $0.9653 \pm 0.0055$ | $0.9654 \pm 0.0046$ | $0.9653^{+0.0084}_{-0.0076}$ |
| $H_0$ | $67.39 \pm 0.96$ | $67.34 \pm 0.89$ | $67.40 \pm 0.88$ | $67.5 \pm 1.0$ | $67.47 \pm 0.87$ | $67.5 \pm 1.3$ |
| $100\,\omega_b$ | $2.240 \pm 0.021$ | $2.241 \pm 0.034$ | $2.240 \pm 0.018$ | $2.240 \pm 0.023$ | $2.240 \pm 0.022$ | $2.242^{+0.035}_{-0.032}$ |
| $\omega_c$ | $0.1200 \pm 0.0021$ | $0.1202 \pm 0.0019$ | $0.1200 \pm 0.0020$ | $0.1198 \pm 0.0023$ | $0.1198 \pm 0.0019$ | $0.1201 \pm 0.0020$ |
| $\tau_{reio}$ | $0.0553 \pm 0.0079$ | $0.0552 \pm 0.0078$ | $0.0555 \pm 0.0075$ | $0.0549 \pm 0.0080$ | $0.0561 \pm 0.0077$ | $0.0550 \pm 0.0080$ |
| $\ln(10^{10} A_s)$ | $3.051 \pm 0.017$ | $3.051 \pm 0.016$ | $3.051 \pm 0.015$ | $3.049 \pm 0.017$ | $3.052 \pm 0.018$ | $3.050 \pm 0.016$ |
| $A_{new}$ | $0.9999 \pm 0.0088$ | $0.998 \pm 0.041$ | $0.90^{+0.44}_{-0.55}$ | $1.007 \pm 0.069$ | $0.9998 \pm 0.010$ | $1.03 \pm 0.30$ |

Table 3.2: Mean values and 68% credible intervals for the minimal ΛCDM parameters plus one phenomenological amplitude, $A_{new}$, for the MCMC chains fit to the Theoretical $TT$ dataset. The values of the parameters used to generate the different simulations are in Table 2.1 and the priors and likelihood used are described in sections 2.3.1 and 2.3.2, respectively. The $R - 1$ parameter for all the runs was set to 0.05 and the instrumental noise is sampled but not shown.

| Param. | $+ A_{SW}$ | $+ A_{eISW}$ | $+ A_{lISW}$ | $+ A_L$ | $+ A_{Dop}$ | $+ A_{Pol}$ |
|---|---|---|---|---|---|---|
| $n_s$ | $0.9647 \pm 0.0032$ | $0.9652 \pm 0.0036$ | $0.9649 \pm 0.0032$ | $0.9652 \pm 0.0032$ | $0.9654 \pm 0.0030$ | $0.9648^{+0.0031}_{-0.0036}$ |
| $H_0$ | $67.38 \pm 0.48$ | $67.35^{+0.50}_{-0.56}$ | $67.38 \pm 0.50$ | $67.42 \pm 0.54$ | $67.42 \pm 0.48$ | $67.36 \pm 0.51$ |
| $100\,\omega_b$ | $2.239^{+0.012}_{-0.014}$ | $2.238 \pm 0.017$ | $2.240 \pm 0.013$ | $2.241^{+0.012}_{-0.014}$ | $2.240^{+0.010}_{-0.012}$ | $2.239 \pm 0.013$ |
| $\omega_c$ | $0.1201 \pm 0.0011$ | $0.1201 \pm 0.0012$ | $0.1201 \pm 0.0011$ | $0.1200 \pm 0.0012$ | $0.1199 \pm 0.0011$ | $0.1201 \pm 0.0012$ |
| $\tau_{reio}$ | $0.0553^{+0.0032}_{-0.0038}$ | $0.0552^{+0.0032}_{-0.0035}$ | $0.0552 \pm 0.0033$ | $0.0553 \pm 0.0032$ | $0.0553^{+0.0033}_{-0.0039}$ | $0.0554^{+0.0033}_{-0.0039}$ |
| $\ln(10^{10} A_s)$ | $3.0506 \pm 0.0080$ | $3.0503^{+0.0065}_{-0.0073}$ | $3.0506 \pm 0.0064$ | $3.0506 \pm 0.0067$ | $3.0505^{+0.0071}_{-0.0084}$ | $3.0510 \pm 0.0071$ |
| $A_{new}$ | $1.0003 \pm 0.0030$ | $1.002 \pm 0.022$ | $0.99 \pm 0.37$ | $0.996 \pm 0.045$ | $0.9999 \pm 0.0043$ | $0.99996^{+0.0019}_{-0.0023}$ |

Table 3.3: Mean values and 68% credible intervals for the minimal ΛCDM parameters plus one phenomenological amplitude, $A_{new}$, for the MCMC chains fit to the Theoretical $TT + EE + TE$ dataset. The values of the parameters used to generate the different simulations are in Table 2.1 and the priors and likelihood used are described in sections 2.3.1 and 2.3.2, respectively. The $R - 1$ parameter for all the runs was set to 0.05 and the instrumental noise is sampled but not shown.

The best constrained phenomenological amplitudes using only the $TT$ data are the Sachs-Wolfe effect, $A_{SW}$, and the doppler effect, $A_{Dop}$. This is easily understood from section 1.4 because those effects have the greatest impact on the CMB temperature power spectrum. The worst determined magnitude is the late Integrated Sachs-Wolfe effect,

$A_{lISW}$, because it dominates at low $\ell$ where cosmic variance has an important contribution which future CMB experiments are unlikely to improve as it is a consequence of having a single Universe realization. In fact, the lISW effect could not be detected using only CMB data (as shown in Figures 3.4 and 3.6) and cross-correlation with other datasets is needed. A $4\sigma$ detection was obtained from the joint cross-correlation from Planck CMB data with different large-scale structure (LSS) tracers, as radio sources from the NVSS catalogue, galaxies from the optical SDSS and the infrared WISE surveys [38].

The second worst constrained phenomenological parameter is $A_{Pol}$ because it has little effect on the temperature power spectrum. Finally, the early Integrated Sachs-Wolfe effect and the lensing effect are determined with almost the same uncertainty.

We are also interested in the correlation of the phenomenological amplitudes with the scalar amplitude, $A_s$, which could be degenerated as it rescales the whole temperature and polarization power spectra. When considering only temperature data, the greatest anti-correlation is obtained for the Sachs-Wolfe effect and the Doppler effect followed by the lensing effect, as the lensing power spectrum is proportional to $A_L$ and $A_s$ [39].

When polarization data are included, all the phenomenological parameters are better constrained. One cause of this might be the reduction of about a 50% in the uncertainty of $A_s$ because the $EE$ power spectrum is rescaled only by $A^2_{Pol}$ and $A_s$. There is a degeneracy between $A_{Pol}$ and $A_s$ when taking into account only the $EE$ power spectrum, but is broken when considering also the $TT$ spectrum as the polarization effect shifts the position of the peaks and does not rescale the spectrum as $A_s$ does. This is why when including polarization data, the polarization effect, $A_{Pol}$, transforms from being one of the worst to the best constrained parameter of the six phenomenological amplitudes of the project. Unfortunately, the late Integrated Sachs-Wolfe effect, although benefiting from polarization data, cannot be considered a detection and is the worst determined parameter.

The anti-correlation effect observed for parameters $A_{SW}$, $A_{Dop}$ and $A_L$ is still observed when polarization data is considered, however, it is reduced notably for those parameters.

Another important aspect is how including an extra parameter affects the constriction of the cosmological parameters. When using only the $TT$ data, the 68% credible intervals of the cosmological parameters stay unaffected except for the early Integrated Sachs-Wolfe effect, $A_{eISW}$, and for the polarization effect, $A_{Pol}$. If we take into consideration the $TT+EE+TE$ dataset, the eISW effect is the only one that affects the uncertainty of the cosmological parameters. The reason might be that polarization effect has an imprint in the polarization power spectra, whereas the early Integrated Sachs-Wolfe effect affects the temperature power spectrum only.

Checking the results obtained in Table 3.2 with [22], an excellent agreement between them has been observed in terms of 68% credible intervals. This is a successful robustness test that allows to state that this study, although assuming a simplified situation, yields to realistic results. For the $TT+EE+TE$ dataset, we can only check the results obtained for three phenomenological parameters: $A_L$ from [37] and $A_{eISW}$ and $A_{lISW}$ from [20]. If we compare the constrains obtained in Table 3.3 for the first two parameters, they are compatible with the results of these articles, and the $A_{lISW}$ cannot be considered a detection which is the same result obtained in [20].

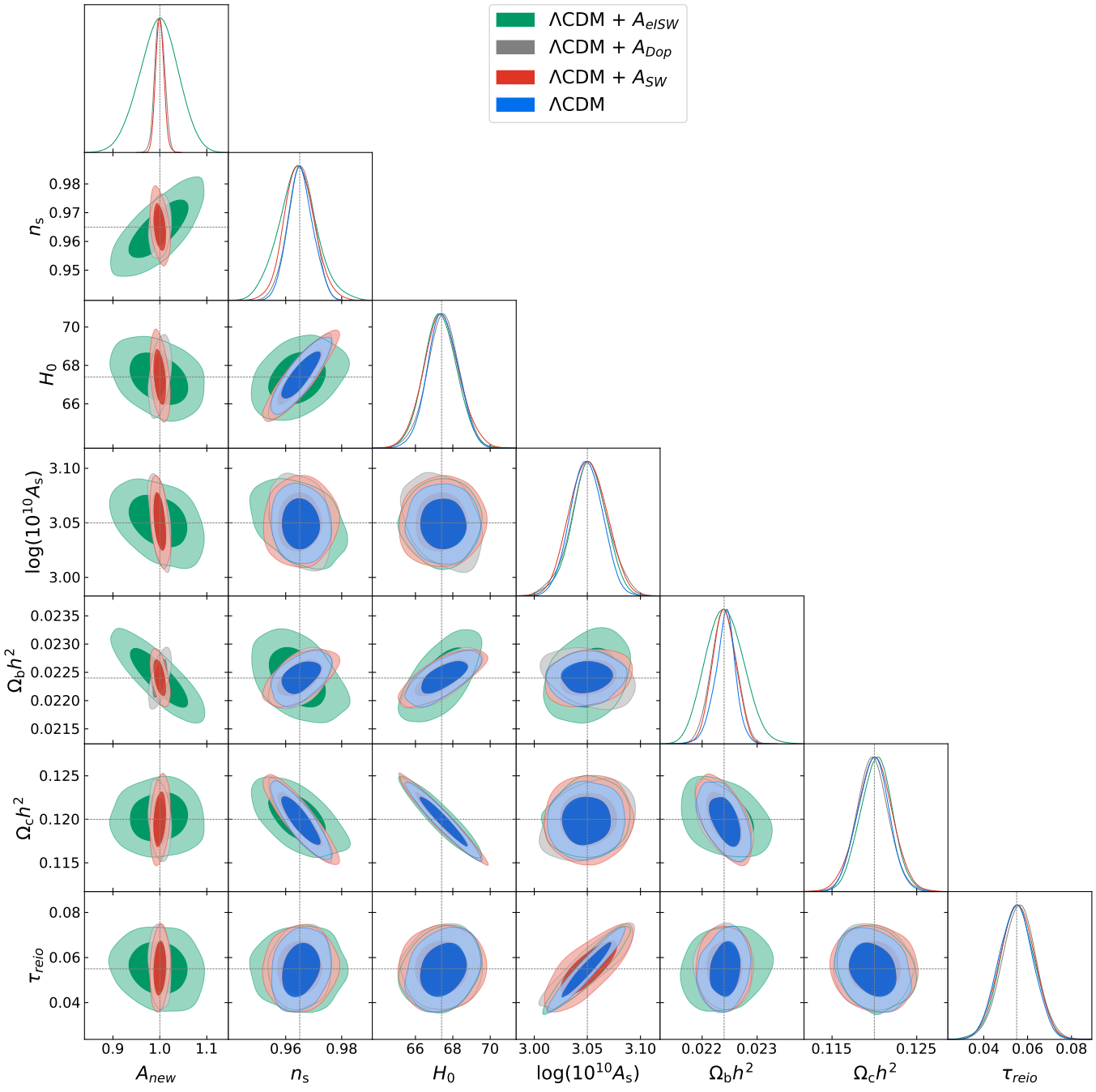


Figure 3.3: *Plots of the marginalized posterior comparison of ΛCDM, ΛCDM + $A_{eISW}$, ΛCDM + $A_{Dop}$ and ΛCDM + $A_{SW}$ fits using the temperature spectrum, TT, from the Theoretical dataset. The phenomenological amplitude is named $A_{new}$ in the plot and the instrumental noise, although sampled, is not plotted. The contours display the 68% and 95% limits and the black dotted lines represent the original parameter values used in the simulations. The $R-1$ parameter for these two runs was set to 0.05. The priors and likelihoods used in this plot are described in detail in sections 2.3.1 and 2.3.2, respectively.*

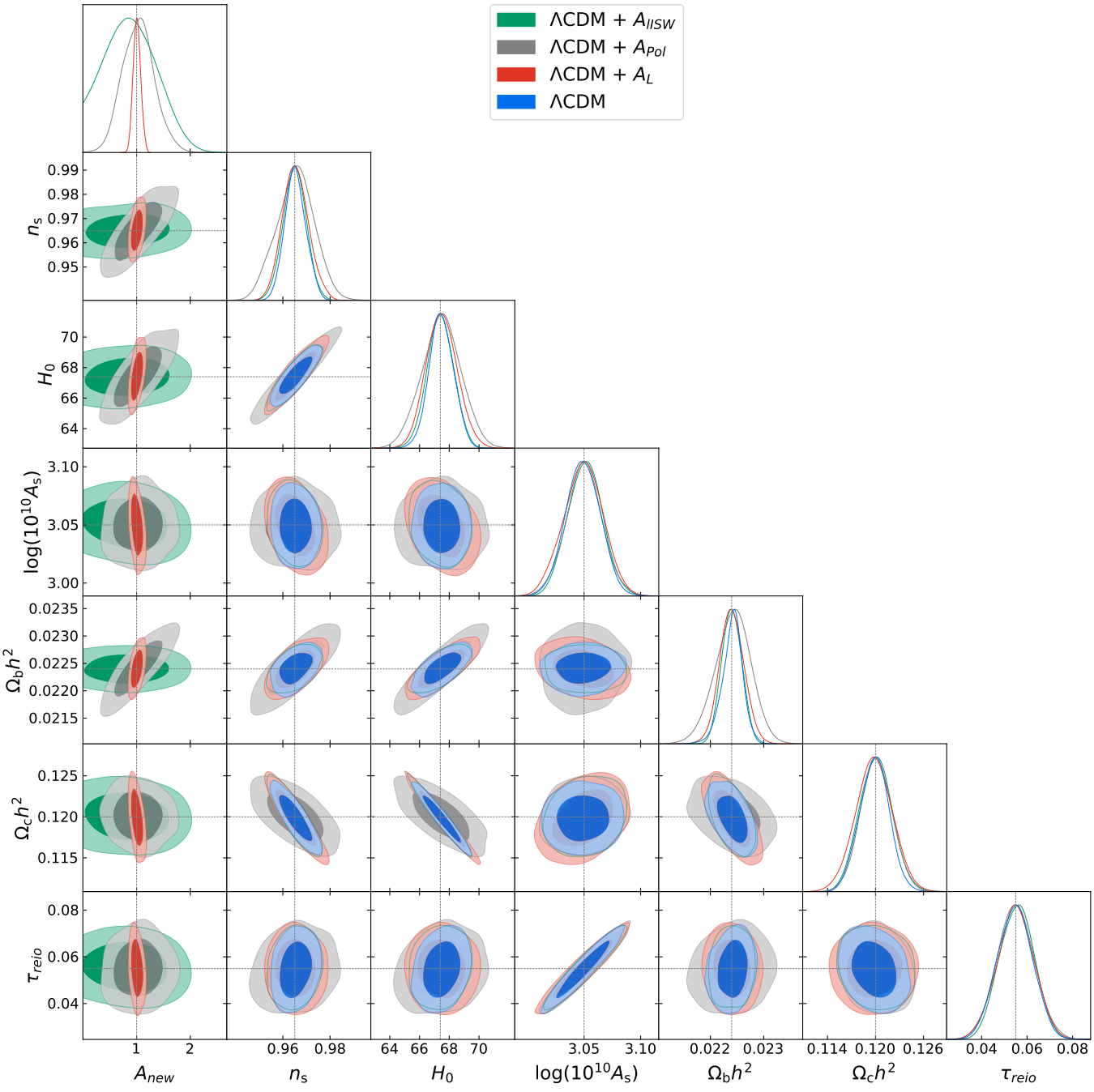


Figure 3.4: *Plots of the marginalized posterior comparison of ΛCDM, ΛCDM + $A_{lISW}$, ΛCDM + $A_{Pol}$ and ΛCDM + $A_L$ fits using the temperature spectrum, TT, from the Theoretical dataset. The phenomenological amplitude is named $A_{new}$ in the plot and the instrumental noise, although sampled, is not plotted. The contours display the 68% and 95% limits and the black dotted lines represent the original parameter values used in the simulations. The $R-1$ parameter for these two runs was set to 0.05. The priors and likelihoods used in this plot are described in detail in sections 2.3.1 and 2.3.2, respectively.*

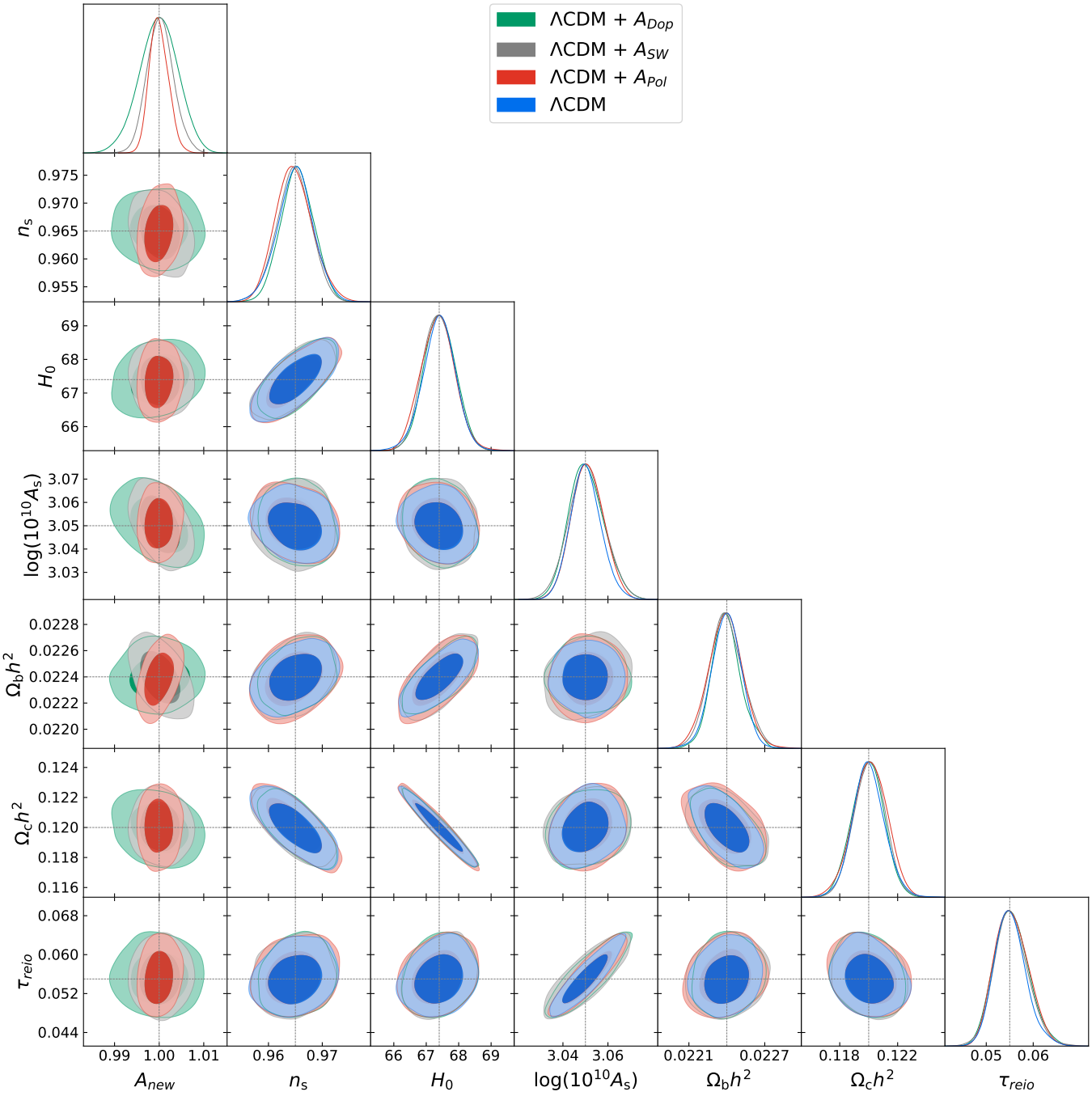


Figure 3.5: *Plots of the marginalized posterior comparison of ΛCDM, ΛCDM + $A_{Dop}$, ΛCDM + $A_{SW}$ and ΛCDM + $A_{Pol}$ fits using the temperature and polarization power spectra, $TT + EE + TE$, from the Theoretical dataset. The phenomenological amplitude is named $A_{new}$ in the plot and the instrumental noise, although sampled, is not plotted. The contours display the 68% and 95% limits and the black dotted lines represent the original parameter values used in the simulations. The $R - 1$ parameter for these two runs was set to 0.05. The priors and likelihoods used in this plot are described in detail in sections 2.3.1 and 2.3.2, respectively.*

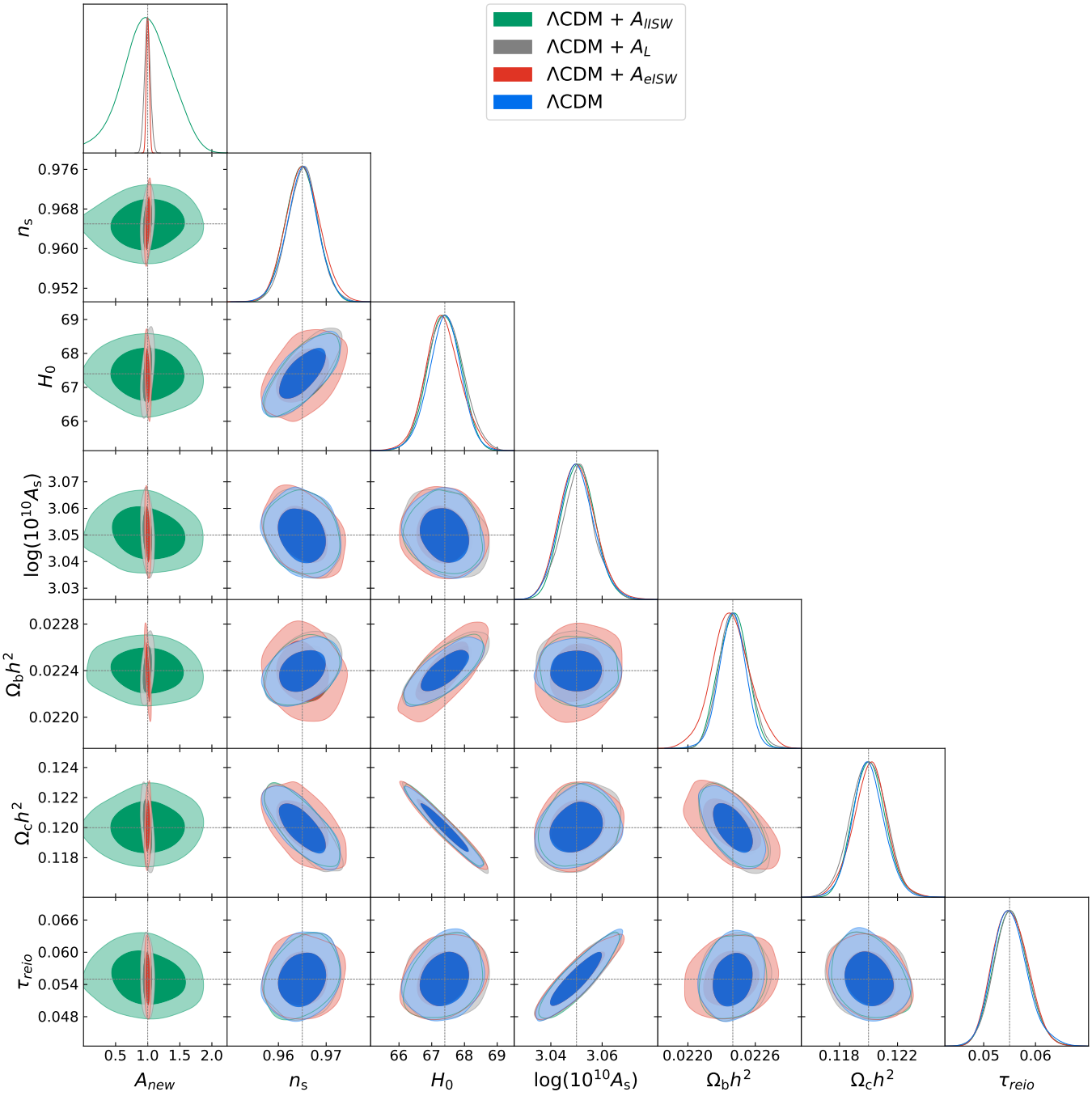


Figure 3.6: *Plots of the marginalized posterior comparison of ΛCDM, ΛCDM + $A_{lISW}$, ΛCDM + $A_L$ and ΛCDM + $A_{eISW}$ fits using the temperature and polarization power spectra, TT+EE+TE, from the Theoretical dataset. The phenomenological amplitude is named $A_{new}$ in the plot and the instrumental noise, although sampled, is not plotted. The contours display the 68% and 95% limits and the black dotted lines represent the original parameter values used in the simulations. The $R-1$ parameter for these two runs was set to 0.05. The priors and likelihoods used in this plot are described in detail in sections 2.3.1 and 2.3.2, respectively.*

## 3.3 Fitting ΛCDM plus several phenomenological amplitudes

In this section we analyse different combinations of phenomenological amplitudes in addition to the ΛCDM cosmological parameters. The objective is to study the capability of Planck experiment to recover different combinations of parameters. Logically, only a few of them could be run due to the high computational cost. First, we have tested combinations of all the cosmological parameters plus two or three phenomenological amplitudes. The results can be seen in Table 3.4 and in Figures 3.7, 3.8 and 3.9.

| | $TT$ | | | $TT+EE+TE$ | | |
|---|---|---|---|---|---|---|
| Param. | $A_{eISW}+A_L$ | $A_{eISW}+A_{lISW}$ | $A_{SW}+A_{eISW}+A_{Dop}$ | $A_{eISW}+A_L$ | $A_{eISW}+A_{lISW}$ | $A_{SW}+A_{eISW}+A_{Dop}$ |
| $n_s$ | $0.9647^{+0.0057}_{-0.0070}$ | $0.9645 \pm 0.0072$ | $0.9656^{+0.0072}_{-0.0064}$ | $0.9648 \pm 0.0037$ | $0.9651 \pm 0.0035$ | $0.9649 \pm 0.0039$ |
| $H_0$ | $67.4 \pm 1.1$ | $67.37 \pm 0.90$ | $67.5 \pm 1.2$ | $67.36 \pm 0.59$ | $67.39^{+0.48}_{-0.56}$ | $67.41 \pm 0.54$ |
| $100\,\omega_b$ | $2.241^{+0.042}_{-0.036}$ | $2.241 \pm 0.035$ | $2.240 \pm 0.042$ | $2.240 \pm 0.018$ | $2.240 \pm 0.017$ | $2.240 \pm 0.018$ |
| $\omega_c$ | $0.1200 \pm 0.0023$ | $0.1201 \pm 0.0020$ | $0.1199 \pm 0.0024$ | $0.1201 \pm 0.0012$ | $0.1200^{+0.0012}_{-0.0011}$ | $0.1200 \pm 0.0012$ |
| $\tau_{reio}$ | $0.0544 \pm 0.0080$ | $0.0549 \pm 0.0077$ | $0.0562 \pm 0.0081$ | $0.0556^{+0.0031}_{-0.0040}$ | $0.0554^{+0.0030}_{-0.0034}$ | $0.0555 \pm 0.0034$ |
| $\ln(10^{10}A_s)$ | $3.049^{+0.018}_{-0.016}$ | $3.050 \pm 0.016$ | $3.039 \pm 0.078$ | $3.0515^{+0.0071}_{-0.0081}$ | $3.0509 \pm 0.0068$ | $3.0506 \pm 0.0080$ |
| $A_{eISW}$ | $0.998^{+0.037}_{-0.045}$ | $0.998 \pm 0.042$ | $1.010 \pm 0.067$ | $1.001^{+0.023}_{-0.021}$ | $1.000 \pm 0.022$ | $1.000 \pm 0.022$ |
| $A_{lISW}$ | – | $< 1.12$ | – | – | $0.93 \pm 0.35$ | – |
| $A_{SW}$ | – | – | $1.007 \pm 0.039$ | – | – | $1.0001 \pm 0.0034$ |
| $A_L$ | $0.995 \pm 0.075$ | – | – | $1.004 \pm 0.046$ | – | – |
| $A_{Dop}$ | – | – | $1.008 \pm 0.044$ | – | – | $1.0003 \pm 0.0053$ |

Table 3.4: Mean values and 68% credible intervals for the minimal ΛCDM parameters plus several phenomenological amplitudes for the MCMC chains fit to the Theoretical $TT$ and $TT+EE+TE$ datasets. The values of the parameters used to generate the different simulations are in Table 2.1 and the priors and likelihood used are described in sections 2.3.1 and 2.3.2, respectively. The $R-1$ parameter for all the runs was set to 0.05, except for the $TT$ ΛCDM $A_{SW}+A_{eISW}+A_{Dop}$ run whose $R-1$ value was set to 0.1. The instrumental noise is sampled but not shown.

From Figure 3.7 it is possible to conclude that the lensing effect and the eISW effect could be constrained together and, as expected, all of the parameters considered are better constrained when taking the polarization spectra into account. The combination of the early and late ISW is studied in Figure 3.8 from which we can state that using only $TT$ data the late ISW effect cannot be constrained at $1\sigma$ level. However, including the late ISW effect does not affect the constriction on the early ISW effect.

The most interesting information is obtained from Figure 3.9, where the combination of $A_{SW}$, $A_{eISW}$ and $A_{Dop}$ is studied. When using only $TT$ data, $\ln(10^{10}A_s)$ is highly anti-correlated with the three phenomenological amplitudes. As explained in [22], increasing these three phenomenological amplitudes $A_{SW}$, $A_{eISW}$ and $A_{Dop}$ has a similar effect to increasing $A_s$. This explains why $\ln(10^{10}A_s)$ is slightly below the original value used in the simulations and the phenomenological amplitudes $A_{SW}$, $A_{eISW}$ and $A_{Dop}$ are above their real value and in exactly the same way the three of them. To understand this result one has to take into account that the late ISW effect has importance only at low $\ell$ and the polarization effect has a very little contribution to the final $TT$ spectrum, so both effects can be neglected. For that reason, the temperature power spectrum is modulated effectively by a product of the scalar amplitude, $A_s$, and a single phenomenological amplitude which rescales all the physical contributions of the temperature transfer function. Consequently, the combination of $A_{SW}$, $A_{eISW}$ and $A_{Dop}$ mimics the effect of $A_s$. Even more fascinating is the fact that when polarization data is included the degeneration is broken. The reason is that the $EE$ power spectrum does not depend on the Sachs-Wolfe effect, the early ISW effect and the Doppler effect as follows from equations (1.44) and (1.46), so $A_s$ can be fully determined.

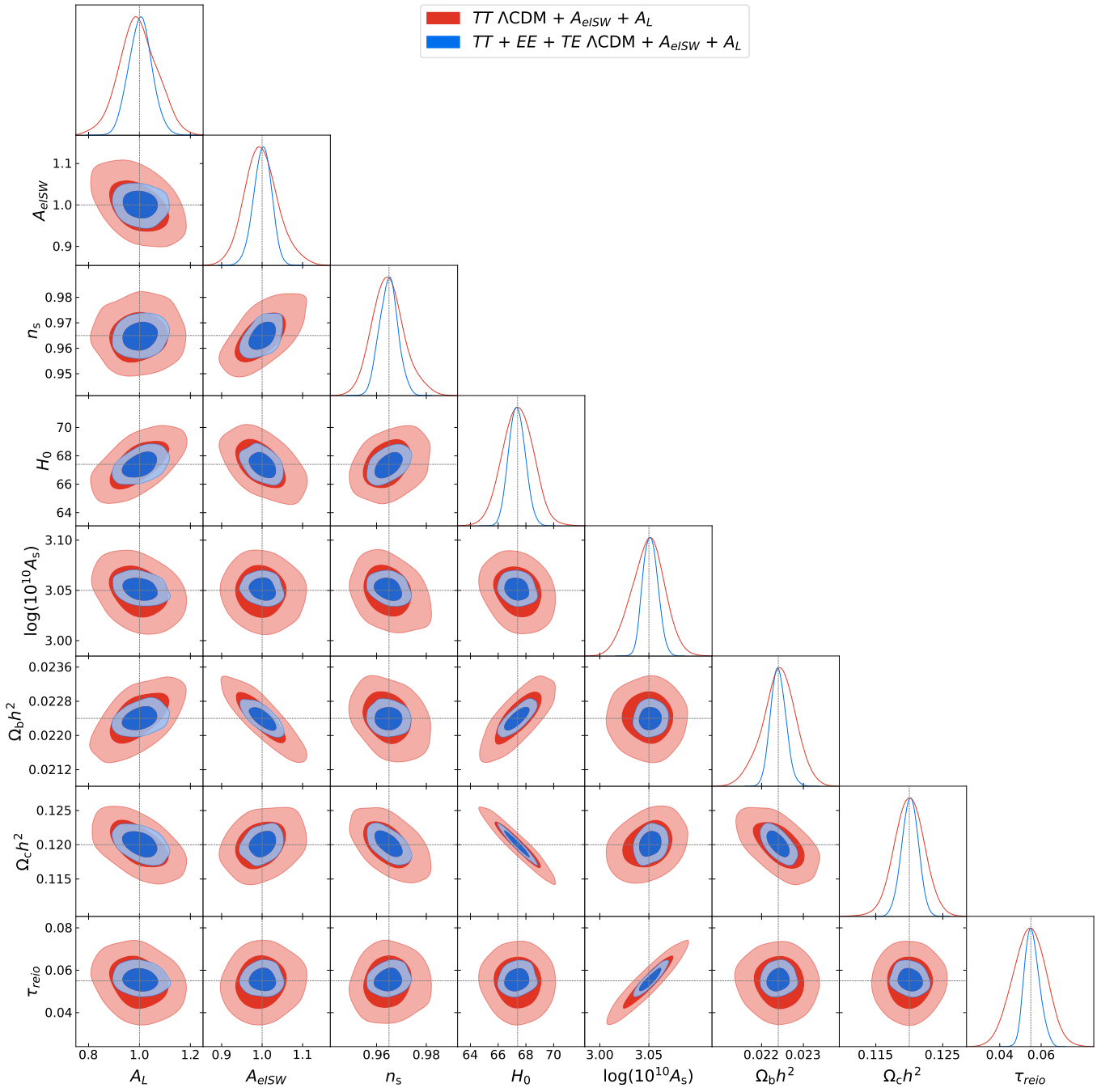


Figure 3.7: *Plots of the marginalized posterior comparison of $\Lambda CDM + A_{eISW} + A_L$ fits using the temperature data, $TT$, and the temperature and polarization data, $TT + EE + TE$, from the Theoretical dataset. The black dotted lines represent the original parameter values and the instrumental noise, although sampled, is not plotted. The contours display the 68% and 95% limits. The $R - 1$ parameter for these two runs was set to 0.05. The priors and likelihoods used in this plot are described in detail in sections 2.3.1 and 2.3.2, respectively.*

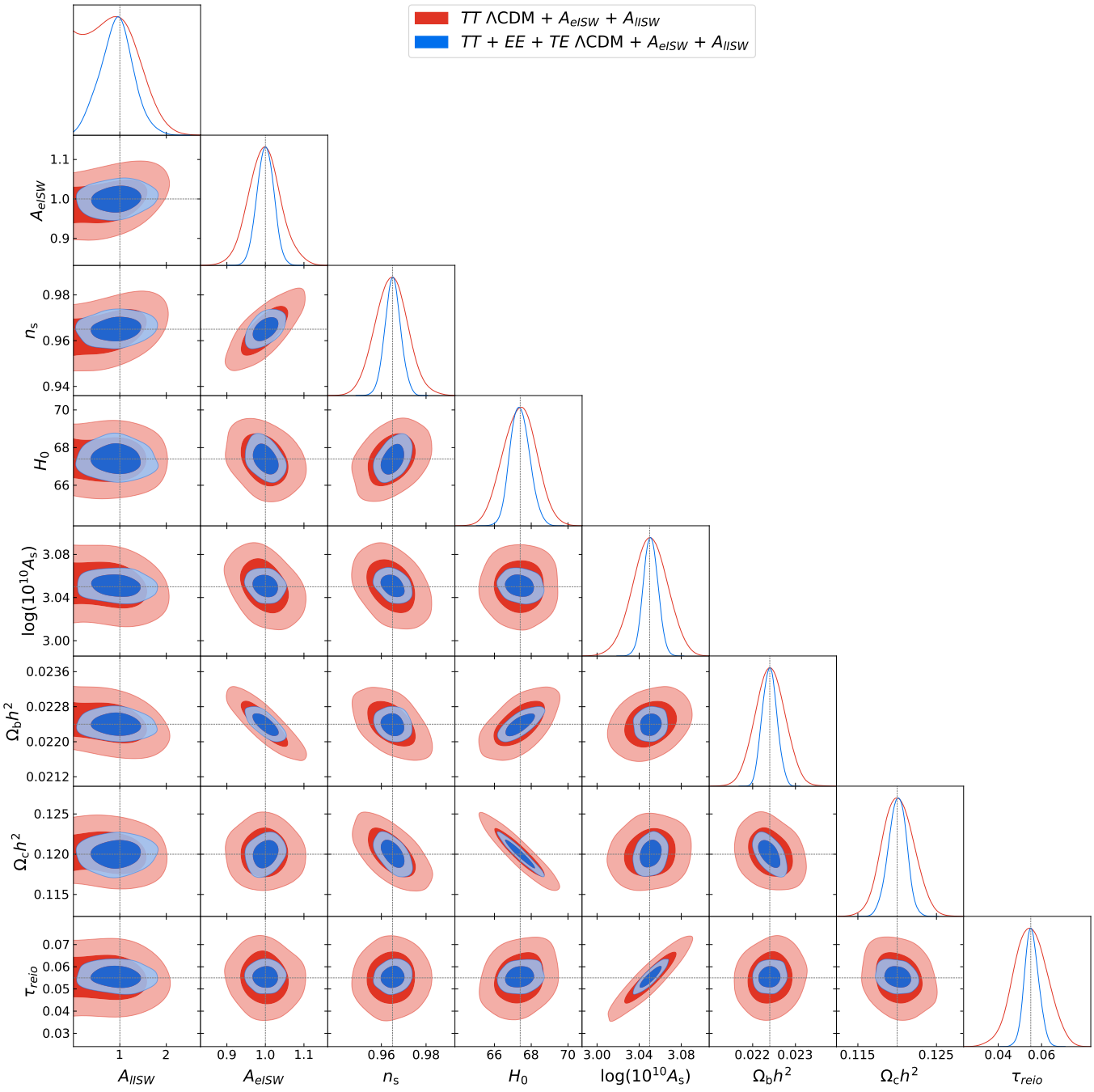


Figure 3.8: *Plots of the marginalized posterior comparison of $\Lambda CDM + A_{eISW} + A_{lISW}$ fits using the temperature data, $TT$, and the temperature and polarization data, $TT + EE + TE$, from the Theoretical dataset. The black dotted lines represent the original parameter values and the instrumental noise, although sampled, is not plotted. The contours display the 68% and 95% limits. The $R - 1$ parameter for these two runs was set to 0.05. The priors and likelihoods used in this plot are described in detail in sections 2.3.1 and 2.3.2, respectively.*

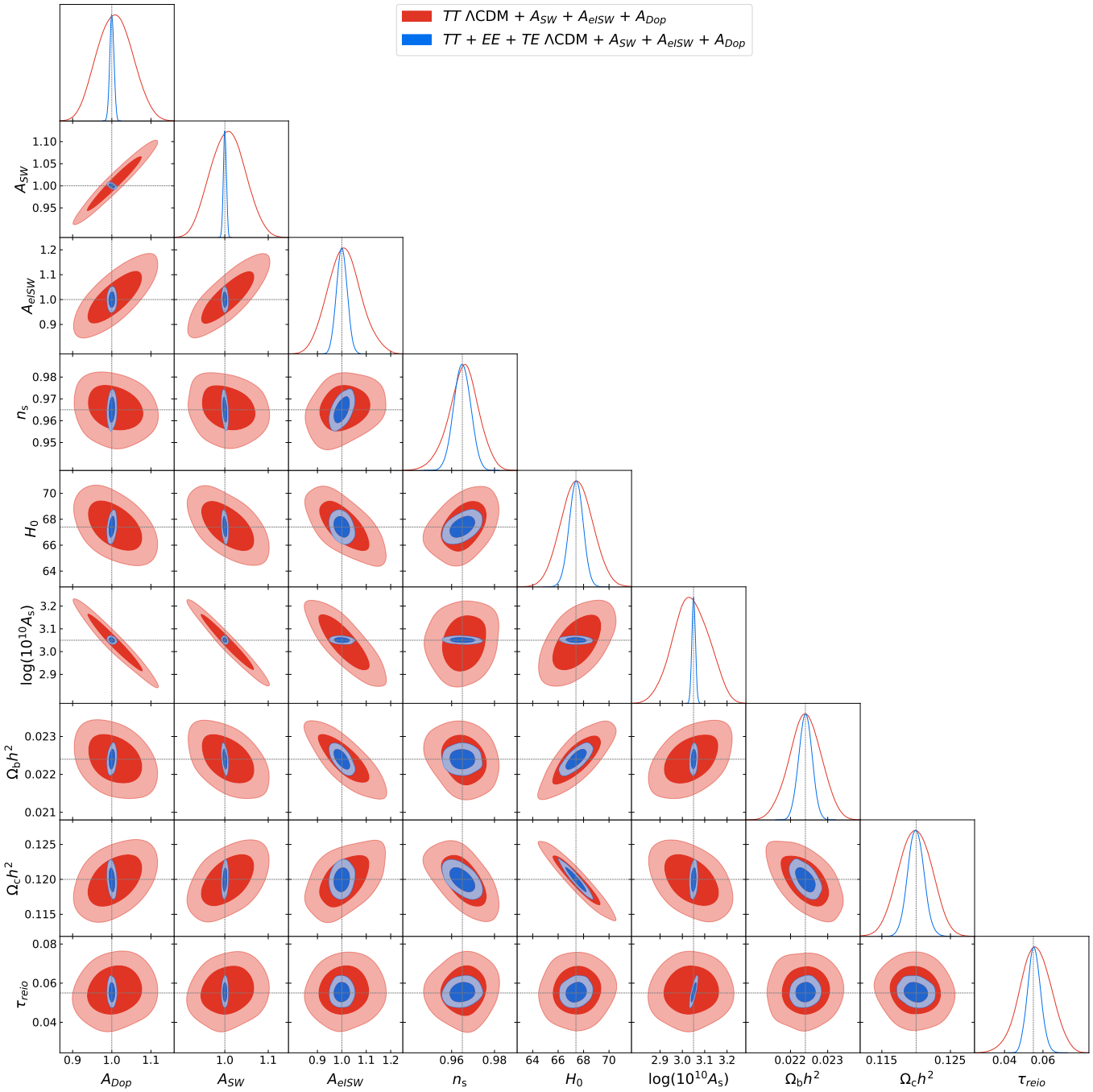


Figure 3.9: *Plots of the marginalized posterior comparison of ΛCDM + $A_{SW}$ + $A_{eISW}$ + $A_{Dop}$ fits using the temperature data, TT, and the temperature and polarization data, TT + EE + TE, from the Theoretical dataset. The black dotted lines represent the original parameter values and the instrumental noise, although sampled, is not plotted. The contours display the 68% and 95% limits. The R − 1 parameter for the TT run was set to 0.1 due to convergence problems and for the TT + EE + TE run was set to 0.05. The priors and likelihoods used in this plot are described in detail in sections 2.3.1 and 2.3.2, respectively.*

At this point, a natural question would be: is it possible to constrain all the ΛCDM parameters and all the phenomenological amplitudes simultaneously? The answer is no. As shown in appendix B, when using only temperature, $TT$, or temperature and polarization, $TT+EE+TE$, datasets, the phenomenological amplitude $A_L$ is unconstrained. The cause, as explained in [22], is the lensing power spectrum, which is proportional to $A_s$ and $A_L$. If the uncertainty of $A_s$ is high and the mean value is shifted from the original value, the uncertainty of $A_L$ would be also high and the mean value would also be shifted, but in the opposite direction of $A_s$. Those two effects cause that we cannot recover successfully the lensing effect.

Not being able to constrain the lensing effect using only the temperature power spectrum is not surprising at all because Figure 3.9 proves that a high uncertainty in $\ln(10^{10}A_s)$ is obtained due to the combined action of $A_{SW}$, $A_{eISW}$ and $A_{Dop}$. But this anti-correlation was broken when the polarization power spectra is included. The Figure 3.10 and the Table 3.5 have the clue to what is happening here. When the polarization effect, $A_{Pol}$, is excluded in the MCMC fit, we are able to constrain all the cosmological and phenomenological parameters successfully, except the late ISW. Otherwise, when the excluded parameter is the lensing effect, strong anti-correlations between the phenomenological amplitudes $A_{SW}$, $A_{eISW}$, $A_{Dop}$ and $A_{Pol}$ and the scalar amplitude $\ln(10^{10}A_s)$ are observed. Curiously, $A_{SW}$, $A_{eISW}$, $A_{Dop}$ were not anti-correlated with $A_s$ because $EE$ power spectra help to constrain the scalar amplitude as the $EE$ spectrum does not depend on the $A_{SW}$, $A_{eISW}$ and $A_{Dop}$ parameters. The same happens with $A_s$ and $A_{Pol}$. This two parameters are extremely anti-correlated in the $EE$ power spectrum, but when the temperature power spectrum is considered, the degeneration disappears. The combined action of these four phenomenological amplitudes provokes the existing anti-correlation with $A_s$.

Notice that no plots with more than three parameters using the temperature power spectrum have been generated due to the difficulties to achieve convergence in the $TT$ ΛCDM $A_{SW}$ + $A_{eISW}$ + $A_{Dop}$ run and the anti-correlation observed.

| Param. | $A_{SW}$ + $A_{eISW}$ + $A_{lISW}$ + $A_{Dop}$ + $A_{Pol}$ | $A_{SW}$ + $A_{eISW}$ + $A_{lISW}$ + $A_{Dop}$ + $A_L$ |
|---|---|---|
| $n_s$ | $0.9649 \pm 0.0037$ | $0.9651 \pm 0.0040$ |
| $H_0$ | $67.35 \pm 0.59$ | $67.42 \pm 0.61$ |
| $100\,\omega_b$ | $2.240 \pm 0.019$ | $2.241 \pm 0.019$ |
| $\omega_c$ | $0.1201 \pm 0.0012$ | $0.1200 \pm 0.0013$ |
| $\tau_{reio}$ | $0.0556 \pm 0.0037$ | $0.0554^{+0.0031}_{-0.0037}$ |
| $\ln(10^{10}A_s)$ | $3.028 \pm 0.057$ | $3.0508 \pm 0.0080$ |
| $A_{eISW}$ | $1.014^{+0.038}_{-0.045}$ | $0.999 \pm 0.022$ |
| $A_{lISW}$ | $0.99^{+0.42}_{-0.36}$ | $0.93^{+0.41}_{-0.36}$ |
| $A_{SW}$ | $1.012 \pm 0.028$ | $1.0002 \pm 0.0038$ |
| $A_{Dop}$ | $1.014 \pm 0.034$ | $0.9995 \pm 0.0060$ |
| $A_L/A_{Pol}$ | $1.012 \pm 0.029$ | $1.005 \pm 0.055$ |

Table 3.5: Mean values and 68% credible intervals ΛCDM + $A_{SW}$ + $A_{eISW}$ + $A_{lISW}$ + $A_{Dop}$ + $A_{Pol}$ and ΛCDM + $A_{SW}$ + $A_{eISW}$ + $A_{lISW}$ + $A_{Dop}$ + $A_L$ for the MCMC chains fit to the Theoretical $TT+EE+TE$ dataset. The values of the parameters used to generate the different simulations are in Table 2.1 and the priors and likelihood used are described in sections 2.3.1 and 2.3.2, respectively. The $R-1$ parameter for all the runs was set to 0.05. The instrumental noise is sampled but not shown.

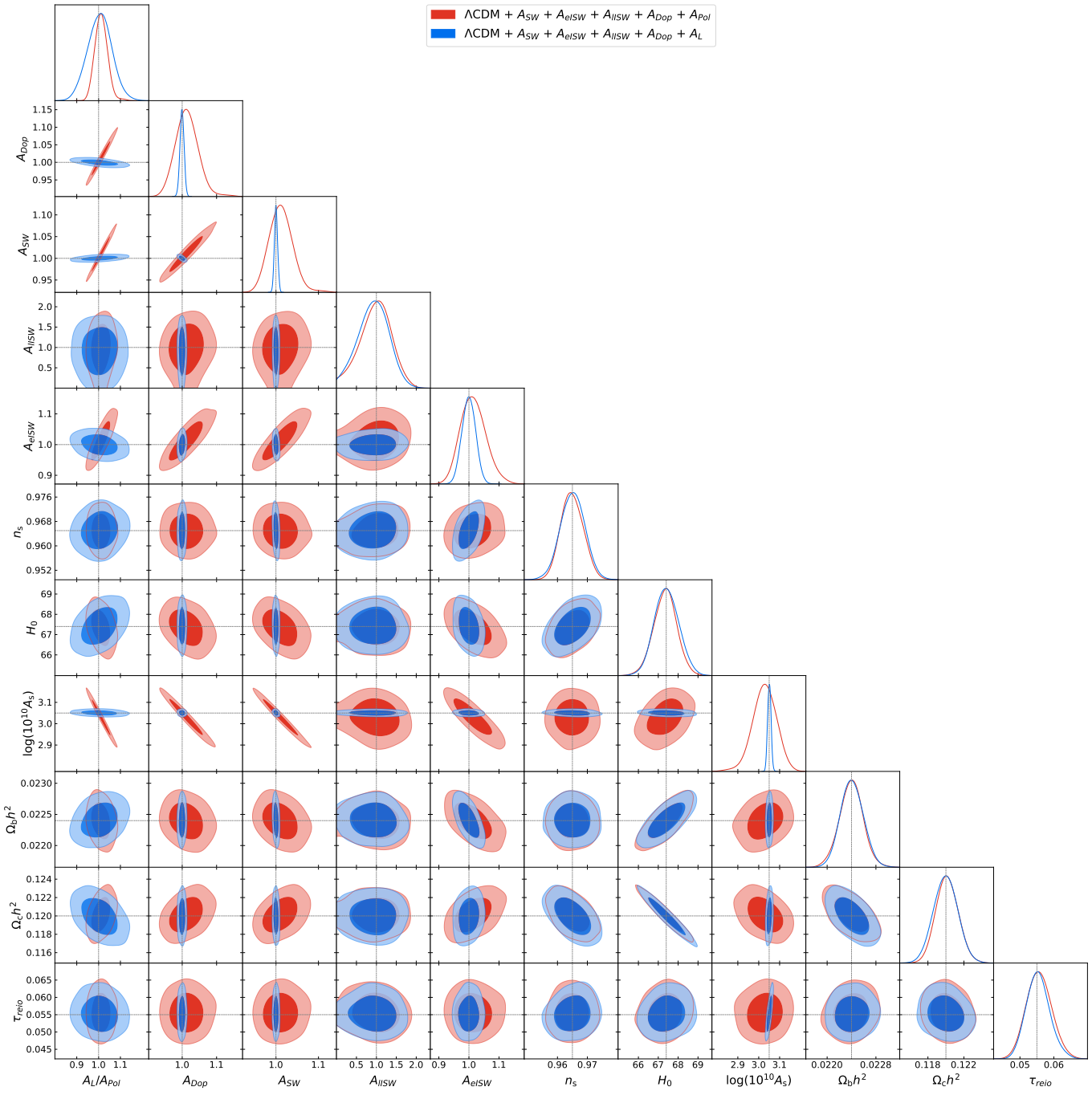


Figure 3.10: *Plots of the marginalized posterior comparison of ΛCDM + $A_{SW}$ + $A_{eISW}$ + $A_{lISW}$ + $A_{Dop}$ + $A_{Pol}$ and ΛCDM + $A_{SW}$ + $A_{eISW}$ + $A_{lISW}$ + $A_{Dop}$ + $A_L$ fits using the temperature and polarization power spectra, $TT+EE+TE$, from the Theoretical dataset. The phenomenological amplitude named $A_L/A_{Pol}$ in the plot represents either the lensing effect or the polarization effect. The instrumental noise, although sampled, is not plotted. The black dotted lines represent the original parameter values and the contours display the 68% and 95% limits. The $R-1$ parameter for these two runs was set to 0.05. The priors and likelihoods used in this plot are described in detail in sections 2.3.1 and 2.3.2, respectively.*

# Chapter 4

# Conclusions and future work

In this work, we introduced phenomenological amplitudes to weight the different physical contributions to the CMB angular power spectra and tested how well Planck experiment is able to constrain different combinations of cosmological parameters and phenomenological amplitudes using simulations of the CMB power spectra. To do so, `CLASS` code was modified to include the new parameters in the calculation of the CMB angular power spectra. Also, the software used for MCMC sampling, called `Cobaya`, was adapted to execute correctly the modifications introduced in `CLASS`. This work is original and scientifically relevant as it is the first time an integral analysis using temperature and polarization CMB simulated data is used to detect the Sachs-Wolfe effect, the early and late Integrated Sachs-Wolfe effect, the Doppler effect, the polarization effect and the lensing effect.

The simulations used are in agreement with the results obtained in Planck experiment [37], in particular when we use only the temperature power spectrum. If temperature and polarization data are used, the simulations are not so realistic because the likelihood considered in this work is simpler than the likelihood used in Planck experiment, thus assuming a simplified experimental framework. As a consequence, the scalar amplitude uncertainty decreases significantly when temperature and polarization data are considered. However, this only affects to the uncertainties of specific parameters not to the conclusions of this work.

The results obtained in this project show that the constrains imposed in the cosmological and phenomenological parameters are tighten when temperature and polarization data are used. Also, a degeneracy between the scalar amplitude $A_s$ and the six phenomenological amplitudes has been observed which made impossible to recover all the parameters properly. This degeneracy could be partially broken when temperature and polarization data are considered, in particular for the combination $\Lambda$CDM + $A_{SW}$ + $A_{eISW}$ + $A_{Dop}$. However, with the combination of $\Lambda$CDM + $A_{SW}$ + $A_{eISW}$ + $A_{Dop}$ + $A_{Pol}$ is explored, strong anti-correlations between the phenomenological amplitudes and $A_s$ are observed, even when temperature and polarization data is used.

Another important aspect which has been observed in this work is a shift in the original values of $A_s$ and the phenomenological amplitudes for certain combinations of parameters, as for example the $\Lambda$CDM + $A_{SW}$ + $A_{eISW}$ + $A_{Dop}$ fit using only temperature data. In [22], this fit was performed with Planck temperature data and the same type of shifts were observed.

The logical continuation of this project is to use real Planck data, which would allow to check if the ΛCDM model is correctly considering each physical contribution. The analysis presented in this work is a good approximation, but we have assumed a simplified experimental scheme. For instance, Planck maps are masked, i.e., a portion of the sky (approximately 30 % for Planck experiment) is removed due to the presence of regions of the sky where foreground emission is expected to be substantial, for example, the Milky Way. Masking the sky introduces correlations between $C_\ell$, which has not been considered in this work. Also, as explained earlier, there are systematics which have not been taken into account. Fitting to real Planck data would allow to perform consistency checks of ΛCDM model which might be the way to resolve cosmological tensions.

# Bibliography


[1] D. J. Fixsen. The temperature of the Cosmic Microwave Background. *The Astrophysical Journal*, 707(2):916–920, 2009.

[2] R Durrer. The cosmic microwave background: the history of its experimental investigation and its significance for cosmology. *Classical and Quantum Gravity*, 32(12), 2015.

[3] S. Dodelson. *Modern Cosmology*. Academic Press, 2003.

[4] R. Durrer. *The Cosmic Microwave Background*. Cambridge University Press, 2008.

[5] S. Weinberg. *Cosmology*. OUP Oxford, 2008.

[6] W. Hu and S. Dodelson. Cosmic Microwave Background Anisotropies. *Annual Review of Astronomy and Astrophysics*, 40(1):171–216, 2002.

[7] A. Challinor. CMB anisotropy science: a review. *Proceedings of the International Astronomical Union*, 8(S288):42–52, 2012.

[8] P. Cabella and M. Kamionkowski. Theory of Cosmic Microwave Background Polarization. *arXiv*, 2008.

[9] A. Kosowsky. Cosmic Microwave Background Polarization. *Annals of Physics*, 246(1):49–85, Feb 1996.

[10] D. Baumann et al. Probing Inflation with CMB Polarization. *AIP Conference Proceedings*, pages 10–120, 06 2009.

[11] M. Zaldarriaga. Cosmic Microwave Background Polarization Experiments. *The Astrophysical Journal*, 503(1):1–15, aug 1998.

[12] M. Zaldarriaga and U. Seljak. All-sky analysis of polarization in the microwave background. *Physical Review D*, 55(4):1830–1840, Feb 1997.

[13] S. Das, S. Mitra, and S. Paulson. Effect of noncircularity of experimental beam on CMB parameter estimation. *Journal of Cosmology and Astroparticle Physics*, 2015(03):048–048, 2015.

[14] A. Challinor et al. All-sky convolution for polarimetry experiments. *Physical Review D*, 62(12), Nov 2000.

[15] M. Kamionkowski, A. Kosowsky, and A. Stebbins. Statistics of cosmic microwave background polarization. *Physical Review D*, 55(12):7368–7388, 1997.

[16] L. Knox. Determination of inflationary observables by cosmic microwave background anisotropy experiments. *Physical Review D*, 52(8):4307–4318, 1995.

[17] L. Verde. A practical guide to Basic Statistical Techniques for Data Analysis in Cosmology. *arXiv*, 2008.

[18] M. Bucher. Physics of the cosmic microwave background anisotropy. *International Journal of Modern Physics D*, 24(02), Feb 2015.

[19] W. Hu and M. White. CMB anisotropies: Total angular momentum method. *Physical Review D*, 56(2):596–615, Jul 1997.

[20] G. Cabass et al. Constraints on the Early and Late Integrated Sachs-Wolfe effects from the Planck 2015 Cosmic Microwave Background Anisotropies in the angular power spectra. *Physical Review D*, 92(6), Sep 2015.

[21] J. Lesgourgues and T. Tram. Fast and accurate CMB computations in non-flat FLRW universes. *Journal of Cosmology and Astroparticle Physics*, 2014(09):032–032, Sep 2014.

[22] J.A. Kable et al. Deconstructing the Planck TT Power Spectrum to Constrain Deviations from ΛCDM. *The Astrophysical Journal*, 905(2):164, Dec 2020.

[23] J. Lesgourgues. Cosmological Perturbations. *arXiv*, 2013.

[24] D. Blas, J. Lesgourgues, and T. Tram. The Cosmic Linear Anisotropy Solving System (CLASS). Part II: Approximation schemes. *Journal of Cosmology and Astroparticle Physics*, 2011(07):034–034, Jul 2011.

[25] J. Lesgourgues. The Cosmic Linear Anisotropy Solving System (CLASS) I: Overview. *arXiv*, 2011.

[26] A. Zonca et al. healpy: equal area pixelization and spherical harmonics transforms for data on the sphere in Python. *Journal of Open Source Software*, 4(35):1298, March 2019.

[27] K. M. Górski et al. HEALPix: A Framework for High-Resolution Discretization and Fast Analysis of Data Distributed on the Sphere. *The Astrophysical Journal*, 622:759–771, April 2005.

[28] Planck Collaboration. Planck 2018 results. *Astronomy & Astrophysics*, 641, Sep 2020.

[29] M.P. Hobson et al. *Bayesian Methods in Cosmology.* Cambridge University Press, 2009.

[30] J. R. Bond, A. H. Jaffe, and L. Knox. Radical Compression of Cosmic Microwave Background Data. *The Astrophysical Journal*, 533(1):19–37, Apr 2000.

[31] R. Trotta. Bayesian Methods in Cosmology. *arXiv*, 2017.

[32] J. Torrado and A Lewis. Cobaya: code for Bayesian analysis of hierarchical physical models. *Journal of Cosmology and Astroparticle Physics*, 2021(05):057, May 2021.

[33] A. Lewis and S. Bridle. Cosmological parameters from CMB and other data: A Monte Carlo approach. *Physical Review D*, 66(10), Nov 2002.

[34] A. Lewis. Efficient sampling of fast and slow cosmological parameters. *Physical Review D*, 87(10), May 2013.

[35] R.M. Neal. Taking Bigger Metropolis Steps by Dragging Fast Variables. *arXiv Mathematics e-prints*, February 2005.

[36] A Lewis. GetDist: a Python package for analysing Monte Carlo samples. *arXiv*, 2019.

[37] Planck Collaboration. Planck 2018 results. *Astronomy & Astrophysics*, 641:A6, Sep 2020.

[38] Planck Collaboration. Planck 2015 results. XXI. The integrated Sachs-Wolfe effect. *Astronomy & Astrophysics*, 594:A21, Sep 2016.

[39] A. Lewis and A. Challinor. Weak gravitational lensing of the CMB. *Physics Reports*, 429(1):1–65, Jun 2006.

# Appendix A

# Cosmological parameters

The effect of varying the cosmological parameters is considered in this appendix for a complete explanation on how the variation of each of the parameters considered in this project affect the CMB power spectra. For this reason, the six cosmological parameters are plotted in Figures A.1-A.6.

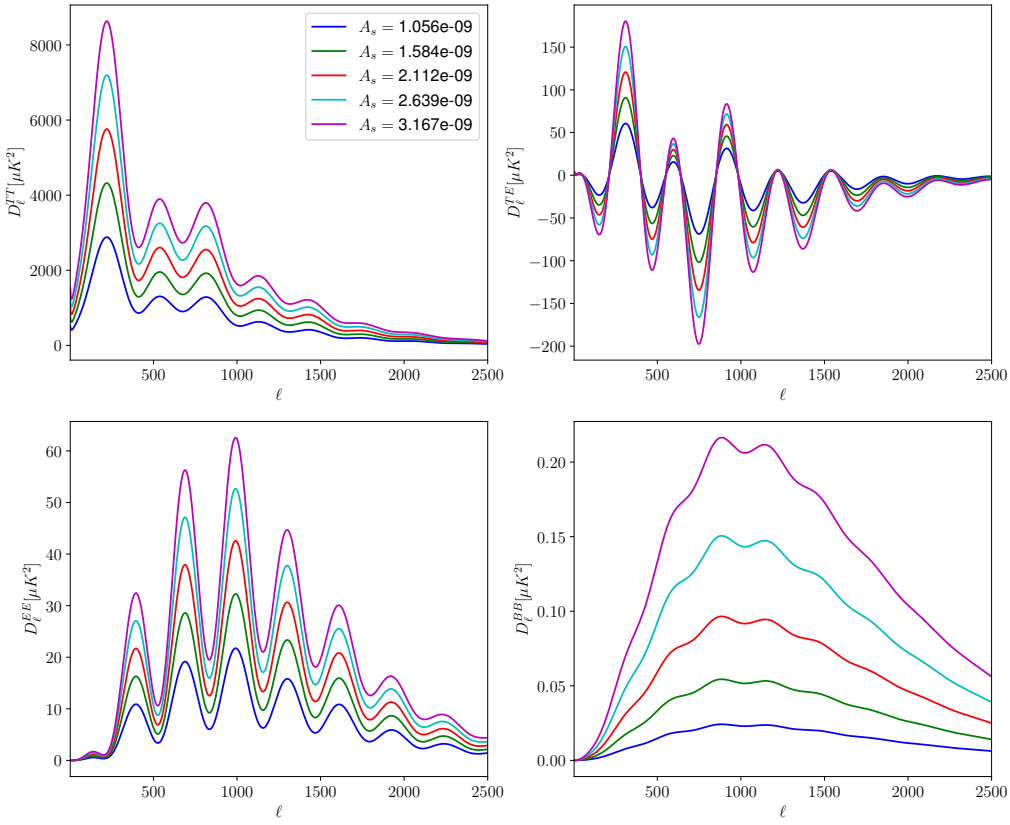


Figure A.1: *Plots of the impact of varying the $A_s$ parameter in the temperature and polarization power spectra. The red line correspond to the power spectra predicted by $\Lambda CDM$ model for the best fit parameters from Planck mission. All plots have the same legend.*

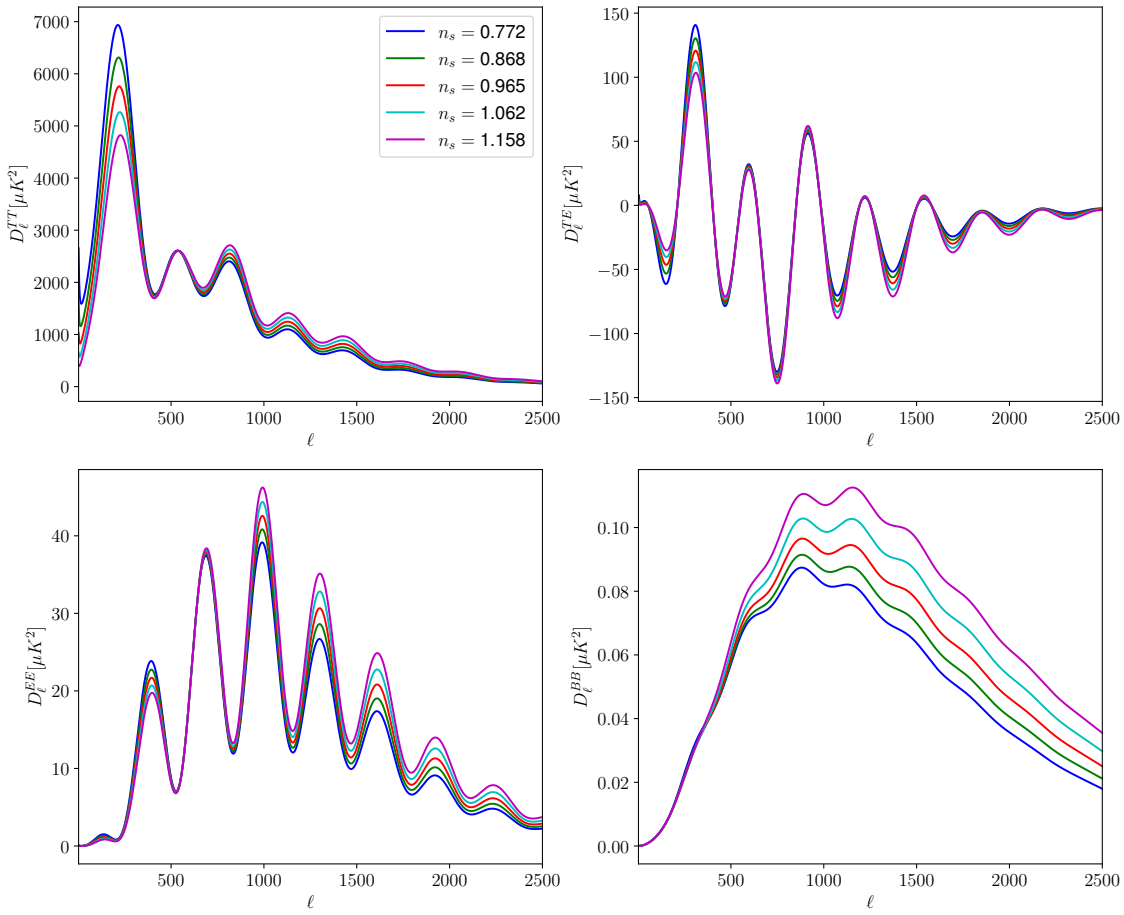


Figure A.2: *Plots of the impact of varying the $n_s$ parameter in the temperature and polarization power spectra. The red line correspond to the power spectra predicted by $\Lambda CDM$ model for the best fit parameters from Planck mission. All plots have the same legend.*

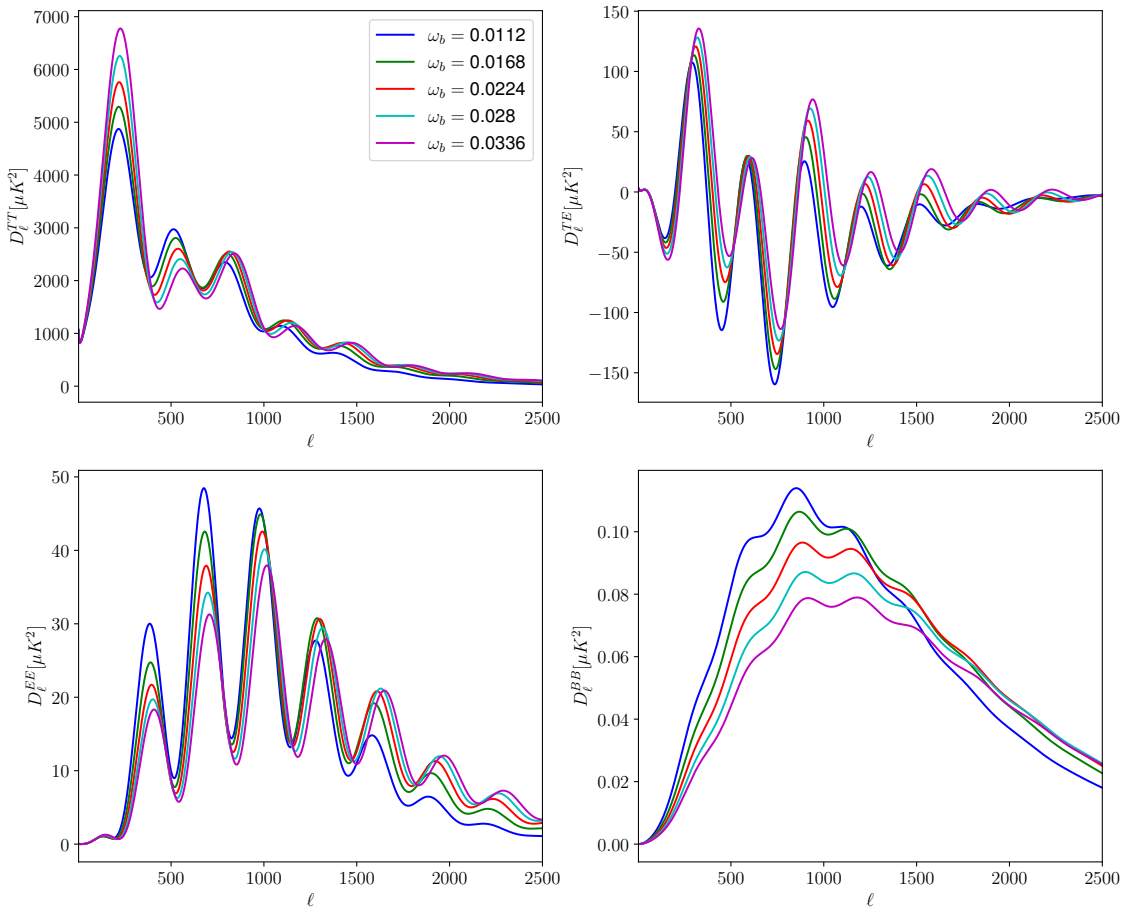


Figure A.3: *Plots of the impact of varying the $\omega_b$ parameter in the temperature and polarization power spectra. The red line correspond to the power spectra predicted by $\Lambda CDM$ model for the best fit parameters from Planck mission. All plots have the same legend.*

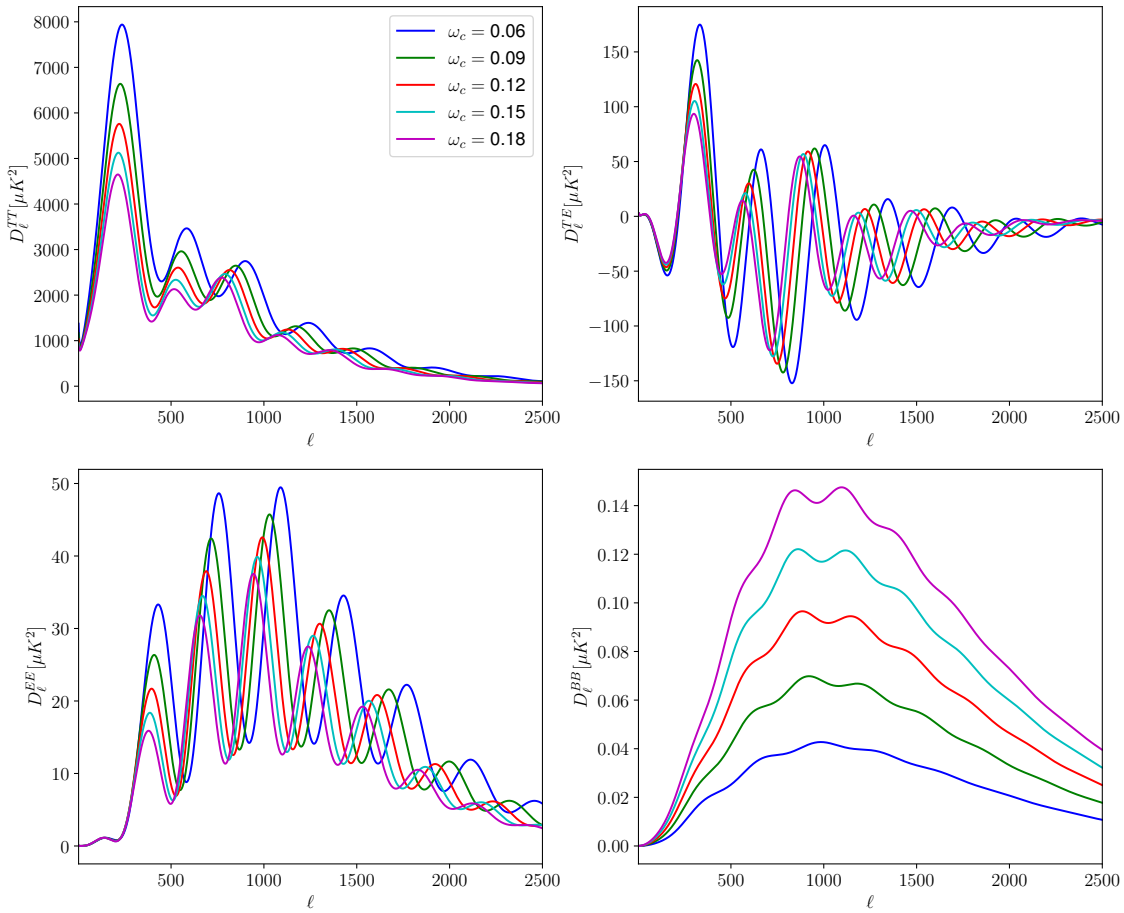


Figure A.4: *Plots of the impact of varying the $\omega_c$ parameter in the temperature and polarization power spectra. The red line correspond to the power spectra predicted by $\Lambda CDM$ model for the best fit parameters from Planck mission. All plots have the same legend.*

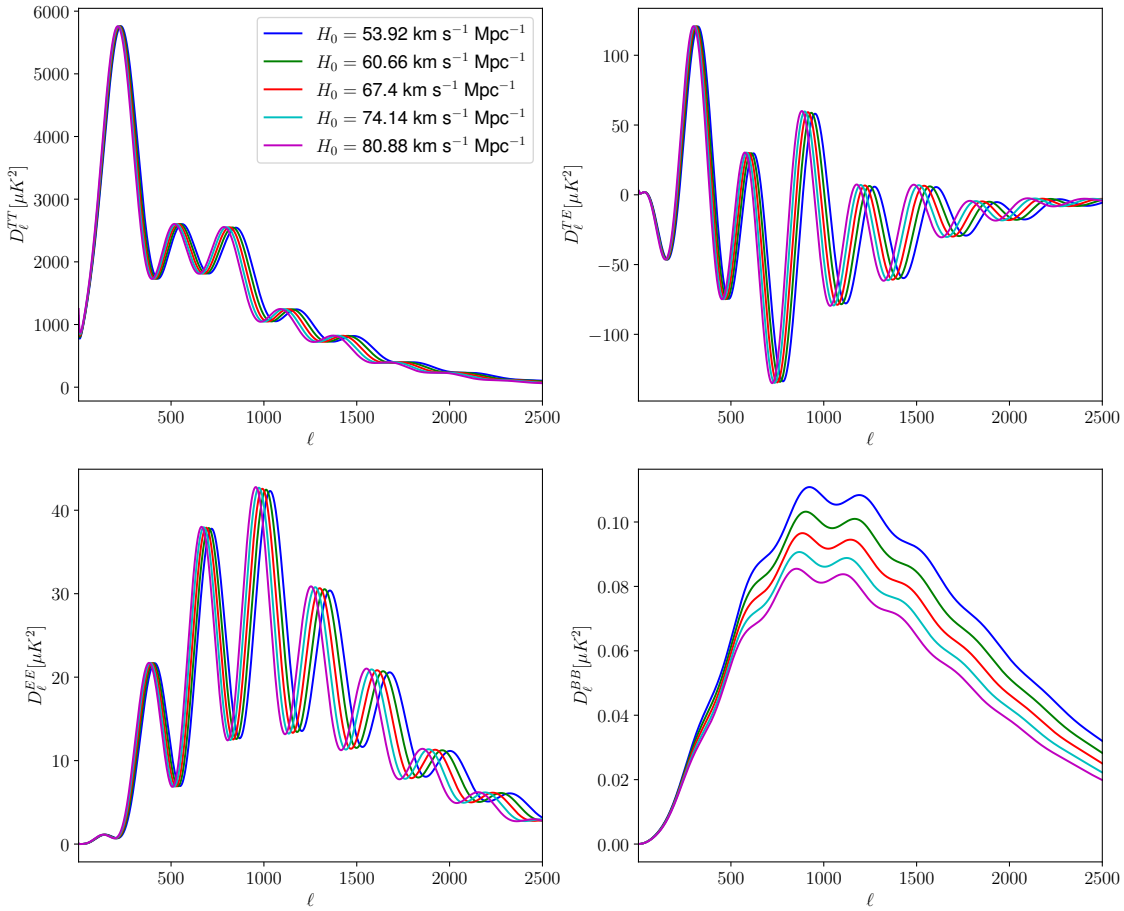


Figure A.5: *Plots of the impact of varying the $H_0$ parameter in the temperature and polarization power spectra. The red line correspond to the power spectra predicted by $\Lambda CDM$ model for the best fit parameters from Planck mission. All plots have the same legend.*

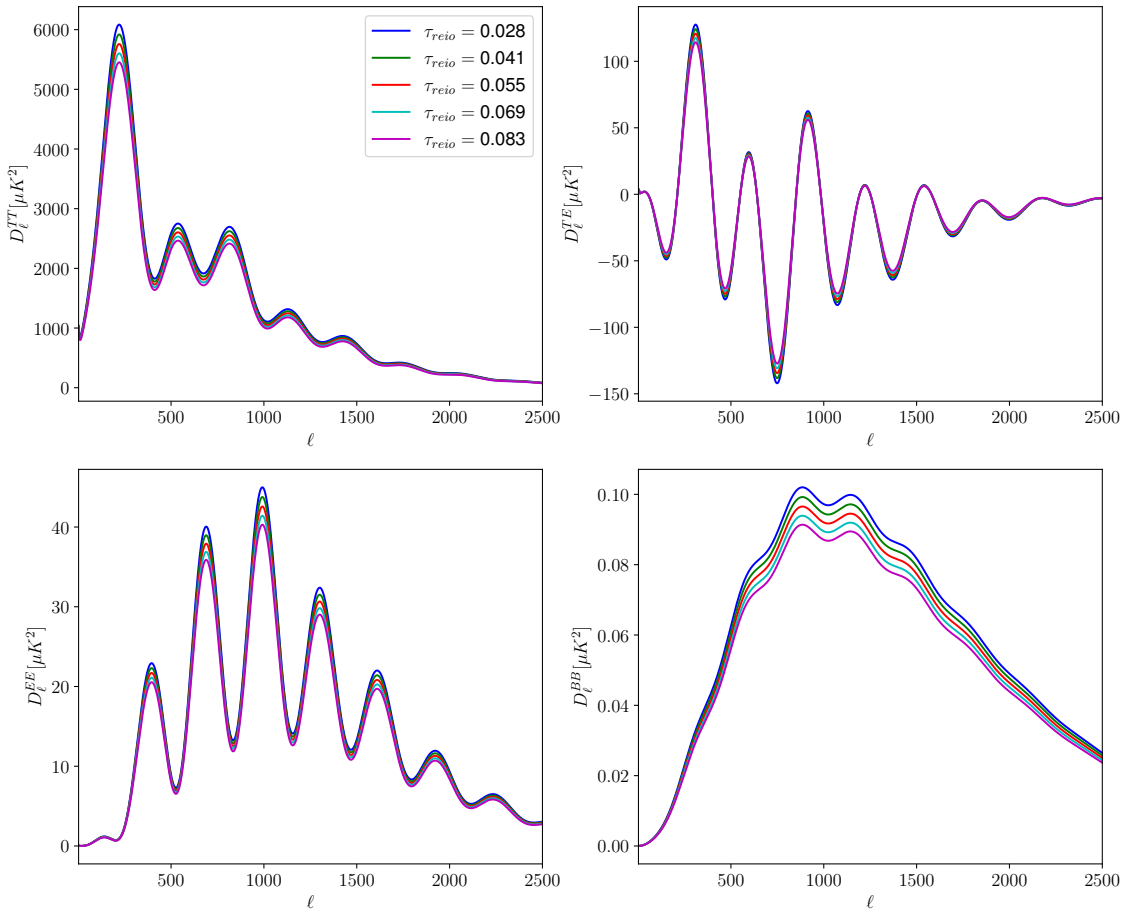


Figure A.6: *Plots of the impact of varying the $\tau_{reio}$ parameter in the temperature and polarization power spectra. The red line correspond to the power spectra predicted by $\Lambda CDM$ model for the best fit parameters from Planck mission. All plots have the same legend.*

# Appendix B

# Fitting $A_S$ plus the six phenomenological amplitudes

The aim of this appendix is to show the impossibility of constraining the ΛCDM cosmological parameters with the six phenomenological parameters considered in this project. To show this, we have only taken into account the scalar amplitude $A_s$ parameter in combination with the phenomenological amplitudes because it is the most problematic cosmological parameter by far. In the Table B.1 and in Figure B.1 the results from the MCMC runs are shown.

| Param. | $TT$ | $TT+EE+TE$ |
|---|---|---|
| $\ln(10^{10}A_s)$ | $2.97^{+0.11}_{-0.14}$ | $2.99^{+0.12}_{-0.19}$ |
| $A_L$ | $> 1.01$ | $> 0.994$ |
| $A_{lISW}$ | $< 1.14$ | $0.99^{+0.39}_{-0.35}$ |
| $A_{eISW}$ | $1.043 \pm 0.064$ | $1.034^{+0.095}_{-0.070}$ |
| $A_{SW}$ | $1.042^{+0.068}_{-0.059}$ | $1.033^{+0.096}_{-0.064}$ |
| $A_{Dop}$ | $1.045 \pm 0.064$ | $1.035^{+0.096}_{-0.070}$ |
| $A_{Pol}$ | $1.036 \pm 0.083$ | $1.034^{+0.095}_{-0.065}$ |

Table B.1: Mean values and 68% credible intervals for $A_s$ + $A_{SW}$ + $A_{eISW}$ + $A_{lISW}$ + $A_{Dop}$ + $A_{Pol}$ + $A_L$ for the MCMC chains fit to the Theoretical $TT$ and $TT+EE+TE$ datasets. The values of the parameters used to generate the different simulations are in Table 2.1 and the priors and likelihood used are described in sections 2.3.1 and 2.3.2, respectively. The $R-1$ parameter for all the runs was set to 0.1. The instrumental noise is sampled but not shown.

Basically, the combination of $A_{SW}$, $A_{eISW}$, $A_{Dop}$ and $A_{Pol}$ produces a similar effect to $A_s$ both in temperature only, $TT$, and in temperature and polarization, $TT+EE+TE$. So, the phenomenological amplitudes mentioned before are anti-correlated with $A_s$, which increases the uncertainty of the scalar amplitude. As the lensing power spectrum is proportional to $A_s$ and $A_L$, the uncertainty of $A_L$ is so high that it is unconstrained and very far from its original value of 1.

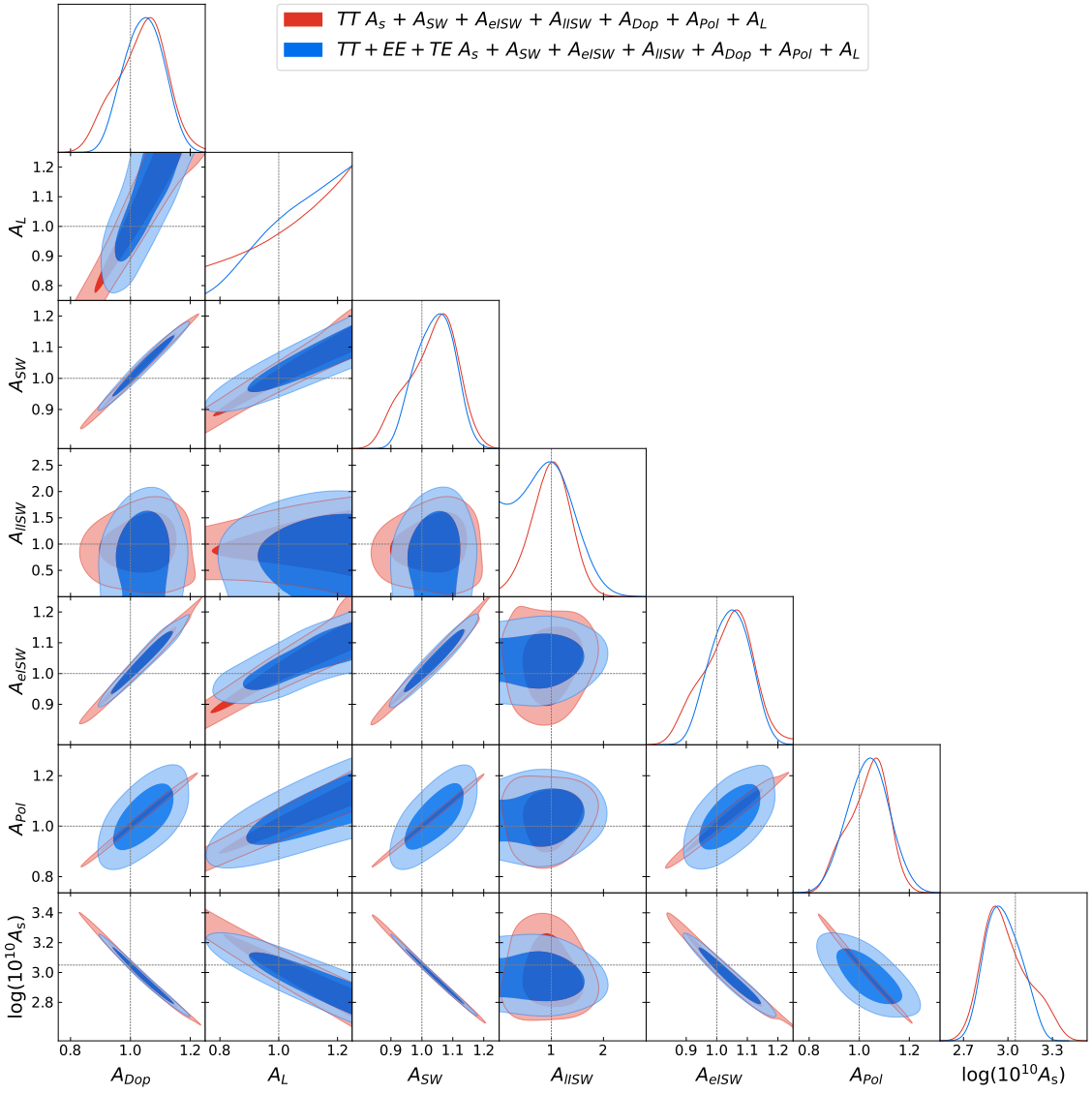


Figure B.1: *Plots of the marginalized posterior comparison of* $A_s + A_{SW} + A_{eISW} + A_{lISW} + A_{Dop} + A_{Pol} + A_L$ *fits using only the temperature power spectrum,* $TT$*, and temperature and polarization power spectra,* $TT + EE + TE$*, from the Theoretical dataset. The instrumental noise, although sampled, is not plotted. The black dotted lines represent the original parameter values and the contours display the 68% and 95% limits. The* $R - 1$ *parameter for these two runs was set to 0.1 because of the difficulty to achieve convergence. The priors and likelihoods used in this plot are described in detail in sections 2.3.1 and 2.3.2, respectively.*

# Appendix C

# Code used in this project

The main programming languages used in this project are Python and C. All the programmes has been installed in two different Linux OS: Ubuntu 18.04 and Centos 7.4.

First, we will show the modifications implemented in `CLASS` to include the six new phenomenological amplitudes introduced in this project. `CLASS` code is written mainly in C programming language and is used to compute the CMB angular power spectra for a given set of cosmological and phenomenological parameters. To introduce these new parameters, first we need to be able to storage them as format double values instead of integer, which is done in the `/class/include/perturbations.h` file for the Sachs-Wolfe effect (`ppt->switch_sw`), the early ISW effect (`ppt->switch_eisw`), the late ISW effect (`ppt->switch_lisw`), Doppler effect (`ppt->switch_dop`) and polarization effect (`ppt->switch_pol`), and in the `/class/ include/lensing.h` file for the lensing effect (`ple->Alens`). Then, in `/class/source/ input.c` file we have introduced a modification to read an input value for each physical contribution and assign it to the corresponding phenomenological amplitude as it is shown in Listing C.1.

```
1691  if (ppt->has_cl_cmb_temperature == _TRUE_) {
1692
1693    class_call(parser_read_string(pfc,"temperature contributions",&string1
      ,&flag1,errmsg),
1694               errmsg,
1695               errmsg);
1696
1697    if (flag1 == _TRUE_) {
1698
1699      ppt->switch_sw = 0.0;
1700      ppt->switch_eisw = 0.0;
1701      ppt->switch_lisw = 0.0;
1702      ppt->switch_dop = 0.0;
1703      ppt->switch_pol = 0.0;
1704
1705      if ((strstr(string1,"tsw") != NULL) || (strstr(string1,"TSW") != NULL
      ))
1706        class_read_double("tsw", ppt->switch_sw);
1707      if ((strstr(string1,"eisw") != NULL) || (strstr(string1,"EISW") !=
      NULL))
1708        class_read_double("eisw", ppt->switch_eisw);
1709      if ((strstr(string1,"lisw") != NULL) || (strstr(string1,"LISW") !=
```

```
    NULL))
1710          class_read_double("lisw", ppt->switch_lisw);
1711        if ((strstr(string1,"dop") != NULL) || (strstr(string1,"Dop") != NULL
    ))
1712          class_read_double("dop", ppt->switch_dop);
1713        if ((strstr(string1,"pol") != NULL) || (strstr(string1,"Pol") != NULL
    ))
1714          class_read_double("pol", ppt->switch_pol);
1715
1716        class_test((ppt->switch_sw == 0) && (ppt->switch_eisw == 0) && (ppt->
    switch_lisw == 0) && (ppt->switch_dop == 0) && (ppt->switch_pol == 0),
1717                   errmsg,
1718                   "In the field 'output', you selected CMB temperature, but
    in the field 'temperature contributions', you removed all contributions
    ");
1719
1720        class_read_double("early/late isw redshift",ppt->eisw_lisw_split_z);
1721
1722      }
1723
1724    }


2456
2457    if ((flag1 == _TRUE_) && ((strstr(string1,"y") != NULL) || (strstr(
      string1,"Y") != NULL))) {
2458
2459      if ((ppt->has_scalars == _TRUE_) &&
2460          ((ppt->has_cl_cmb_temperature == _TRUE_) || (ppt->
    has_cl_cmb_polarization == _TRUE_)) &&
2461          (ppt->has_cl_cmb_lensing_potential == _TRUE_)) {
2462        ple->has_lensed_cls = _TRUE_;
2463        class_read_double("Alens",ple->Alens); /* Alens fiducial parameter*/
2464      }
2465      else {
2466        class_stop(errmsg,"you asked for lensed CMB Cls, but this requires a
    minimal number of options: 'modes' should include 's', 'output' should
    include 'tCl' and/or 'pCL', and also, importantly, 'lCl', the CMB
    lensing potential spectrum. You forgot one of those in your input.");
2467      }

3434    /** - lensing structure */
3435
3436    ple->has_lensed_cls = _FALSE_;
3437    ple->Alens = 1.0;
```

Listing C.1: Parts of `/class/source/input.c` where modifications to include the phenomenological amplitudes have been performed.

Next, `perturbations.c` and `lensing.c` files are modified to take account correctly of the early and late ISW effects, the polarization effect in the polarization angular power spectra and the lensing effect. The parts where modifications have been done can be seen in Listings C.2 and C.3.

```
7214      /** - --> for each type, compute source terms */
7215
7216      /* scalar temperature */
7217      if (ppt->has_source_t == _TRUE_) {
7218
```

```
7219      /* Assign eisw or lisw term to isw effect in function of z*/
7220
7221      if (z >= ppt->eisw_lisw_split_z){
7222        switch_isw = ppt->switch_eisw;
7223      }
7224      if (z < ppt->eisw_lisw_split_z) {
7225        switch_isw = ppt->switch_lisw;
7226      }
7227
7228      /* newtonian gauge: slightly more complicated form, but more
     efficient numerically */
7229
7230      if (ppt->gauge == newtonian) {
7231        _set_source_(ppt->index_tp_t0) =
7232          ppt->switch_sw * pvecthermo[pth->index_th_g] * (delta_g / 4. +
     pvecmetric[ppw->index_mt_psi])
7233          + switch_isw * (pvecthermo[pth->index_th_g] * (y[ppw->pv->
     index_pt_phi]-pvecmetric[ppw->index_mt_psi])
7234                          + pvecthermo[pth->index_th_exp_m_kappa] * 2. *
     pvecmetric[ppw->index_mt_phi_prime])
7235          + ppt->switch_dop /k/k * (pvecthermo[pth->index_th_g] * dy[ppw->
     pv->index_pt_theta_b]
7236                                    + pvecthermo[pth->index_th_dg] * y[ppw
     ->pv->index_pt_theta_b]);
7237
7238        _set_source_(ppt->index_tp_t1) = switch_isw * pvecthermo[pth->
     index_th_exp_m_kappa] * k* (pvecmetric[ppw->index_mt_psi]-y[ppw->pv->
     index_pt_phi]);
7239
7240        _set_source_(ppt->index_tp_t2) = ppt->switch_pol * pvecthermo[pth->
     index_th_g] * P;
7241      }
7242
7243      /* synchronous gauge: slightly more complicated form, but more
     efficient numerically */
7244
7245      if (ppt->gauge == synchronous) {
7246
7247        _set_source_(ppt->index_tp_t0) =
7248          ppt->switch_sw * pvecthermo[pth->index_th_g] * (delta_g/4. +
     pvecmetric[ppw->index_mt_alpha_prime])
7249          + switch_isw * (pvecthermo[pth->index_th_g] * (y[ppw->pv->
     index_pt_eta]
7250                                                         - pvecmetric[ppw->
     index_mt_alpha_prime]
7251                                                         - 2 *
     a_prime_over_a * pvecmetric[ppw->index_mt_alpha])
7252                          + pvecthermo[pth->index_th_exp_m_kappa] * 2. * (
     pvecmetric[ppw->index_mt_eta_prime]
7253                                                                          -
      a_prime_over_a_prime * pvecmetric[ppw->index_mt_alpha]
7254                                                                          -
      a_prime_over_a * pvecmetric[ppw->index_mt_alpha_prime]))
7255          + ppt->switch_dop * (pvecthermo[pth->index_th_g] * (dy[ppw->pv->
     index_pt_theta_b]/k/k + pvecmetric[ppw->index_mt_alpha_prime])
7256                               +pvecthermo[pth->index_th_dg] * (y[ppw->pv->
     index_pt_theta_b]/k/k + pvecmetric[ppw->index_mt_alpha]));
7257
```

```
7258          _set_source_(ppt->index_tp_t1) =
7259            switch_isw * pvecthermo[pth->index_th_exp_m_kappa] * k * (
    pvecmetric[ppw->index_mt_alpha_prime]
7260                                                                  + 2. *
    a_prime_over_a * pvecmetric[ppw->index_mt_alpha]
7261                                                                  - y[ppw
    ->pv->index_pt_eta]);
7262
7263          _set_source_(ppt->index_tp_t2) =
7264            ppt->switch_pol * pvecthermo[pth->index_th_g] * P;
7265        }
7266      }
7267
7268      /* scalar polarization */
7269      if (ppt->has_source_p == _TRUE_) {
7270
7271        /* all gauges. Note that the correct formula for the E source
7272           should have a minus sign, as shown in Hu & White. We put a
7273           plus sign to comply with the 'historical convention'
7274           established in CMBFAST and CAMB. */
7275
7276        _set_source_(ppt->index_tp_p) = ppt->switch_pol * sqrt(6.) *
    pvecthermo[pth->index_th_g] * P;
7277
7278      }
```

Listing C.2: Parts of `/class/source/perturbations.c` where the transfer functions are calculated. The modifications to include correctly the late and early ISW effects and polarization effect are shown.

```
468   for (l=2; l<=ple->l_unlensed_max; l++) {
469     class_call(spectra_cl_at_l(psp,l,cl_unlensed,cl_md,cl_md_ic),
470                psp->error_message,
471                ple->error_message);
472     cl_tt[l] = cl_unlensed[ple->index_lt_tt];
473     cl_pp[l] = cl_unlensed[ple->index_lt_pp] * ple->Alens;
474     if (ple->has_te==_TRUE_) {
475       cl_te[l] = cl_unlensed[ple->index_lt_te];
476     }
477     if (ple->has_ee==_TRUE_ || ple->has_bb==_TRUE_) {
478       cl_ee[l] = cl_unlensed[ple->index_lt_ee];
479       cl_bb[l] = cl_unlensed[ple->index_lt_bb];
480     }
481   }
```

Listing C.3: Part of `/class/source/lensing.c` where a modification to include the phenomenological amplitude corresponding to the lensing effect have been performed.

To execute `CLASS` with these new modifications using the Python package containing `CLASS` (called Python wrapper), the dictionary of parameters must contain `'temperature contributions': 'tsw, eisw, lisw, dop, pol'` and the different values assigned to each phenomenological amplitude using the variables `'tsw'`, `'eisw'`, `'lisw'`, `'dop'`, `'pol'`, `'Alens'`.

As explained in Chapter 2, `Cobaya` calls `CLASS` code in the likelihood calculation using `/cobaya/cobaya/theories/classy/classy.py` Python file. This file assumes that no phenomenological amplitudes are introduced in the calculation of the CMB angular power

spectra and an error arises. To fix this problem a line containing `self.extra_args[ 'temperature contributions'] = ' tsw eisw lisw dop pol'` must be added.

As explained in Chapter 2, we have simulated the CMB angular power spectra observed by Planck experiment using a combination of `CLASS` and `healpy`. The software developed for that purpose is original and showed in Listing C.4.

```
# Packages
# ------------------------------------------------------------------------
import healpy as hp
from classy import Class
from cobaya.model import get_model
import numpy as np
import matplotlib.pyplot as plt
# ------------------------------------------------------------------------
# Simulates the CMB angular power spectra using a combination of CLASS
# and healpy.
# Author: Miguel Ruiz Granda
# ------------------------------------------------------------------------
# PARAMETERS (taking as reference FWHM and temperature noise level of
    channel 143 GHz of Planck Mission)
nside = 2 ** 11
beam_FWHM = 7.22  # arcmin
beam_FWHM_rad = beam_FWHM * np.pi / (60 * 180)  # radians
T_CMB = 2.7255e6  # muK
noise_std_pixel = 0.55 * (60 / hp.nside2resol(nside, arcmin=True)) / T_CMB
     # adimensional
l_max = 2500
packages_path = '/home/miguel/Desktop/class'

# CLASS is executed using python wrapper to calculate CMB lensed
    temperature spectrum.
cosmo = Class()
cosmo.set(
    {'l_max_scalars': l_max, 'output': 'tCl, lCl, pCl', 'modes': 's', '
    lensing': 'yes', 'temperature contributions': 'tsw, eisw, lisw, dop,
    pol',
     'tsw': 1.0, 'eisw': 1.0, 'lisw': 1.0, 'dop': 1.0, 'pol': 1.0, 'Alens':
     1.0, 'omega_b': 0.0224,
     'omega_cdm': 0.12, 'H0': 67.4, 'tau_reio':  0.055, 'ln10^{10}A_s':
    3.05, 'n_s': 0.965, 'early/late isw redshift': 30})
cosmo.compute()
cl = cosmo.lensed_cl()
factor = (T_CMB ** 2 / (2 * np.pi)) * np.multiply(cl['ell'], (cl['ell'] +
    1))  # (T_CMB**2)*l*(l+1)/(2*pi) factor.

# Gaussian beam function and pixel window function are calculated to
    convolve the Cl sky and obtain Cl map.
beam_function = hp.sphtfunc.gauss_beam(beam_FWHM_rad, l_max, pol=True)
beam_function_squared = np.multiply(beam_function, beam_function)
pixel_window_function = hp.sphtfunc.pixwin(nside, pol=True, lmax=l_max)
pixel_window_function_squared = np.multiply(pixel_window_function,
    pixel_window_function)

# TT, EE, TE, EE angular power spectra (adimensional)
cl_healpy = []
cl_healpy.append(np.multiply(np.multiply(cl['tt'], beam_function_squared[:,
     0]),
```

```
                          pixel_window_function_squared[0, :]))  # Cl TT
cl_healpy.append(np.multiply(np.multiply(cl['ee'], beam_function_squared[:,
    1]),
                          pixel_window_function_squared[1, :]))  # Cl EE
cl_healpy.append(np.multiply(np.multiply(cl['bb'], beam_function_squared[:,
    2]),
                          pixel_window_function_squared[1, :])) # Cl BB
cl_healpy.append(np.multiply(np.multiply(cl['te'], beam_function_squared[:,
    3]),
                          pixel_window_function_squared[1, :]))  # Cl TE


# The map is generated using cl_healpy and the function synfast.
mapGenerated = hp.sphtfunc.synfast(cl_healpy, nside, new=True)

# We add instrumental random gaussian noise to the convolved map.
npix = hp.pixelfunc.nside2npix(nside)
electronicNoise1 = np.random.normal(0, noise_std_pixel, npix)
electronicNoise2 = np.random.normal(0, np.sqrt(2)*noise_std_pixel, npix)
electronicNoise3 = np.random.normal(0, np.sqrt(2)*noise_std_pixel, npix)

mapGenerated[0] = mapGenerated[0] + electronicNoise1
mapGenerated[1] = mapGenerated[1] + electronicNoise2
mapGenerated[2] = mapGenerated[2] + electronicNoise3

# Using the function anafast, the Cl from the map are recovered.
cl_recovered = hp.sphtfunc.anafast(mapGenerated, lmax=l_max, use_weights=
    True)

cl_save = []
cl_save.append(np.divide(np.divide(cl_recovered[0][2:],
    beam_function_squared[2:, 0]), pixel_window_function_squared[0, 2:])) #
     Cl TT
cl_save.append(np.divide(np.divide(cl_recovered[1][2:],
    beam_function_squared[2:, 1]), pixel_window_function_squared[1, 2:])) #
     Cl EE
cl_save.append(np.divide(np.divide(cl_recovered[3][2:],
    beam_function_squared[2:, 3]), pixel_window_function_squared[1, 2:])) #
     Cl TE
cl_save.append(beam_function_squared[2:, 0]) # Squared beam function
    temperature (TT)
cl_save.append(np.array(beam_function_squared[2:, 1])) # Squared beam
    function (EE)
cl_save.append(np.array(beam_function_squared[2:, 3])) # Squared beam
    function (TE)
cl_save.append(np.array(pixel_window_function_squared[0, 2:])) # Squared
    pixel window function-Temperature
cl_save.append(np.array(pixel_window_function_squared[1, 2:])) # Squared
    pixel window function-Polarization
np.savetxt('dataclTTAndPol.csv', cl_save, delimiter=',')
```

Listing C.4: Python code used to generate the CMB angular power spectra from the Simulated dataset, i.e., going through `healpy`.

Finally, the crucial part of this project: the MCMC runs with `Cobaya`. As the code developed for the Theoretical and Simulated datasets are very similar, and $TT$ and $TT + EE + TE$ codes differ basically in the likelihood used, we will show as an example the code used in $TT + EE + TE$ Theoretical dataset in Listing C.5.

```
from cobaya.model import get_model
import numpy as np
import sys
from cobaya.run import run
import healpy as hp
import matplotlib.pyplot as plt
#-----------------------------------------------------
# Runs MCMC from Cobaya using the TT + EE + TE
# Theoretical dataset and the temperature and
# polarization for a certain set of sampled parameters.
# Author: Miguel Ruiz Granda
#-----------------------------------------------------
# Folder where the MCMC chains are stored
output_folder = sys.argv[1]
output_path = '/home/miguel/Desktop/' + output_folder + '/' + output_folder

# Theoretical cosmological parameters used to compute the CMB TT spectrum.
fiducial_params = {
    'eisw': 1.0, 'lisw': 1.0, 'dop': 1.0, 'pol': 1.0, 'Alens': 1.0, '
    omega_b': 0.0224, 'tsw': 1.0,
    'omega_cdm': 0.12, 'H0': 67.4, 'tau_reio': 0.055, 'ln10^{10}A_s': 3.05,
     'n_s': 0.965, 'early/late isw redshift': 30}
l_max = 2500
# Path to CLASS code
packages_path = '/home/miguel/Desktop/class'
info_fiducial = {
    'params': fiducial_params,
    'likelihood': {'one': None},
    'Debug': False,
    'theory': {'classy': {"extra_args": {"N_ncdm": 1, "N_ur": 2.0328}, "
    path": packages_path}},
    'packages_path': packages_path}

model_fiducial = get_model(info_fiducial)

# Calculates the Cls using CLASS using the fiducial_parms defined above.
model_fiducial.add_requirements({"Cl": {'tt': l_max, 'ee': l_max}})

# Compute and extract the CMB power spectrum
# (In muK^-2, without l(l+1)/(2pi) factor)
# notice the empty dictionary below: all parameters are fixed
model_fiducial.logposterior({})
Cls = model_fiducial.provider.get_Cl(ell_factor=False, units="muK2")

# Our fiducial power spectrum
Cl_est_TT = Cls['tt'][:l_max + 1]
Cl_est_EE = Cls['ee'][:l_max + 1]
Cl_est_TE = Cls['te'][:l_max + 1]

# Parameters used in the likelihood:
beam_FWHM_rad = 7.22 * np.pi / (60 * 180) # deg
healpix_Nside = 2048
T_CMB = 2.7255e6  # muK
noise_std_pixel = 7.04870790577218e-06
pixel_area_rad = np.pi / (3 * healpix_Nside ** 2)
weight_per_solid_angle = ((noise_std_pixel * T_CMB) ** 2 * pixel_area_rad)
    ** -1

```

```
beam_function = hp.sphtfunc.gauss_beam(beam_FWHM_rad, l_max, pol=True)
beam_function_squared = np.multiply(beam_function, beam_function)
pixel_window_function = hp.sphtfunc.pixwin(healpix_Nside, pol=True, lmax=
    l_max)
pixel_window_function_squared = np.multiply(pixel_window_function,
    pixel_window_function)
ells = np.arange(l_max + 1)
# Noise spectrum, beam-corrected
Nl1 = 1 / (weight_per_solid_angle * beam_function_squared[:, 0][2:] *
    pixel_window_function_squared[0, :][2:])
Nl2 = 2 / (weight_per_solid_angle * beam_function_squared[:, 1][2:] *
    pixel_window_function_squared[1, :][2:])
# Cl of the map: data + noise
Cl_map_TT = Cl_est_TT[2:] + Nl1
Cl_map_EE = (Cl_est_EE[2:] + Nl2)[:1999]
Cl_map_EE = np.concatenate((Cl_map_EE, np.ones(500)))
Cl_map_TE = (Cl_est_TE)[2:2001]
Cl_map_TE = np.concatenate((Cl_map_TE, np.zeros(500)))

# The likelihood
def my_like(noise_std_pixel=7e-6, _self=None):
    weight_per_solid_angle = ((noise_std_pixel * T_CMB) ** 2 *
    pixel_area_rad) ** -1
    ells = np.arange(2, l_max + 1)
    # Noise spectrum, beam-corrected
    Nl1 = 1 / (weight_per_solid_angle * beam_function_squared[:, 0][2:] *
    pixel_window_function_squared[0, :][2:])
    Nl2 = 2 / (weight_per_solid_angle * beam_function_squared[:, 1][2:] *
    pixel_window_function_squared[1, :][2:])
    # Cl of the map: data + noise
    # Request the Cl from the provider
    Cl_theo_TT = _self.provider.get_Cl(ell_factor=False, units="muK2")['tt'
    ][2:l_max + 1] + Nl1
    Cl_theo_EE = (_self.provider.get_Cl(ell_factor=False, units="muK2")['ee
    '][2:l_max + 1] + Nl2)[:1999]
    Cl_theo_EE = np.concatenate((Cl_theo_EE, np.ones(500)))
    Cl_theo_TE = (_self.provider.get_Cl(ell_factor=False, units="muK2")['te
    '][2:l_max + 1])[:1999]
    Cl_theo_TE = np.concatenate((Cl_theo_TE, np.zeros(500)))
    # Compute the log-likelihood
    V1 = (Cl_theo_TT * Cl_theo_EE - Cl_theo_TE * Cl_theo_TE) / (Cl_map_TT*
    Cl_map_EE - Cl_map_TE*Cl_map_TE)
    V2 = (Cl_map_TT * Cl_theo_EE + Cl_theo_TT * Cl_map_EE - 2*Cl_map_TE*
    Cl_theo_TE) / (Cl_theo_TT*Cl_theo_EE - Cl_theo_TE*Cl_theo_TE)
    logp = np.sum(-0.7 * 0.5*(2 * ells + 1) * (V2 + np.log(V1) - 2))
    return logp

info = {
    'params': {
        # Fixed
        'Alens': 1.0, # 'tsw': 1.0, 'lisw': 1.0, 'dop': 1.0, 'pol': 1.0, '
    eisw': 1.0,
        # 'omega_cdm': 0.12, 'H0': 67.4, 'tau_reio': 0.055, 'ln10^{10}A_s':
     3.05, 'n_s': 0.965, 'omega_b': 0.0224,
        'early/late isw redshift': 30,
        # Sampled
        # Phenomenological amplitudes
        'dop': {'latex': 'A_{Dop}', 'prior': {'max': 1.25, 'min': 0.75}, '
```

```
    proposal': 0.05,
99              'ref': {'dist': 'norm', 'loc': 1.0, 'scale': 0.001}},
100         # 'Alens': {'latex': 'A_{L}', 'prior': {'max': 1.25, 'min': 0.75},
    'proposal': 0.05,
101         #           'ref': {'dist': 'norm', 'loc': 1.0, 'scale': 0.001}},
102         'tsw': {'latex': 'A_{SW}', 'prior': {'max': 1.25, 'min': 0.75}, '
    proposal': 0.05,
103             'ref': {'dist': 'norm', 'loc': 1.0, 'scale': 0.001}},
104         'lisw': {'latex': 'A_{lISW}', 'prior': {'max': 4.0, 'min': 0.0}, '
    proposal': 0.05,
105             'ref': {'dist': 'norm', 'loc': 1.0, 'scale': 0.001}},
106         'eisw': {'latex': 'A_{eISW}', 'prior': {'max': 1.25, 'min': 0.75},
    'proposal': 0.05,
107              'ref': {'dist': 'norm', 'loc': 1.0, 'scale': 0.001}},
108         'pol': {'latex': 'A_{Pol}', 'prior': {'max': 3.0, 'min': 0.0}, '
    proposal': 0.05,
109             'ref': {'dist': 'norm', 'loc': 1.0, 'scale': 0.001}},
110         # LambdaCDM parameters
111         'n_s': {'prior': {'min': 0.8, 'max': 1.2},
112                 'ref': {'dist': 'norm', 'loc': 0.965, 'scale': 0.004}, '
    proposal': 0.002, 'latex': 'n_\\mathrm{s}'},
113         'A_s': {'latex': 'A_\\mathrm{s}', 'value': 'lambda logA: 1e-10*np.
    exp(logA)'},
114         'H0': {'latex': 'H_0', 'prior': {'max': 100, 'min': 20},
115                 'proposal': 2, 'ref': {'dist': 'norm', 'loc': 67.556, '
    scale': 2}},
116         'logA': {'drop': True, 'latex': '\\log(10^{10} A_\\mathrm{s})',
117                  'prior': {'max': 3.91, 'min': 1.61},
118                  'proposal': 0.001,
119                  'ref': {'dist': 'norm', 'loc': 3.05, 'scale': 0.001}},
120         'omega_b': {'latex': '\\Omega_\\mathrm{b} h^2',
121                     'prior': {'max': 0.1, 'min': 0.005},
122                     'proposal': 0.0001,
123                     'ref': {'dist': 'norm',
124                             'loc': 0.0224,
125                             'scale': 0.0001}},
126         'omega_cdm': {'latex': '\\Omega_\\mathrm{c} h^2',
127                       'prior': {'max': 0.99, 'min': 0.001},
128                       'proposal': 0.0005,
129                       'ref': {'dist': 'norm', 'loc': 0.12, 'scale':
    0.001}},
130         'tau_reio': {'latex': '\\tau_{reio}', 'prior': {'max': 0.8, 'min':
    0.01},
131                      'proposal': 0.003, 'ref': {'dist': 'norm', 'loc':
    0.055, 'scale': 0.006}},
132         'clamp': {'derived': 'lambda A_s, tau_reio: 1e9*A_s*np.exp(-2*
    tau_reio)',
133                   'latex': '10^9 A_\\mathrm{s} e^{-2\\tau}'},
134         'noise_std_pixel': {
135            'prior': {'dist': 'norm', 'loc': 7.05e-06, 'scale': 1e-8},
136            'latex': r'\sigma_\mathrm{pix}'}},
137     'likelihood': {'my_cl_like': {"external": my_like, "requires": {'Cl': {
    'tt': l_max, 'ee': l_max}}}},
138     'theory': {'classy': {"extra_args": {"N_ncdm": 1, "N_ur": 2.0328}, '
    path': packages_path, 'stop_at_error': True}},
139     'packages_path': packages_path,
140     'debug': False,
141     'sampler': {'mcmc': {"burn_in": 0, 'Rminus1_stop': 0.05, '
```

```
    Rminus1_cl_stop': 0.2,
                        'covmat': 'auto', 'drag': False, 'oversample_power
    ': 0.4, 'proposal_scale': 1.9}},
     'output': output_path}

model = get_model(info)

updated_info, sampler = run(info)
```

Listing C.5: Python code used to run Markov Chain Monte Carlo (MCMC) method from `Cobaya` using the $TT + EE + TE$ Theoretical dataset and sampling all cosmological and phenomenological parameters, except $A_L$.

All the figures that appear in this document are elaborated explicitly for this Final Degree Project, except those which are properly cited. For their elaboration, the package `matplotlib`[1] of Python was used and original scripts were written.

[1] `https://matplotlib.org/`